

Technical University of Lodz

Faculty of Electrical, Electronic, Computer and Control Engineering

Department of Microelectronics and Computer Science

**Smart Materials
as Sensors and Actuators
for
Lorentz Force Tuning System**

Dissertation

written by Przemysław Sękalski

supervised by prof. Andrzej Napieralski

**Łódź
September 2006**

Dla Kochanej Ewunii, Zosii oraz Fistaszka

Acknowledgement

I would like to express my gratitude to my advisor, professor Andrzej Napieralski, for his support, patience, and encouragement throughout my studies. His technical and editorial advice was essential to the completion of this dissertation and has taught me countless lessons and insights on the workings of academic research in general.

Special thanks are addressed to doctor Mariusz Grecki and professor Dieter Proch who have encouraged me to take part in the CARE project.

I would like to thank doctor Stefan Simrock for his invaluable comments, constant support and what is the most important for his trust in young people. I would like to show my gratitude to doctor Lutz Lilje, who helped me to understand the physics which stands behind the project and who encouraged me to exceed the limits. I would like to express special thanks to Clemens Albrecht and all cryogenic team from DESY for their continuous support in the preparation and execution of experiments as well as their valuable comments.

Special thanks are addressed to the colleagues from IPN-Orsay, INFN-Milan and CEA-Saclay laboratories for their collective work. Especially, I would like to thank Mohammed Fouaidy for long discussions, Angelo Bosotti for research inspirations, Rocco Papparella for knowledge exchange and Pierre Bosland for explanation of mechanics.

Special thanks are addressed to professor Tadeusz Pustelny for his valuable remarks and comments regarding the dissertation.

Finally, I would like to express my gratitude to my Family, who have encouraged me to continue my studies. Moreover, I would like to greatly appreciate my wife Ewa for her patience, support and inspiration.

I acknowledge the support of the European Community-Research Infrastructure Activity under the FP6 “Structuring the European Research Area” program (CARE, contract number RII3-CT-2003-506395), and Polish National Science Council Grant”138/E-370/SPB/6.PR UE/DIE 354/2004-2007” and “3 T10C 036 30”.

Index

Used shortcuts	3
Chapter 1. Introduction	4
Chapter 2. State of the art of the cavity tuners	8
2.1. Introduction	8
2.2. Superconducting accelerators	8
2.3. Vacuum Ultra Violet Free Electron Laser	10
2.4. Current tuners development	16
Chapter 3. Detuning sources	21
3.1. Lorentz force phenomenon description	21
3.2. Microphonics	24
3.3. Mechanical model of cavity	27
3.3.2. Direct and inverse transfer functions between piezostack and RF field	28
3.4. Cavity model description	30
3.5. Detuning measurement	34
3.5.1. Multi-pulse detuning measurement	34
3.5.2. Single pulse detuning measurement	35
3.5.3. Comparison of single and multi-pulse detuning measurement	36
3.6. Conclusion	37
Chapter 4. Smart materials	39
4.1. Introduction	39
4.2. Piezoelectric stacks	40
4.2.1. Piezoelement characterization and comparison	42
4.3. Magnetostrictive rods	48
4.4. Conclusion	52
Chapter 5. Force measurement	53
5.1. Introduction	53
5.2. Strain gauge	54
5.3. Shift of piezoelectric stack resonant frequency	58
5.3.1. Measurement at room temperature	60
5.3.2. Measurement at LHe temperature	63
5.4. Capacitance change	67
5.5. Conclusion	69

Chapter 6. Fast tuning system	70
6.1. Introduction	70
6.2. Mechanical part – Cold Tuning System	71
6.3. Electronic part	73
6.4. Software part	74
6.4.1. Single pulse compensation method	76
6.4.2. Multi-pulse compensation method	81
6.4.3. Feed forward algorithm for Lorentz force compensation	87
6.5. Measurements and results	88
Chapter 7. Summary and conclusion	92
Bibliography	95
Index of figures	101
Index of tables	105
Appendix A Piezo Control Panel PCP description	106
Appendix B Measurements of coefficients of linearized detuning for different accelerating field gradient.	109

Used shortcuts

CTS	- Cold Tuner System
DOOCS	- Distributed Object Oriented Control System
FG	- function generator
FLASH	- F ree Electron L aser in H amburg
ILC	- International Linear Collider,
K_L	- Lorentz force detuning constant
LCR	- an electrical circuit consisting of a resistor (R), an inductor (L), and a capacitor (C)
LHC	- Large Hadron Collider
NC	- normal conducting
PI	- Physik Instrumente GmbH & Co. KG
PTS	- Piezo Tuner System
PZD	- Piezo Driver Transducer
PZM	- Piezo Driver Receiver (Measurement)
PZT	- a piezoelectric material, which contains lead zirconium titanate
QL	- loaded quality factor
Q_0	- unloaded quality factor
SASE	- self amplified spontaneous emission
SC	- superconducting
TCE	- temperature coefficient of expansion,
TESLA	- Tera-eV Superconducting Linear Accelerator,
TTF	- TESLA Test Facility,
VUV-FEL	- Vacuum Ultra-Violet Free Electron Laser,
X-FEL	- X-Ray Free Electron Laser,

Chapter 1. Introduction

During the last century the understanding of the nature, especially at the level of its smallest constituents have been significantly improved. The last achievement – the so-called Standard Model becomes a fundamental theory for the particle physics. However, the presented model needs to be verified by experiment. The only method to validate the hypothesis covered in Standard Model is to design particle accelerators, which are able to provide an extremely high energy of range of millions of millions of eV and higher.

The first precursor of nowadays machines – the cyclotron – was constructed by E. Lawrence in 1929. This device was operated at energy up to 1 MeV. For comparison, the Large Hadron Collider (LHC), which is constructed at CERN, Switzerland will be able to provide the centre-of-mass energy of 14 TeV. However, there is need to remark that during the collision this energy will be shared with quarks of protons therefore the energy of the collision will be much lower. In other words, products of collision will capture part of energy. This “energy sharing” might be eliminated by using the fundamental particles, which make up all the other particles found in Nature, and are not themselves made up of smaller particles. As a consequence, the $e^- e^+$ colliders are promising for the current and future research. The advantages of such a machine were proved by the biggest storage ring called Large Electron-Positron Collider (LEP). Its energy was around 200GeV and the beam luminosity was in range of $10^{33} \text{ cm}^{-2}\text{s}^{-1}$. In high energy physics community is strong believe that after the great success of previous machine, there is need to build new accelerator, which will be able to provide an energy of collision over 1 TeV.

Across the world there are several groups, which are working on the successor of LEP. One of them is a TESLA Technology Collaboration, which proposes to use a nine-cell superconducting standing wave accelerating structures made of pure niobium [Brinkmann 2001]. The cavities will be operated at 1.3 GHz and the average accelerating field gradient in each cavity will be above 35 MV/m. The over 30 km long accelerator will be able to provide the required energy of collision of positrons and electrons of 1 TeV.

The proposed machine is a linear accelerator. It is the only solution to eliminate the synchrotron radiation, which prevent reaching the high energy by electrons and positrons. This radiation is generated while the electrons, which move near the speed of light, flight through magnetic fields perpendicular to the direction of movement. Then the photons are generated, which carry out part of electron energy. In case of ring accelerator the magnetic field are used to change the direction of beam.

The reason of using the superconducting cavities is its efficiency. The small power dissipation in the cavity walls is guaranteed by using the pure nine-cell niobium cavities cooled by superfluid

helium to 2 K. As a consequence, the unloaded quality factor of single cavity is in order of 10^{10} . However, for high accelerating gradients (above the 20 MV/m) there is need to operate the machine in pulse mode to keep the average cryogenic losses in acceptable limits. In case of proposed solution, the pulse length is set to 1.3 ms, where the first 500 μs is used for filling the cavity with RF field and during the next 800 μs the field is kept constant (so-called flat-top). This is also a great advantage of the superconducting structure over the normal conducting ones, in which only microseconds pulses might be reached.

The performance of TESLA technology significantly evaluated since last decade. Since the first test of single cavity, through TTF I - the 100 m TESLA Test Facility and TTF II (its 260 m long upgrade), to VUV-FEL¹ (Vacuum Ultra Violet Free Electron Laser), the improvement in reliability and performance of used technology has been done. All of these machines were constructed at DESY-Hamburg, Germany with international collaboration of many countries including Poland.

As it was mentioned above the TESLA technology allows building not only the linear collider, but also a free electron laser. In the second type of the device the fast high-energy electrons are moving through undulators in which a high magnetic field forces the particles to undergo oscillations and radiate. As a consequence, the phenomenon of synchrotron radiation, which prevents from reaching high energy in ring accelerators, is used to generate a high brilliant and coherent light of very short wavelength. Currently, the wavelength of FLASH is in range of several nanometers. The next machine of length of 3 km will be able to provide a light of X-ray regime – X-FEL (X-ray Free Electron Laser). The possible application of FEL is not limited to high-energy physics but also covers the biology, medicine, solid physic and many others.

The cavities used in TESLA and X-FEL projects are powered by the wave with constant radio frequency equal to 1.3 GHz (RF). This frequency was adjusted to internal frequency of the TESLA cavity, because the cavity should work on resonance. As it was mentioned, the quality factor of unloaded cavity is more than 10^{10} whereas the quality factor of loaded cavity (with couplers, tuner, etc) is $Q_L=3*10^6$. It corresponds to cavity measured half-bandwidth around $\omega_{1/2} \approx 230$ Hz. There is need to point, that each cavity is slightly different, what causes that each cavity need to be tuned before operation.

The resonant frequency of the cavity depends on its dimension. As a result, a sophisticated system, which can shrink and stretch the single cavity, was build to reach the frequency of master oscillator. The tuning system consists of a stepper motor, which adjust the shape of the cavity after cooling down and pumping. Because there is need to tune cavities before operating, therefore this process is commonly named pre-detuning. The system is also equipped with piezoelectric stack,

¹ VUV-FEL was recently renamed to FLASH (Free-Electron LASer in Hamburg)

which are using for Lorentz force and microphonics cancellation. The second part of the system is commonly named a fast tuner.

The principle of fast tuner operation is described in thesis of M. Liepe [Liepe 2001b]. However, the presented solution was checked with only one cavity, and the driving signal was set manually. In case of FLASH, there will be six modules, but probably only two of them will be equipped with the fast tuners. It means that there will be at least 16 compensation systems. In case of future machine, like X-FEL there will be at least 1000 of tuners. For longer machines, like ILC few tens of thousands of tuners is predicted. As a consequence, there is need to automate the algorithm for compensation. Another important issue is a reliability of used actuator. According to the literature [Zickgraf 1995, PI web] the lifetime of the piezoelectric stacks depends on preload force. As a result, a static force measurement at cryogenic environment becomes an important topic.

The main objective of the thesis is to present the recent development of the fast tuner attached to TESLA type cavities assembled in FLASH accelerator. Especially the thesis proofs, that:

- it is possible to automate the Lorentz force compensation system used for Vacuum Ultra Violet Free Electron Laser,
- it is possible to use a piezoelectric stack itself to measure the static force (preload) applied to the actuator in wide range of temperatures from 2 to 300 K,

The dissertation is organized in seven chapters. At the beginning the general information about the accelerator technology is presented. The second chapter provide also a terminology used in the high-energy physics field, which allows easy understanding for experts from other disciplines. Moreover, the TESLA type cavity is presented with its dimensions and mechanical properties. Beside of that, it also covers the information about alternative development of tuners, which might be used for TESLA type cavities for future machines.

Chapter 3 summarizes the information about detuning sources. The mechanical and electromechanical models of cavity compared to performed measurements are presented. Also the old (multi-pulse) and new (single pulse) methods of detuning measurement are described.

In chapter 4 the smart materials, which might be used for fast tuning system, are presented. Especially, there results of experiments performed at cryogenic and room temperature of piezoelectric stacks from five different manufacturers and two types of magnetostrictive rods are shown. Moreover, the problems related with reliability of the active element are investigated.

The lifetime of the piezoelectric actuator depends on the preload force. As a result there is need to measure the static force applied to the piezoelement. The innovative method of using the active

element itself to estimate the preload is presented in Chapter 5. Moreover, it is compared to existing method, which relies on the strain gauges.

Next chapter is dedicated to the fast tuning system used for FLASH accelerator. At the beginning the mechanical part is briefly presented. The main part of this chapter is the automation of Lorentz force compensation system.

At the end a summary and plan for the further research is presented. Moreover, a list of used bibliography is attached. The thesis is finished with two appendixes. The first of them describes the control panel used for Lorentz force compensation (Appendix A). The second one presents a study of linearized detuning coefficients for different accelerating field gradient (Appendix B).

Chapter 2. State of the art of the cavity tuners

2.1. Introduction

The main aim of this chapter is to give a brief introduction to the accelerators technology, especially for the experts from non-high-energy-physics fields. At the beginning, the principle of superconducting cavities (SC) is presented. In general, the work covered in the thesis is connected with TESLA type cavities and as a result only this type of the structure will be presented in this Chapter. Then, the Vacuum Ultra Violet Free Electron Laser is described as the example of machine, which uses the SC cavities. At the end of this chapter different variation of proposed tuners are shown

2.2. Superconducting accelerators

Nowadays, the physics of accelerator is well established and described in plenty of books and papers. The most interesting, valuable and complex are the one presented by A. W. Chao and H. Padamsee [Padamsee 1998, Chao 1999]. The work presented in the thesis focuses on the recent development done at DESY in Hamburg, Germany. Especially, the recent development connected with Vacuum Ultra Violet Free Electron Laser will be presented. Nevertheless, several references to other machines are given.

As it was written in the introduction the superconducting SC technology becomes more and more interesting for low current, pulsed mode machines as for the one developed at DESY in Hamburg, Germany [Schmueser 2003]. The key part of any accelerator is a resonant cavity. In technology developed at DESY, commonly named TESLA, it is a nine-cell structure build of pure niobium (see Figure 2.1) [Brinkmann 2001]. The niobium of high RRR² (over 300) used for the design becomes a superconductor when cooled below 9.2 K. Thanks to superconductivity, the particles in an accelerator can be brought up to highest energies with hardly any power loss (the efficiency of energy transmission between the accelerating field and the beam is almost 100 %). However, the cavity operation temperature is set to 1.8 K to eliminate temporary surface warm up (called quench), caused by imperfection of the surface and high electromagnetic fields. Additionally, the lower temperature causes lower power losses. The resistance of niobium decreases by almost two orders of magnitude when cooled down from 4 K to 1.8 K.

² RRR - the Residual Resistivity Ratio is defined as the ratio of electrical resistivity at 295K to electrical resistivity at 4.2K

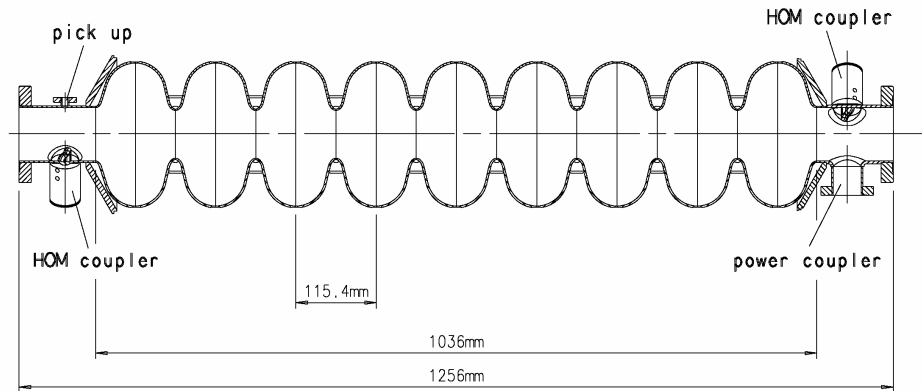


Figure 2.1 Nine-cell cavity used at FLASH. [Brinkmann 2001]

The power losses in the resonator walls are negligible and almost all the power can be transferred to the particle beam. As a consequence the energy consumption is vastly decreased. The energy is mainly spending on the cryogenic system. However, the overall energy consumed to accelerate low current beam remains lower than for normal conducting NC systems. It is hard to judge which technology is better because it depends on the purpose for what the accelerator is used. Moreover, both NC and SC technologies are still developing and the breakthroughs open new possibilities of application.

Additional advantage of SC technology is extremely high quality of so created particle beam. Thanks to vanishing electrical resistance, fewer interference fields arise and thus the resonator can be made bigger than for NC's one. As a consequence, it is possible to produce a particle beam with higher energy and smaller cross-section. This allows obtaining higher collision rate at the detector, and the energy of the collision is also higher.

The cavity is powered by 1.3 GHz radio frequency wave, supplied from klystrons via waveguides and couplers. The cavity shape is adjusted in such a way, that the given RF field creates a standing wave inside it. The quality factor of presented system is over 10^{10} without any load (Q_0) and more than $3 \cdot 10^6$ when equipped with couplers and pick-up antenna (Q_L). Due to the high quality factor the half-bandwidth is reasonably small and it is in order of few hundreds of Hertz. In case of FLASH it is only 230 Hz and slightly varies from cavity to cavity. Nevertheless, it is very important to precisely adjust the shape of the cavity because any geometry disturbance changes the frequency of cavity resonance. The system detunes and as a result the quality factor of resonator is reduced.

Tesla Test Facility I (TTF I), which was successfully commissioned in 1997, proved the principle of operation of TESLA technology. The laser radiation was generated for the first time using the free-electron laser on February 2000. During next two years the test facility was used for experiments in physics. Since late 2002 an upgrade to 260-meter-long test facility was began.

Nowadays, the machine, after major upgrade and tuning of used devices (i.e. klystrons, LLRF control system,), evaluated to Vacuum Ultra Violet Free Electron Laser (VUV-FEL). Beside the improvement and expansion of the system, the principles of operation remain untouched. Furthermore, it is already decided that for X-Ray Free Electron Laser (X-FEL) the same technology will be used. To continue, a new biggest linear accelerator called International Linear Collider (ILC) will base on the current development.

2.3. Vacuum Ultra Violet Free Electron Laser

The free-electron laser (FEL) that provides tuneable radiation from the vacuum-ultraviolet (VUV) to soft X-rays is built at Deutsche Elektronen-Synchrotron (DESY) laboratory in Hamburg, Germany. It is a 260 meter-long extension of TTF I additionally equipped with undulators, in which the accelerated electrons are induced to emit flashes of X-ray laser light [Brinkmann 2002]. The first system ended lasing operation in March 2002 with great success. The SASE (self amplified spontaneous emission) principle has been proven for wavelengths from 180 nm down to 80 nm.

However, after minor modification the VUV-FEL will be able to operate at energy of 1 GeV. Then it should serve the light of the wavelengths down to 6 nm in the first harmonic of the SASE FEL. However, the most recent achievement (mid of 2006) indicates that the VUV-FEL stably lasing at wavelength of 13 nm. The overview of the machine with localization of each section is presented in Figure 2.2.

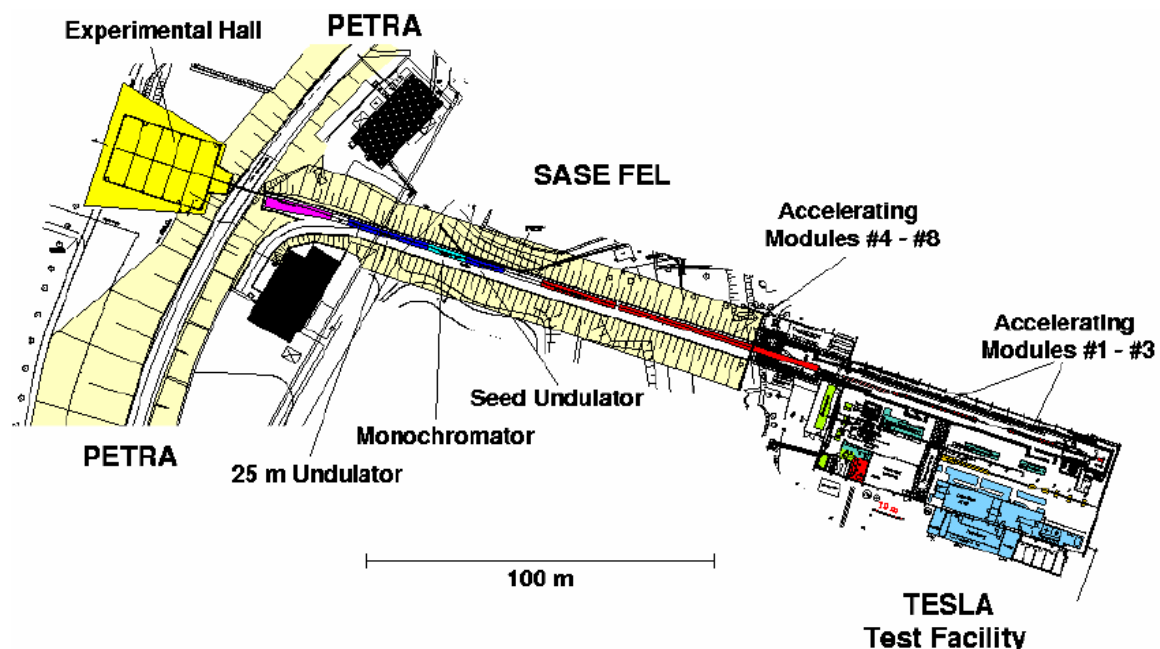


Figure 2.2 Overview of VUV-FEL localization. [DESY web]

Simultaneously, the VUV-FEL is an experimental facility for future generations of lasers and accelerators. After success of SASE operation, the construction of European X-Ray Free Electron Laser (X-FEL) was scheduled for years 2008-2012. It will consist of almost 2000-meter-long accelerator ended with several undulators. The beam energy is planned to be over 20 GeV. To reach higher energy either a longer accelerator needs to be built or cavities, which will allow obtaining higher gradients needs to be used (or at least combination of both parameters).

At the moment, at VUV-FEL there are five modules (called ACC1÷ACC5) equipped with eight cavities each. The average accelerating field gradient of single module varies from 15 to 20 MV/m. However, particular cavities (i.e. module ACC1, cavity 5) might reach higher gradients up to 25 MV/m. On the other hand, at horizontal test stand named CHECHIA, which can hold a single fully dressed cavity, nine-cell structure were stably operated at field gradient of 37 MV/m [Lilje 2004a]. Moreover, at the end of 2006 a new module (ACC6) equipped with 8 high gradient cavities will be inserted in line to VUV-FEL. Nevertheless, there is still a room for cavity development because the theoretical limit of superconductivity allows operation at 50 MV/m. [Liepe 2001b]

All cavities used for TESLA technology has similar nine-cell shape presented in Figure 2.3. However, the first and the last cell are slightly different that the one in the middle to ensure equal field amplitudes in all 9 cells. Moreover, there is a slight asymmetry between left (closer to the gun - endcup1) and right end cell (farther to the gun - endcup2), which prevents trapping of higher-order modes [Aune 2000]. The contour of single cell is presented in Figure 2.3 and the appropriate values of dimension are gathered in Table 2.1 [Brinkmann 2001].

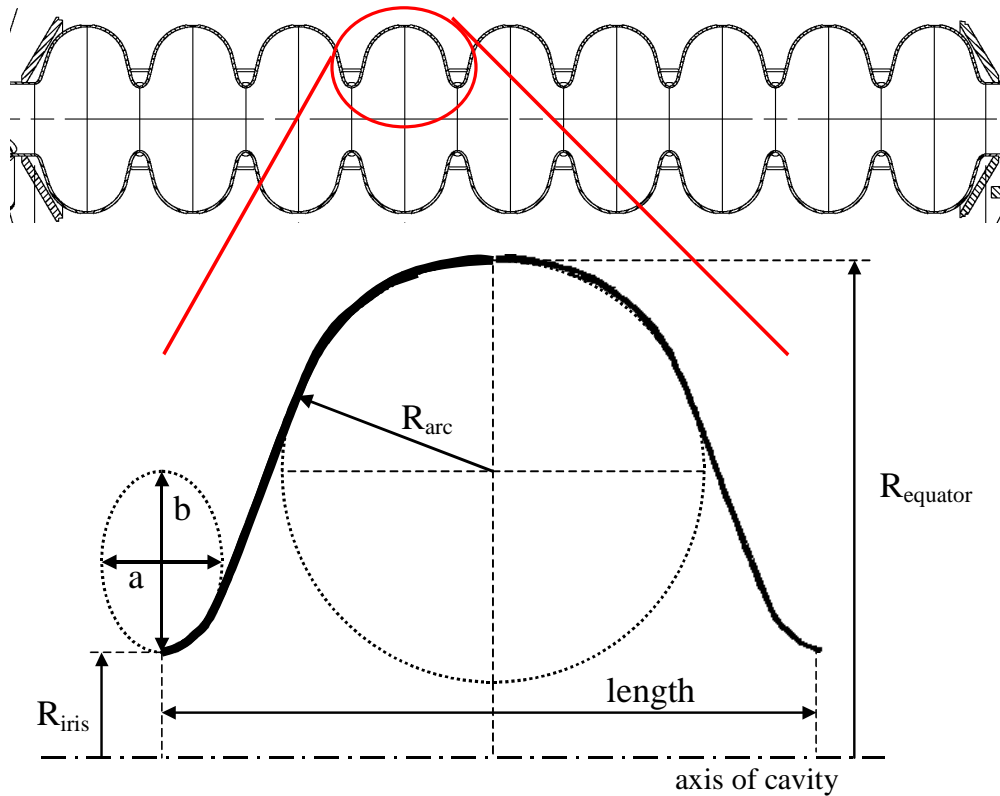


Figure 2.3 Dimension of single cell used in TESLA technology

Table 2.1 Dimension in mm of single cell used in TESLA technology

Parameters of cavity shape	Midcup	Endcup1	Endcup2
Length	57.7	56.0	57.0
Equator radius $R_{equator}$	103.3	103.3	103.3
Iris radius R_{iris}	35.0	39.0	39.0
Radius of circular arc R_{arc}	42.0	40.3	42.0
Horizontal axis a	24.0	20.0	18.0
Vertical axis b	38.0	27.0	25.6

The thickness of the cavity walls is only 2.8 mm. Therefore stiffening rings are assembled between the single cells to improve the cavity stiffness. The stiffness of the cavity with rings is slightly above 3 kN/mm, whereas the without them is twice smaller [Gassot 2001]. The stiffness of the cavity varies from one to another because of the production procedure (i.e. the wall thickness control).

The cavities used in VUV-FEL are operated in the pulsed mode. The single pulse of RF field lasts 1300 μ s. During the first 500 μ s the cavity is filled up and the accelerating gradient is increasing exponentially. During the next 800 μ s the field need to be kept constant. For the period of so-called ‘flat-top’ the beam is activated. During each RF pulse up to 800 electron bunches of few nano Coulombs with 1 μ s delay between each might be passed through the accelerator. After that the forward power decrease to zero and the gradient inside cavity decays. The curves of the input power, the beam current, the accelerating voltage and phase of the field inside the cavity during

the single pulse are presented in Figure 2.4. The cavity during the pulse needs to be reloaded with frequency of 1.3 GHz. The macroscopic effect of that is a dynamic Lorentz forces, which changes the shape of the cavity. As a consequence the cavity is detuned. The example of detuning is marked in Figure 2.4 as a dashed line. The above-described phenomenon is presented in detail in Chapter 3.

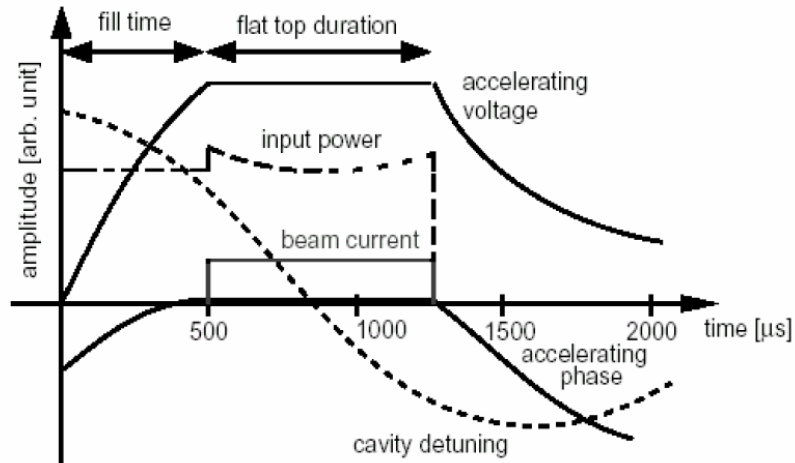


Figure 2.4 Structure of pulse used in VUV-FEL accelerator. [Schilcher 1998]

Nowadays, the RF pulses are repeated with frequency of 5 Hz. However, the maximum repetition rate will be increased in the future. The goal is to reach in current machine 10 Hz. On the other hand, for further accelerators based on the TESLA technology it is planned to operate with repetition rate of 50 Hz (or even 75 Hz).

The main parameters of VUV-FEL are gathered in Table 2.2. However, it is worth to mention that it is a test facility and therefore these values might change when any breakthrough is done. As an example the accelerating gradient of single cavity might be given. Few years ago, it was planned to install the cavities, which can hold up to 15 MV/m, but nowadays the ones, which may be operated at 35 MV/m, are mounted.

Table 2.2 Parameters of VUV-FEL

Parameter name	Value
Energy	1 GeV
Bunch to Bunch energy spread $\sigma E/E$	$< 2 \cdot 10^{-3}$
RF frequency	1.3 GHz
Accelerating gradient	15 (25, 30) MV/m
RF pulse length	1300 μ s (flat-top 800 μ s)
Repetition Rate	10 Hz
Particles per Bunch	$5.4 \cdot 10^{10}$
Bunch Separation	1 μ s
Number of bunches per pulse	800
Beam current	8 mA
Cavity fill time	510 μ s
Cavity Q_L	$3 \cdot 10^6$
Cavity Q_0	$3 \cdot 10^9$

Cells per cavity	9
Active cavity length	1.036 m
Number of cavities	64 (8 modules)
Number of cavities per klystron	32
RF power per cavity @ 25 MV/m	200 kW

As it was mentioned before, the cavity must be operated at resonance. That is the reason to use a tuner. It must perform two different types of operations. On one hand, it must be able to tune cavity, just after cooling down and pumping, in wide range. On the other hand, it must be able to act very fast during pulse duration, especially during the ‘flat-top’. It is very hard to design electromechanical system, which will be able to fulfil both requirements using only one active device. Therefore, in the presented solution, a stepping motor and piezostack are assembled together. The mechanical design was done by CEA-Saclay in France and is called Cold Tuning System (CTS).

The slow tuner, based on stepping motor and Harmonic Drive gearbox, is used for pre-tuning stage. The engine is made by PHYTRON. Due to some special modifications it might work at LHe temperature (i.e. dedicated ball bearings). It allows moving the cavity by ± 5 mm, which corresponds to frequency shift of ± 2.6 MHz. The theoretical resolution of stepper motor is 1.5 nm for one step. However, due a mechanical backlash of system, effect of motion is visible only when stepping motor is moving by thousand of steps. Moreover, the device is too slow for fast tuning, which is necessary for microphonics and Lorentz force deformation. As a consequence, a fast tuner based on smart materials is combined.

The previous described part of tuner was designed for low gradient cavities used before. During these time the most important thing was to be close enough to the resonance frequency (bandwidth of these cavities was wider). However, with field gradient improvement and cavity bandwidth narrowing, other effect like Lorentz force and microphonics become more and more important. Currently, not only cavity initial frequency needs to be controlled, but also its shift during RF pulse needs to be guarded and then minimized. Thus, the old tuner was slightly modified. Instead of one of the support, a fixture for a piezostack was assembled. Depending of its type it may hold one or two piezoelements (see Figure 2.5). Elongation of piezoelements is too small to use them for pre-tuning stage, however they are enough fast for Lorentz force and microphonics compensation. The solution was proposed and initially tested by M. Liepe [Liepe 2001]. The author continues the development and proposes automation of control system.

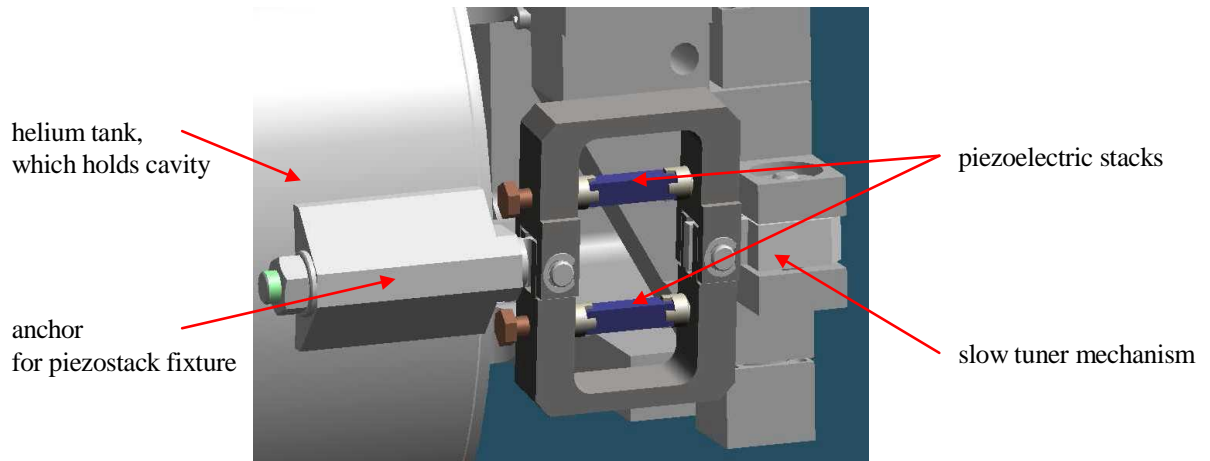


Figure 2.5 Fixture for two piezoelements attached instead of old tuner support.

The whole tuner attached to the end of the cavity as it is presented in Figure 2.6. On the right photo a bellow is visible, which connects two nearest cavities. It allows adjusting shape of single cavity without significant interference to the other ones.

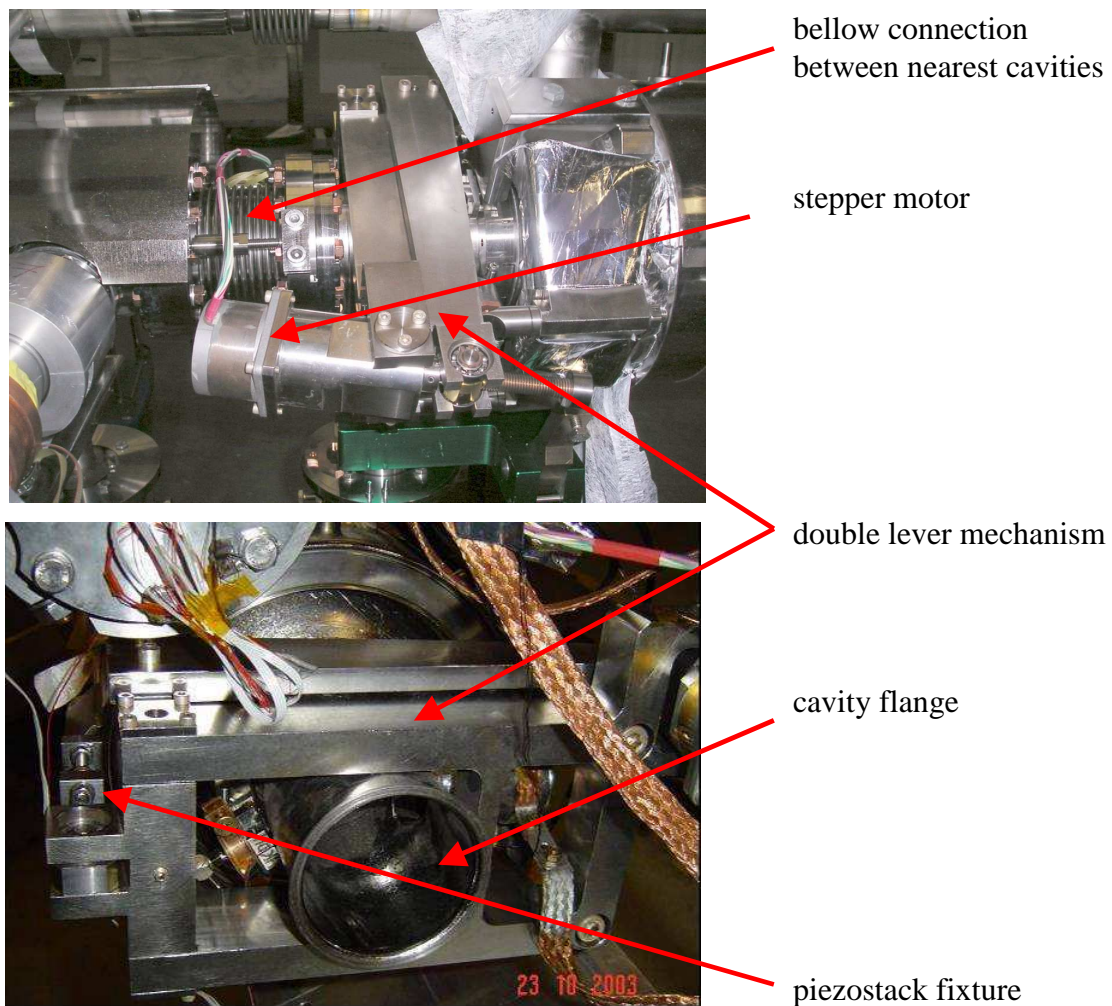


Figure 2.6 Photographs of cavity tuner.

The above-presented solution is not the only one, which was proposed for TESLA type cavities. Several other designs are developed at KEK, INFN, CEA and Thomas Jefferson Laboratory. The summary of current designs is presented in next subchapter.

2.4. Current tuners development

Since the decision that International Linear Collider (ILC) will be based on superconducting TESLA-like cavities several different tuner design has been proposed [Liepe 2005]. Beside the presented-above two other solutions are developed in European Union in framework of Coordinated Accelerator Research in Europe (CARE) program. The first of them is the Piezo Tuning System (PTS) proposed by CEA-Saclay (see Figure 2.7) and the second is a coaxial blade tuner projected by INFN-Milan (shown in Figure 2.8). Also o KEK, Japan proposed two tuner prototypes – the Slide Jack Tuner and the coaxial ball screw one (both presented in Figure 2.9). The last but not least, is a tuner from TJLAF module upgrade called renascence tuner (Figure 2.10). The main parameters of all tuners are presented in Table 2.3.

Table 2.3 Different tuners for TESLA type cavities [Liepe 2005]

	Europe developed in framework of CARE project			Japan		USA
	CEA-Saclay CTS	CEA-Saclay PTS	INFN Blade tuner	KEK Slide Jack Tuner	KEK coaxial ball screw	TJLAF Renescence tuner
Coarse Range [kHz]	±220	±250	±250	±550	±2760	±250
Coarse Res. [Hz]	<1	<1	<1		<1	<1
Fast actuator	Piezo or magnetostr.	Piezo	Piezo	Piezo	Piezo	Piezo or magnetostr.
Fast range [Hz]	500	1000	1200	1200	2500	1000/ 30000
Tuning direction	Tensile and compression	Tensile and compression	Tensile and compression			
Position of fast actuator	4 K, vacuum	4 K, vacuum	4 K, vacuum	5 K, vacuum	80 K, vacuum	5 K, vacuum
Position of motor	4 K, vacuum	4 K, vacuum	4 K, vacuum	Warm	80 K, vacuum	5 K, vacuum
Position of tuner	At the end of the cavity	At the end of the cavity	In the middle of the cavity	In the middle of the cavity	In the middle of the cavity	In the middle of the cavity

All of the presented tuners might work either directly with TESLA type cavities or need some minor modification (i.e. the anchor interface). Every single one has two mechanisms – for slow and fast tuning. In general for fast tuning a piezostack are used. However, for some of them it is possible to exchange the piezoelements with magnetostrictive rods (see Chapter 4 for details). The range of fast tuning is quite similar and stays over 1 kHz, except the one, which is used nowadays (CTS) and the second one, which is designed for TJLAF (it might have much higher fast tuning range up to 30 kHz, but test of prototype is needed).

According to the experience, the fast tuning of 1000 Hz allows to compensate Lorentz force caused by RF field of gradient below 25 MV/m. In case of old CEA design, where fast tuning range is even smaller, the operation is limited to gradient of 15 MV/m. However, the method presented in Chapter 6 allows to counteract to the dynamic Lorentz force generated by accelerating field of gradient of 20 MV/m.

Regarding position of the tuner it is possible to split them into two groups. In one of them (CEA-Saclay's designs) the tuner is mounted at the end of the cavity and therefore there is need to keep more space between nearest cavities. In the other group the tuner is mounted around cavity and as a consequence there is no need to leave additional gap. In case of INFN solution, it allows to reduce the total length of the whole accelerator by 5%. It is required to perform a financial calculation to find, what is more reasonable - use more complex and expensive tuner or to provide extra cost needed for longer machine.

Concerning the position of active elements of tuners, there are three main classes. In the first solution, both stepper motor and piezoelement are assembled in cryogenic temperature of 2÷5 K (European and US designs). Two other ideas are developed in KEK. In one of them the motor is mounted outside the cryostat and therefore the maintenance is possible, but the piezoelectric actuators are located close to the cavity (operating temperature of 5 K). In second solution (Slide Jack Tuner), both piezostacks and stepper motors are placed at intermediate temperature inside of the vacuum vessel.

The localization of active elements of fast and slow tuner is extremely important due to the maintenance and replacement in case of failure. Only the solution proposed by KEK allows exchanging the stepper motor without warming up the cryomodule. However, as it is expected the price of such solution is the highest.

Nevertheless, any of the presented solutions allows exchanging the piezoelement. As a consequence the lifetime of the actuator is one of the major issues. If the piezoelectric element is breakdown, the cavity will not be able to operate at high gradient (over 30 MV/m). On the other hand the lifetime of the actuator is strongly depends on the preload force [Zickgraf 1995]. As a consequence, one of the important issues is measurement and control of static force applied to the element. The innovative methods developed by author are presented in Chapter 5.

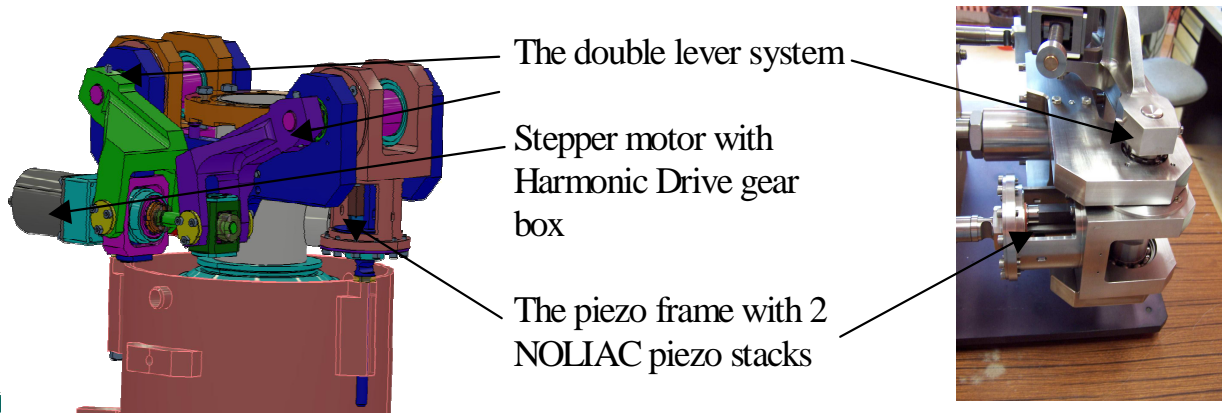


Figure 2.7 Drawing and photo of new design of CEA-Saclay - PTS tuner. [Bosland 2005]

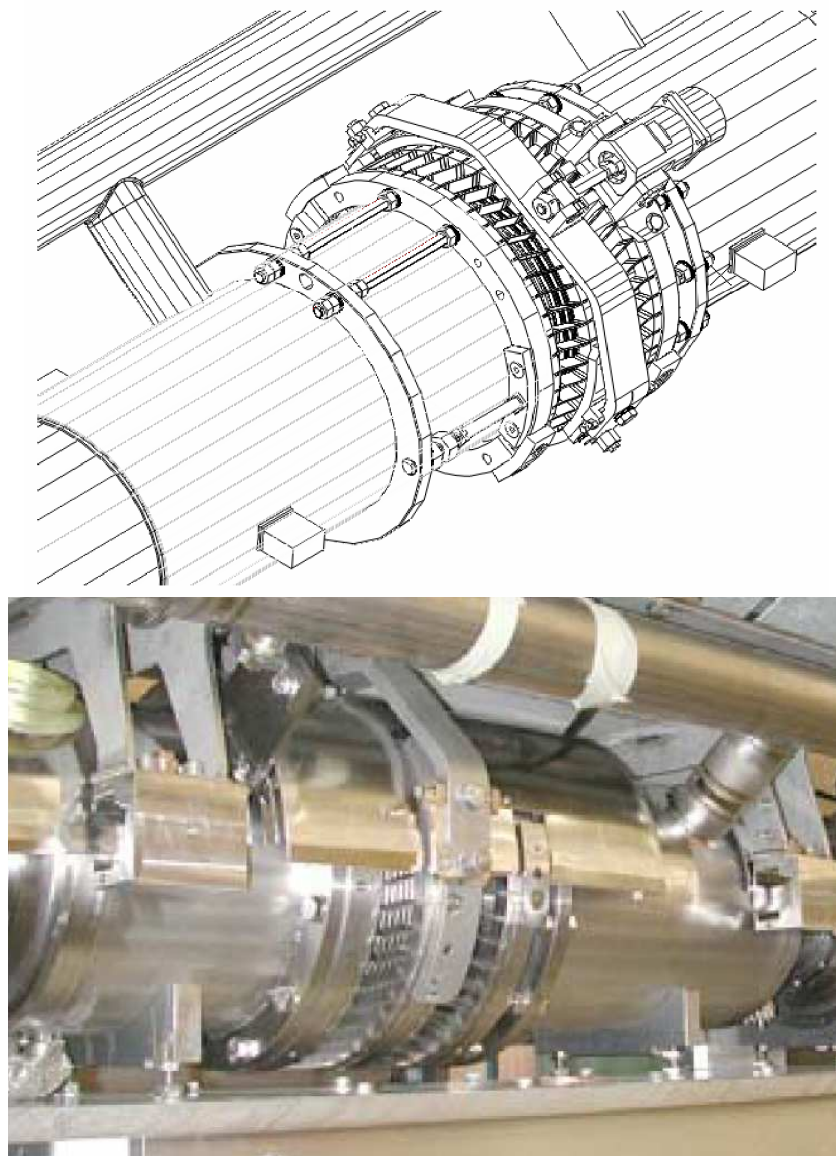


Figure 2.8 Drawing and photo of INFN blade coaxial tuner [Pagani 2005]

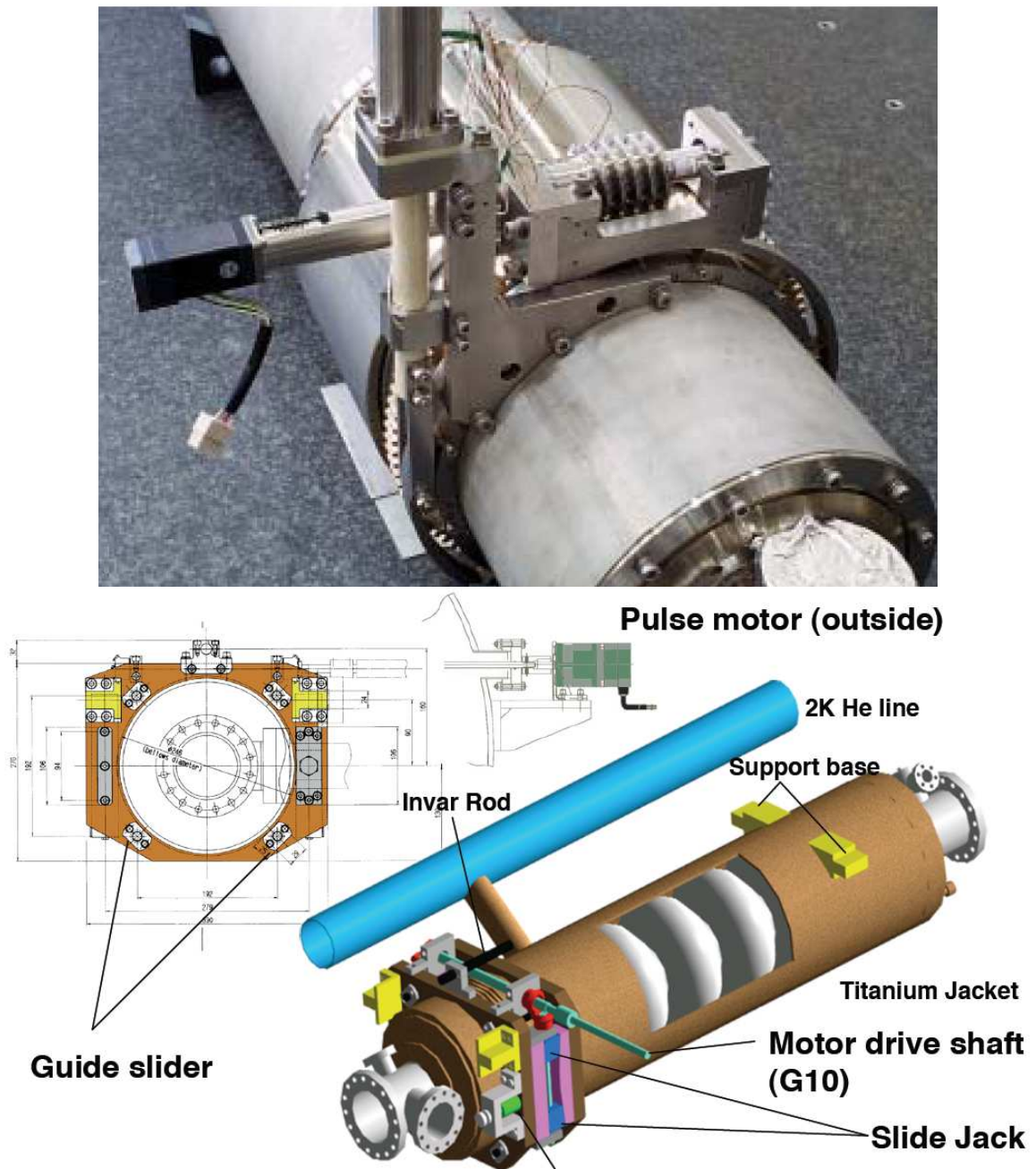


Figure 2.9 KEK tuners - coaxial ball screw tuner (left) and slide jack tuner (right).[Liepe 2005]

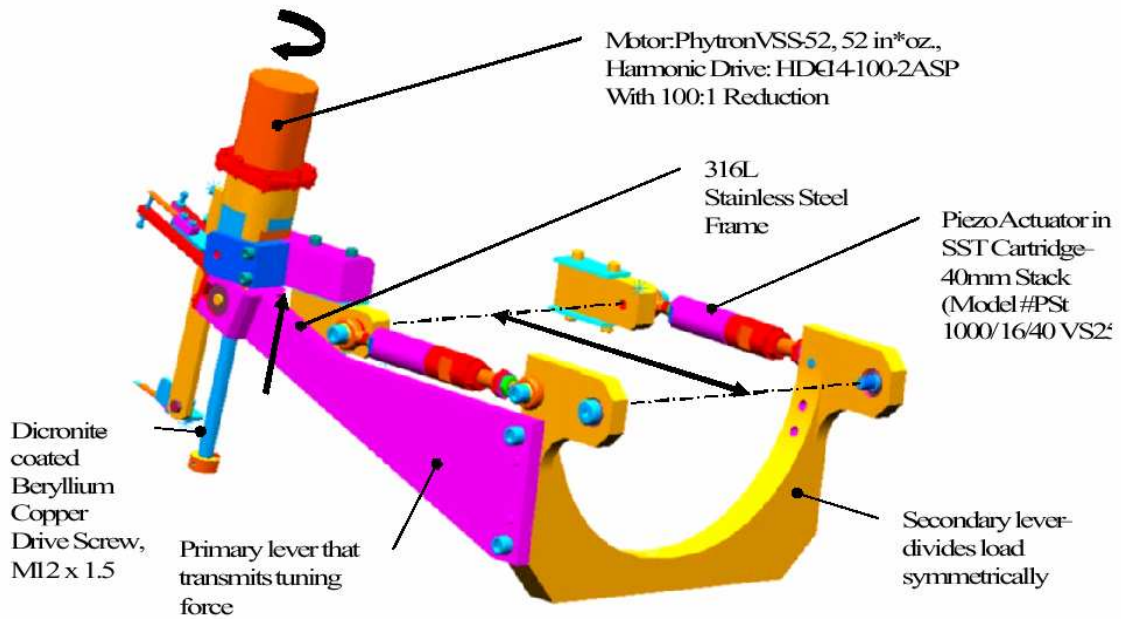


Figure 2.10 TJNAF tuner [Liepe 2005]

At the end of this chapter, there is need to stress once again, that the theoretical limit of accelerating field gradient, which might be obtained in TESLA-like cavity, is slightly below 50 MV/m. Currently, the VUV-FEL operates with much smaller gradients, which is set up to 20 MV/m, due to the technological processes connected with cavity preparations and due to the RF losses described below. However, next module called ACC6, which will be inserted to VUV-FEL in 2007 will consist of eight high gradient cavities and will be probably operated with average gradient of 35 MV/m.

Since the VUV-FEL is operated by the end user, there was the decision made by DESY government to rename the accelerator to FLASH. This abbreviation stands for Free Electron Laser in Hamburg. As a result of this decision, in further part of the dissertation, the new name will be used even if the experiments refer to the previous name of the machine.

Chapter 3. Detuning sources

In this chapter a detailed description of the detuning sources are given. As it was mentioned previously, it is possible to split the cavity deformation sources into two main groups. One of them is a Lorentz force, which is predictable and depends on the cavity parameters and accelerating field gradient. The second one is microphonics – mechanical vibrations of surrounding environment, which is fully stochastic. Both types of perturbation are presented in subsections 3.1 and 3.2 respectively.

Both phenomena were investigated previously in several papers and thesis. The most important works in the field are the thesis of H. Gassot [Gassot 2001], M. Liepe [Liepe 2001b] and M. Doleans [Doleans 2003a]. The first of them concentrate on the mechanical aspects of the Lorentz force and as a result of the research the stiffening rings were introduced. These special rings are mounted between the cells to improve the stiffness and reduce the detuning caused by Lorentz force by factor of 2. The second thesis focuses on the manual method of compensation of Lorentz force. The author proposes to use a piezostack for the purpose. He also proved the principle of the method. The third one is focused on the system dedicated for the medium-beta cavities used for Spallation Neutron Source SNS project. However, the analytical investigation can be applied to the TESLA type cavities.

3.1. Lorentz force phenomenon description

The accelerating field gradients inside the single cell are equal to teens of MV/m. In case of TESLA type cavity the RF reloaded frequency is set to 1.3GHz. As a consequence, a huge charge flow through the thin surface layer of the cavity walls is caused. The movement of charges in electromagnetic field is affected by the Lorentz force. The pressure, which is caused by these forces, acts on the cavity wall. The radiation pressure P_s is calculated from equation:

$$P_s = \frac{1}{4} \left(\mu_0 |\vec{H}|^2 - \epsilon_0 |\vec{E}|^2 \right) \quad (3.1)$$

where \vec{H} and \vec{E} are correspondently the magnetic and electric vectors of field

The distribution of Lorentz forces is presented in Figure 3.1. As it is shown the forces act inward near the cell equator and outward near the cell bore. Due to the coaxial symmetry a 2 dimensional model might be regarded. Only a single cell is investigated analytically due to the complexity of calculation. The full nine-cell cavity was examined using Finite Element Method in PhD thesis of H. Gassot [Gassot 2001].

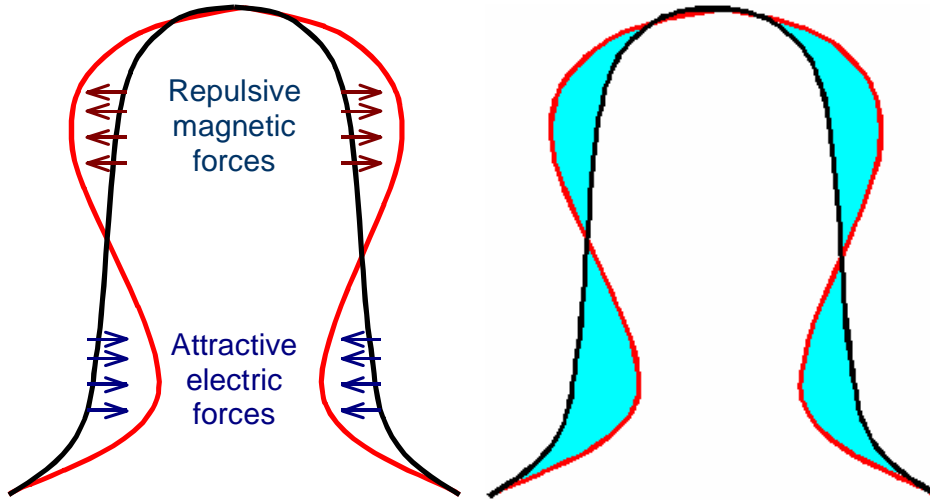


Figure 3.1 Single cell deformation due to the internal electromagnetic forces (left side) and the volume change caused by Lorentz force ΔV (right side).

As a result of the radiation pressure the cavity deforms, leading to a change in its shape. The resonance frequency depends on the geometrical dimensions of the cavity; therefore finally the Lorentz forces cause the resonance frequency modification. According to the Slater theory the change of frequency caused by small change of the volume is given by formula [Slater 1950]:

$$\Delta f = \frac{f_0}{4E_{stored}} \int_{\Delta V} (\epsilon_0 E^2 - \mu_0 H^2) dV \quad (3.2)$$

where

$$E_{stored} = \frac{1}{4} \int_V (\epsilon_0 E^2 - \mu_0 H^2) dV \text{ is a stored energy in no deformed cavity}$$

V is a volume of no deformed cavity

ΔV is a change of the cavity volume caused by Lorentz force (see Figure 3.1)

f_0 is a resonance frequency of unperturbed cavity

The distribution of the electromagnetic field in the cavity shows that close to the cell iris the electric field dominates, but near the equator the magnetic part is larger. The calculation done for a field gradient equal to 25 MV/m shows that the frequency shift is around 900 Hz. The computation was performed using two assumptions. First of them is that the cavity is not stiffened. The second necessary statement is the value of wall thickness of the cavity, which was set to 2.8 mm. The frequency shift of less than 1 kHz seems to be very small comparing with the resonance frequency of the cavity, which is 1.3 GHz. However, the loaded quality factor Q_L of cavity (equipped with the main coupler and antennas) is equal to $3 \cdot 10^6$. Therefore the full bandwidth of the cavity is only 430 Hz. As a consequence, the reinforcement of the cavity is needed. To make the cavity stiffer it is possibly to increase the thickness of the wall. However, this is a very expensive solution because

of cost of pure niobium used for cavities. It is stimulation for searching a new type of the cavities i.e. the one made of copper and coated inside by thin layer of niobium [Bousson 2000].

Another disadvantage of this solution is a problem with the pre-detuning. There is need to adjust the frequency of the cavity, after cooling down and helium pumping, to the frequency of master oscillator. For TESLA type cavities the stiffness rings are used which are welded in between the adjacent cells. However, the welded ring reduces the deformation of the cavity close to the iris, but the cavity elasticity remains unchanged close to the equator of each cell. This simple solution reduces the frequency shift caused by RF field of gradient of 25 MV/m to only 500 Hz [Gassot 2001].

Measurement of the static detuning was done at CHECHIA stand test at DESY [Schilcher 1998]. The cavity D39 was driven by continues RF wave. According to experiment the static detuning is proportional to square of the magnitude of accelerating field gradient:

$$\Delta f \sim -K_L E_{acc}^2 \quad (3.3)$$

where K_L is a Lorentz force detuning constant equal to $0.9 \text{ Hz}/(\text{MV}/\text{m})^2$

E_{acc} is a magnitude of accelerating field

The value of Lorentz force detuning constant K_L was measured on the cavity (see Figure 3.2). This constant varies slightly from cavity to cavity. Nowadays, it is assumed to be around $1 \text{ Hz}/(\text{MV}/\text{m})^2$.

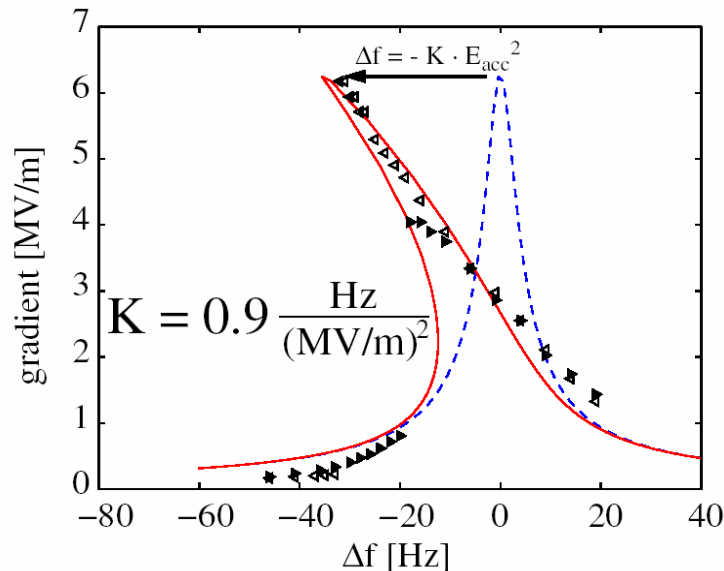


Figure 3.2 Static Lorentz force detuning and Lorentz force coefficient. [Schilcher 1998]

In case of normal operation of FLASH, the cavities are operated in pulsed mode with repetition of RF pulse between 1 to 10Hz. As a result, a dynamic Lorentz forces detuning need to be taken under consideration. Proper measurements for different acceleration gradients were performed several

times. The example of detuning caused by the dynamic Lorentz force is presented in Figure 3.3. It is visible that for gradients above the 20 MV/m the frequency change is higher than cavity half-bandwidth (~ 230 Hz).

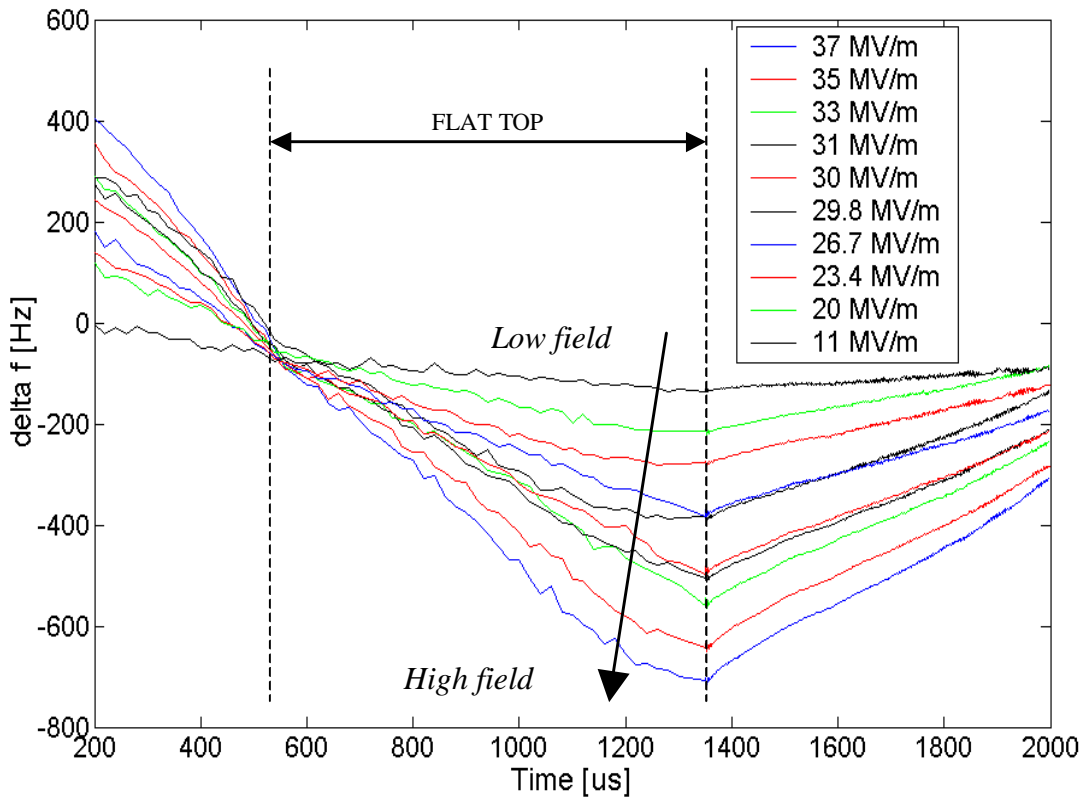


Figure 3.3 Detuning caused by Lorentz force for different accelerating field gradients

3.2. Microphonics

The cavity is also deformed by the mechanical vibrations caused by external sources, which are commonly called microphonics. There are plenty sources of them, for instance both the liquid hydrogen and water cooling systems – especially pumps generates noise. Even a nonlinear flow of LHe itself might disturb the geometry of the cavity. Another source is a human activity: walking people, car traffic above the tunnel, civil works, etc. At last but not least, the seismic movement of ground need to be taken under consideration.

The change of cavity frequency caused by microphonics is very low in comparison to Lorentz force, and usually remains below 20 Hz. The measurement of microphonics influence was performed in CHECHIA cryostat. The cavity was operated in continuous-wave (cw) mode. Both, the detuning caused by microphonics in function of time and the distribution of resonance frequency are presented in Figure 3.4 [Liepe 2001b].

It is also possible to measure the vibrations caused by Lorentz force and microphonics using the piezoelectric element, which is inserted in fast tuner. The typical spectrum of the actuator response

for CHECHIA stand test is presented in Figure 3.6. The left figure shows the spectrum of signal response when cavity was operated in cw mode. The right figure shows the ordinary spectrum of piezostack output voltage excited by RF pulse. The accelerating field gradient was set 30 MV/m. The RF pulse length was 800 μ s.

The mechanical resonance around 287 Hz is clearly visible in both figures. It will be used later in automatic Lorentz force compensation system (Chapter 6). Nevertheless, there are also others frequencies, which correspond to microphonics (i.e. He system, pumps). It is also visible that above 500 Hz there are no other resonances. As a consequence, the cavity damp higher frequencies and the mechanical resonance cannot be excited.

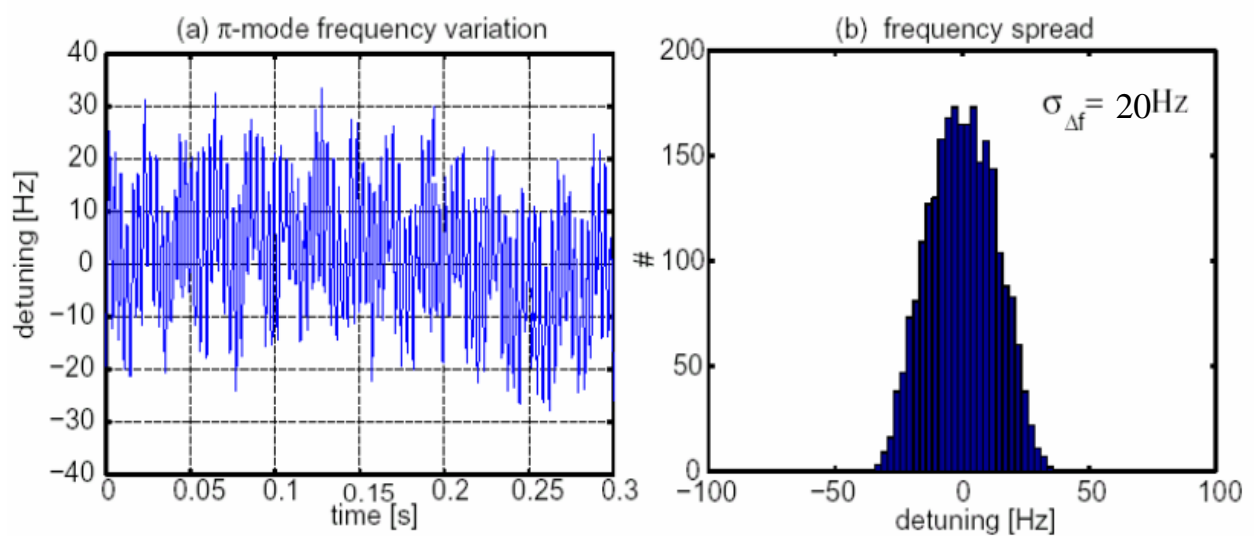


Figure 3.4 Noise measured in cavity and distribution of frequency caused by microphonics. The cavity was operated in cw mode in CHECHIA cryostat [Liepe 2001b].

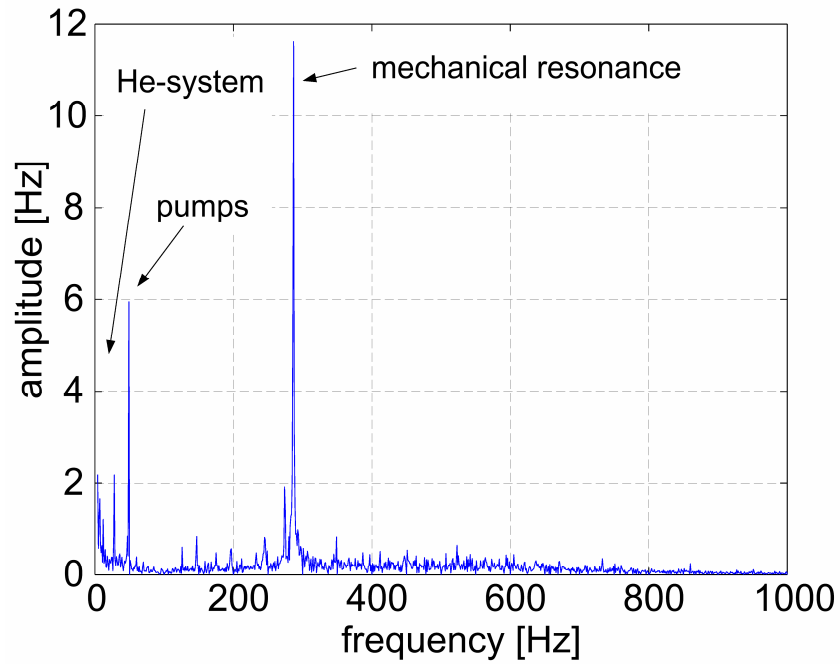


Figure 3.5 Spectrum of piezostack output voltage. Data from CHECHIA stand test. Figure shows the response in cw mode [Liepe 2001]

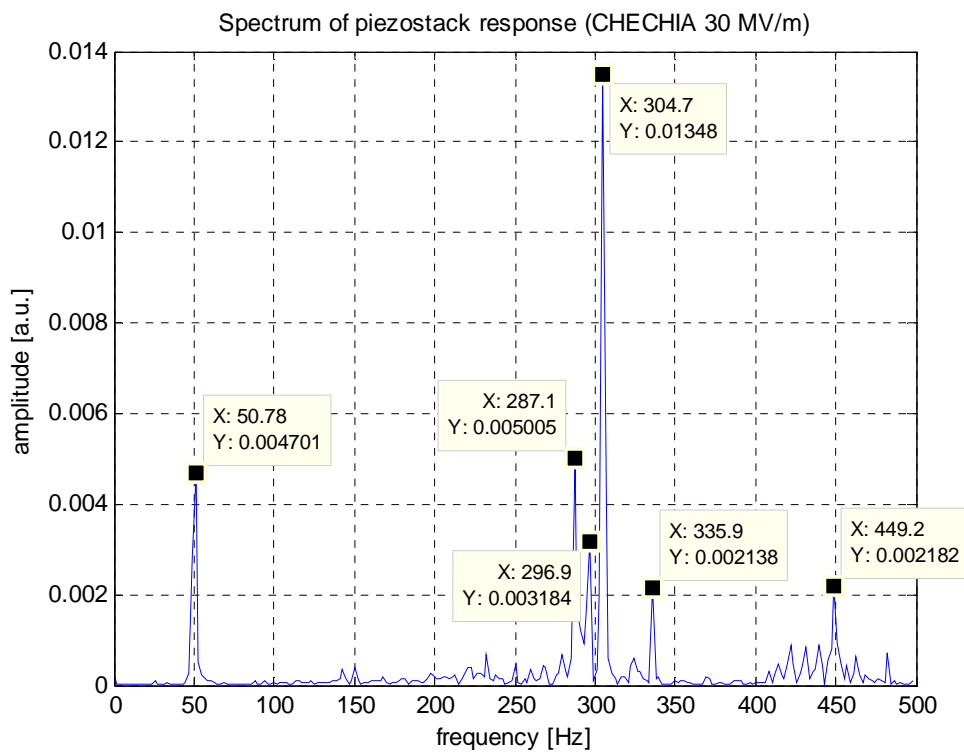


Figure 3.6 Spectrum of piezostack output voltage. Data from CHECHIA stand test. Figure shows the response to RF field, accelerating field gradient 30 MV/m.

The microphonics might be compensated only by feedback system. The PID controllers cannot be used because according to performed study, system is observable but not controllable. At this moment study of single cell cavity is performed at INFN Milan [Paparella 2005]. Further work will be soon published by the team, which is led by A. Bosotti.

3.3. Mechanical model of cavity

The mechanical model of the cavity was investigated in details by Hui Min Gassot in her thesis [Gassot 2001]. Due to the complexity of mechanical behaviour of the nine-cell cavity the finite element method implemented in CAST3M software was used. Furthermore, the comparison of the model simulations and measurements was done. The results are presented in Figure 3.8 and Figure 3.8. It is visible a good correlation between the calculation and reality. It is important to remark that due to the symmetry of the cavity only a two dimensional model of half-cavity might be considered.

However, also a full nine-cell model was investigated to find mechanical modes of the cavity. The results of the simulation are very close to the one obtained from measurement and presented in Figure 3.6.

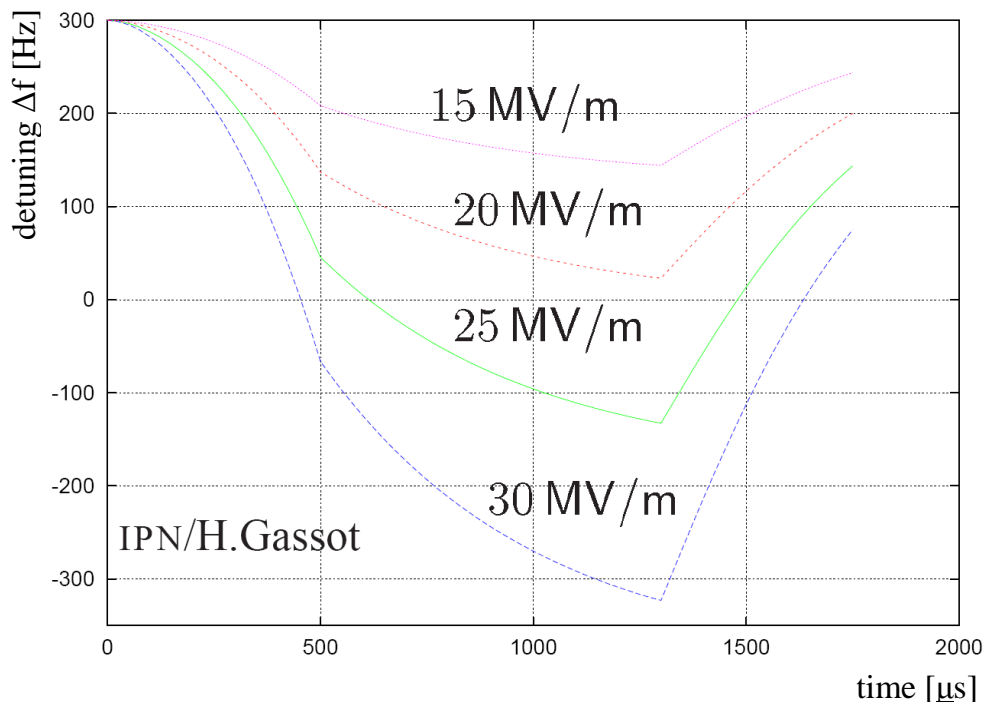


Figure 3.7 The cavity detuning obtained from FEM simulation done using CAST3M [Gassot 2001].

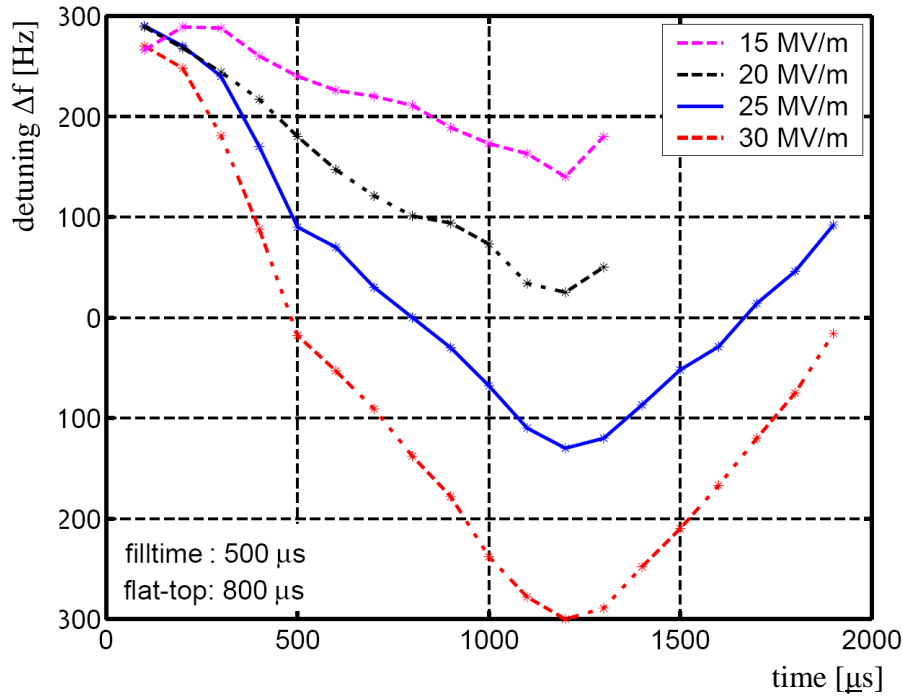


Figure 3.8 The cavity detuning obtained from measurement done at DESY.

3.3.2. Direct and inverse transfer functions between piezostack and RF field

For optimal controller of piezoelement it would be very helpful to measure the transfer functions between the RF field and the piezostack and the inverse one. Since, it is easy to measure the piezoelement response to particular field (i.e. Figure 3.9), it is hard to measure the opposite effect.

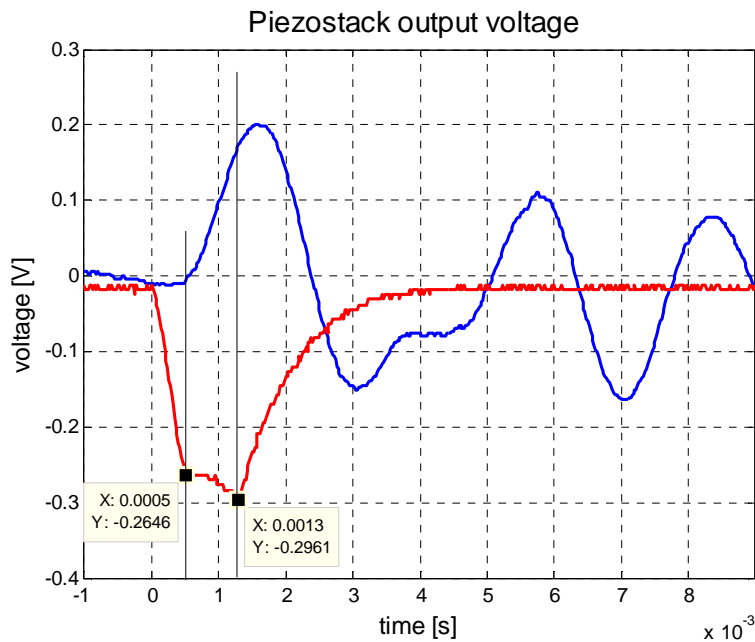


Figure 3.9 Output voltage of piezostack inserted in CHECHIA stand test. (red line represents the RF field, blue line is a piezostack response).

The transfer function between the piezostack and the RF field might be measured when cavity is operated in continuous wave (cw) mode. Preliminary attempts were performed by L. Lilje in the “Cryo Workshop” (workbench in the warm) in 2002 (see Figure 3.10). The attempts to measure this transfer function in the cold in CHECHIA cryostat fails due to insufficient coupling caused by incorrect antenna configuration for the high-power test.

The research group, which works for SNS, was able to operate their cavities (similar to the TESLA one) in cw mode at the cold. The results of the study are presented in several papers [Dalayen 2001 and Doleans 2003a/b]. Especially interesting is the identification of cavity response, analytical approximation and usage for feedback loop closing.

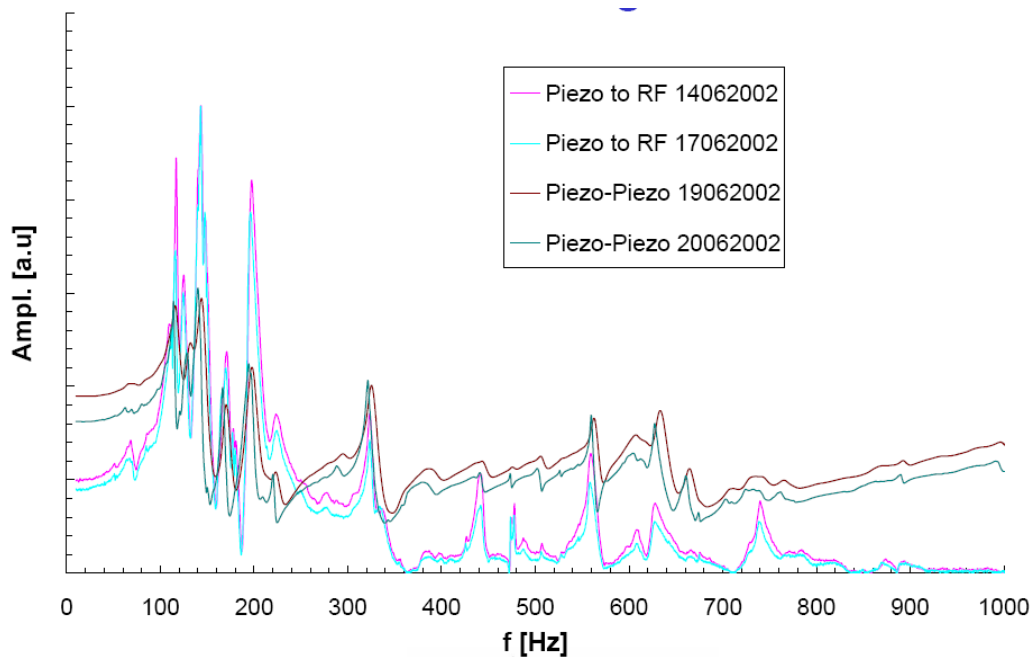


Figure 3.10 The measurement of transfer function between two piezoelements and piezoelement and the RF field. [from L. Lilje]

Another attempt to measure the response of the cavity to the pulse applied to piezostack was performed with cavity 5, ACC1 by the author. The half-sine wave pulse was used as a signal pulse. Using the single-pulse detuning measurement algorithm (refer to chapter 3.5.2) the frequency change during the flat-top (800 μ s) was measured. Next, the pulse was delayed versus the RF pulse and another measurement was performed. As a result the “measurement window” was swept over the whole time between the nearest pulses (500 ms). The measured detuning was glued with respect to the time. As a consequence, a response to signal applied to piezostack and RF field was measured.

Then the same measurement was performed, but the signal applied to the piezostack was zero. Assuming linearity of the system, there is possibility to subtract both responses. As a result, the

frequency change caused by only piezostack was acquired. The spectrum of this response is presented in Figure 3.11. There are several main resonances, which corresponds to the one obtained in the warm experiment.

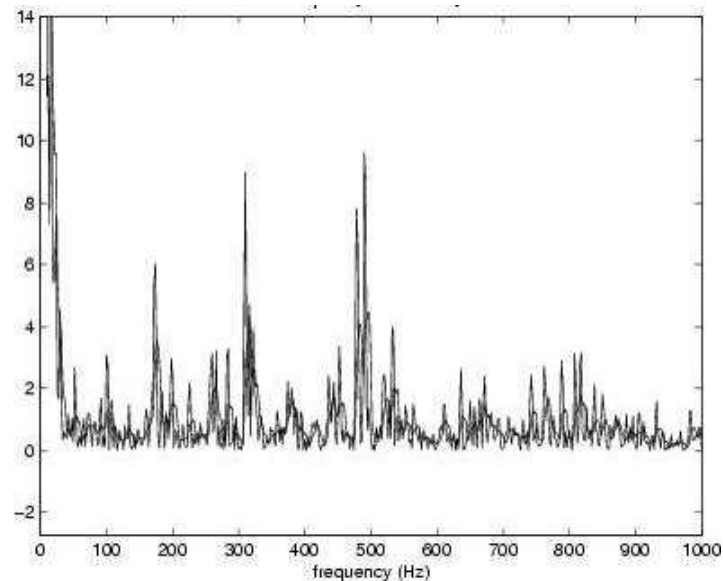


Figure 3.11 Spectrum of pulse response. A half-sine wave signal of frequency of 800Hz was used as an input pulse.

3.4. Cavity model description

The cavity with the klystron and coupler might be modelled as it presented in Figure 3.12 [Schilcher 1998]. This model was initially designed for vector sum controller. The klystron is represented as a current source I_{gen} , which is coupled to transmission line of impedance equal to Z_0 (usually it is a waveguide, but in particular solution it could be also a coaxial cable). The circulator, which is inserted between the coupler and the klystron, protects the last mentioned one from reflecting waves. All waves that travel back from the cavity are deviated to the load, which is matched with the transmission line impedance Z_0 . The coupler is modelled as an ideal transformer of ratio of 1:N. At the second side of the coupler, the cavity of impedance Z_{cav} is represented as an RLC circuit. At least the beam is showed as a current source I_{beam} .

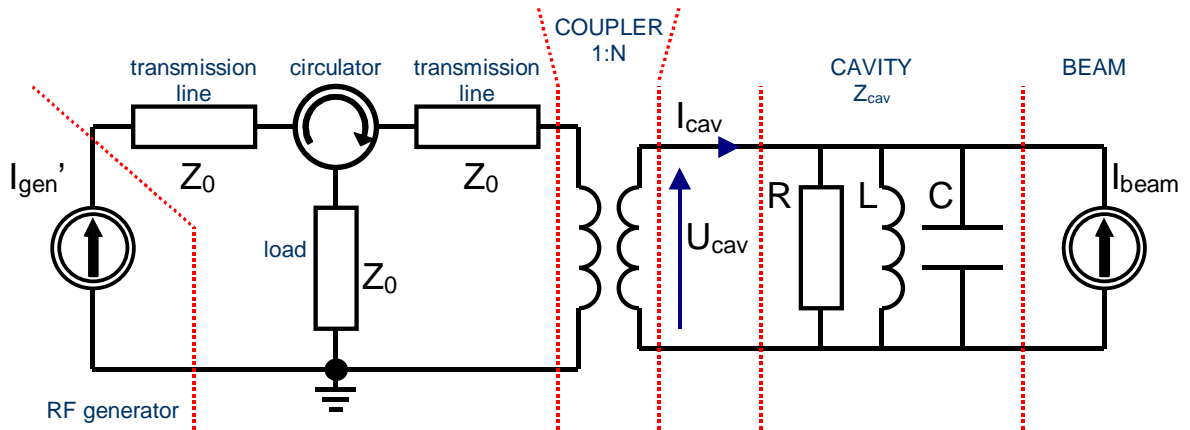
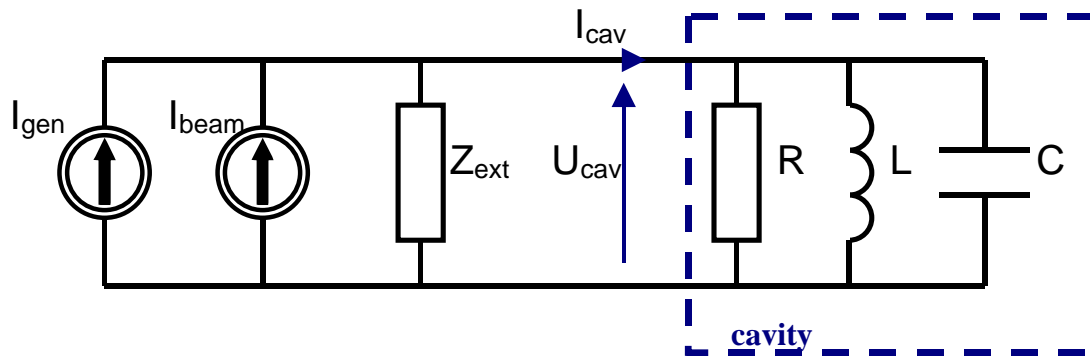


Figure 3.12 The model of cavity connected to a RF generator by coupler and transmission lines
[Schilcher 1998]

For further investigations, it is more useful to operate with the model, which is seen from cavity side (see Figure 3.13). As previously, the resonant cavity is considered as a special case of resonant RLC circuit where the inductance L and the capacitance C represent a lumped element or its distributed equivalent, and the resistance R symbolizes the losses in the circuit connected with capacitance and inductance imperfection as well as with the wall losses of the cavity resonator. The Z_{ext} represents external losses (in example coaxial cable, in general $Z_{ext} = N^2 \cdot Z_0$). As previously the current sources represent the RF field source (I_{gen}) and the beam (I_{beam}). Due to the circulator and the coupler the current, which represents RF source is equal to $I_{gen}' = 2I_{gen}/N$.



$$X_L = j\omega L$$

$$X_C = \frac{1}{j\omega C}$$

$$X_R = R$$

Figure 3.13 The simplified model of cavity circuit.

Since the cavity is a resonance device it is useful to introduce the parameter, which describes its efficiency – a quality factor Q . From the general definition of Q factor, it is given as:

$$Q = 2\pi \frac{\text{Total stored energy at resonance frequency}}{\text{Energy dissipated at one period of resonance frequency}} = \frac{\omega_0 W_{\text{stored}}}{P_{\text{dissipated}}} \quad (3.4)$$

where: ω_0 is the resonant frequency.

In case of circuit showed in Figure 3.13 the quality factor of unloaded cavity Q_{unload} is rewritten to:

$$Q_{\text{unload}} = \omega_0 \frac{\frac{1}{2} CV_{\text{max}}^2 \big|_{\omega=\omega_0}}{\frac{1}{R} V_{\text{rms}}^2 \big|_{\omega=\omega_0}} = \omega_0 RC = \frac{R}{\omega_0 L} \quad (3.5)$$

where R, L and C are the resistance, the inductance and the capacitance of model presented in Figure 3.12

V_{max} is a maximal voltage applied to the cavity

The above equation is true if the circuit will be driven by sinusoidal wave as it is in case of FLASH (or any other one which fulfill the following relation $V_{\text{max}} = \sqrt{2}V_{\text{rms}}$).

In case of superconducting TESLA type cavities the quality factor of unloaded cavity is very high and stays in range of $5 \cdot 10^9$. It is necessary to calculate the external quality factor Q_{ext} to determine the quality factor of load cavity Q_{load} . The stored energy remains constant, whereas the dissipated energy might be treated as a sum of the one loosed in external devices and in cavity itself. Using the definition, the loaded cavity Q factor is described by formula:

$$\frac{1}{Q_{\text{load}}} = \frac{1}{Q_{\text{unload}}} + \frac{1}{Q_{\text{ext}}} \quad (3.6)$$

where Q_{unload} is quality factor of unloaded cavity,

Q_{ext} is a quality factor of external circuit.

In case of cavities used for FLASH purpose the Q_{load} factor is around $3 \cdot 10^6$. As a result, it might be found that the TESLA shape superconducting cavities are limited by the external devices (i.e. couplers) rather than by the cavities itself ($Q_{\text{unload}} \gg Q_{\text{load}} \rightarrow Q_{\text{load}} \approx Q_{\text{ext}}$).

The admittance of the modelled cavity is given by formula:

$$Y = \frac{1}{R} + j \left(\omega C - \frac{1}{\omega L} \right) \quad (3.7)$$

where R, L and C are the resistance, the inductance and the capacitance of model presented in Figure 3.12

The resonance appears when both reactive components X_L and X_C compensate each other. Then the resonance frequency ω_0 is found from equation:

$$\omega_0 = \frac{1}{\sqrt{LC}} \quad (3.8)$$

For TESLA shape cavity the resonance frequency f_0 is set to 1.3GHz. The steady-state description of the circuit showed in Figure 3.13 is given by equation:

$$\frac{d^2V(t)}{dt} + \left(\frac{1}{R} + \frac{1}{Z_{ext}} \right) \frac{1}{C} \frac{dV(t)}{dt} + \frac{1}{LC} V(t) = \frac{1}{C} \frac{dI(t)}{dt} \quad (3.9)$$

where $I = I_{beam} + I_{gen}$ is a sum of the beam current and the RF field current.

The above equation may be rewritten using the quality factor and resonance frequency to:

$$\frac{d^2V(t)}{dt} + \frac{\omega_0}{Q_{load}} \frac{dV(t)}{dt} + \omega_0^2 V(t) = \frac{\omega_0 R_L}{Q_{load}} \frac{dI(t)}{dt} \quad (3.10)$$

where R_L is a parallel connection of resistance R and Z_{ext}

However, the system is operated in pulse mode, therefore there is need to introduce a transient behaviour description instead of steady-state one. Several assumptions have to be made:

the beam and the RF generator current are turned on for a long time compared to characteristic filling time of the cavity,

the cavity is weakly damped system ($1/Q_{load} \ll 1$) therefore the resonance frequency ω_{res} equal to:

$$\omega_{res} = \omega_0 \sqrt{1 - \frac{1}{4Q_{load}^2}} \text{ is approximated to } \omega_0,$$

the second order time derivatives are neglected.

By applying the above assumption to equation (3.10), a state space equation might be written:

$$\underbrace{\frac{d}{dt} \begin{pmatrix} V_{Re} \\ V_{Im g} \end{pmatrix}}_{\dot{x}} = \underbrace{\begin{pmatrix} -\omega_{1/2} & -\Delta\omega \\ \Delta\omega & -\omega_{1/2} \end{pmatrix}}_{\mathbf{A}} \underbrace{\begin{pmatrix} V_{Re} \\ V_{Im g} \end{pmatrix}}_x + \underbrace{\begin{pmatrix} R_L \omega_{1/2} & 0 \\ 0 & R_L \omega_{1/2} \end{pmatrix}}_{\mathbf{B}} \underbrace{\begin{pmatrix} I_{Re} \\ I_{Im g} \end{pmatrix}}_u \quad (3.11)$$

where $\vec{V}(t) = (V_{Re}(t) + iV_{Im g}(t))e^{i\omega t}$ represents a complex field vector,
 $\vec{I}(t) = (I_{Re}(t) + iI_{Im g}(t))e^{i\omega t}$

$$\omega_{1/2} = \frac{\omega_0}{2Q_{load}} \text{ is the bandwidth of cavity resonator equal to 216 Hz,}$$

the measured value is around 230 Hz

$\Delta\omega = \omega_0 - \omega$ is a detuning of the cavity.

Using the matrix notation the differential equation becomes:

$$\dot{x}(t) = \mathbf{A}x(t) + \mathbf{B}u(t) \quad (3.12)$$

where \mathbf{A} and \mathbf{B} matrices are the one from equation

The general solution of equation (3.10) is given as:

$$x(t) = e^{\mathbf{A}t} x(0) + \int_0^t e^{\mathbf{A}(t-t')} \mathbf{B}u(t') dt' \quad (3.13)$$

where

$$e^{\mathbf{A}t} = e^{-\omega_1/2t} \begin{pmatrix} \cos(\Delta\omega t) & -\sin(\Delta\omega t) \\ \sin(\Delta\omega t) & \cos(\Delta\omega t) \end{pmatrix},$$

$$\text{the initial state for } t_0=0 \Rightarrow x(0) = \begin{pmatrix} V_{\text{Re}}(0) \\ V_{\text{Im},g}(0) \end{pmatrix}.$$

The above equation introduces the cavity detuning from master oscillator frequency $\Delta\omega$. The cavity shape determines the resonance frequency. Thus, any mechanical perturbation influences on the electrical parameters of the resonator. From measurement performed at DESY, one can find that if the over-one-meter-long cavity is compressed by 1 μm , then the resonance frequency change is around 300 Hz.

3.5. Detuning measurement

Measurement of detuning is one of the mayor issues for tuning system. There is possibly to estimate the detuning using the piezoelement, however it is more reasonable to use forward, reflected and probe signal acquired from the cavity itself. The second solution uses electromechanical model presented in previous subchapter.

There are two methods of detuning measurement: multi-pulse and single pulse one. First of them was proposed by T. Schilcher in his thesis [Schilcher 1998]. The second one was developed during the research with A. Brandt. Both methods are shortly presented bellow and then a comparison is given.

3.5.1. Multi-pulse detuning measurement

During the operation the cavity is pulsed with RF field. However, when forward power is removed the stored RF field starts oscillation with frequency of the detuned cavity. The frequency shift might be measured by comparison of phase of free ringing cavity versus the master oscillator clock. The slope of the phase is proportional to the detuning (see Figure 3.14) [Schilcher 1998].

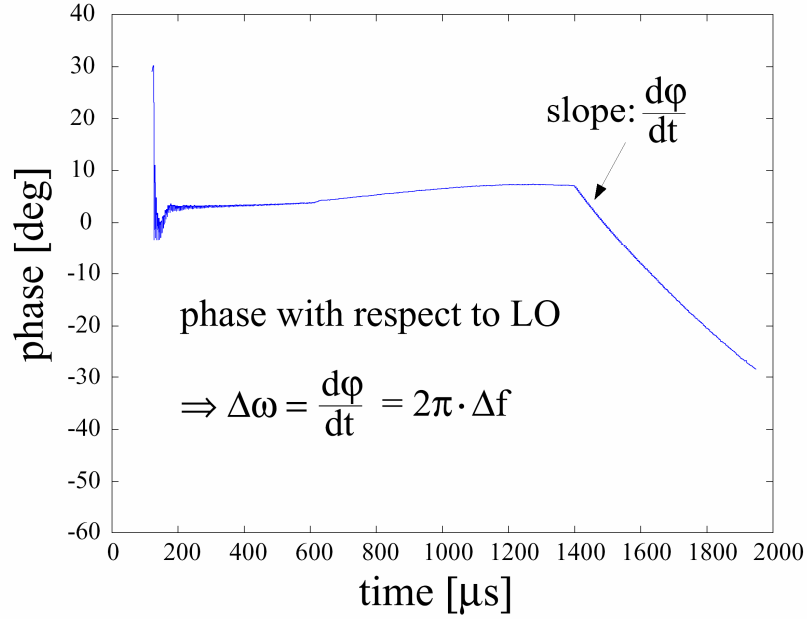


Figure 3.14 Principle of detuning measurement in multi-pulse method [Schilcher 1998].

Using this method it is possible to measure the detuning during whole pulse. However, there is need to shorten the forward power pulse and measure the slope of the phase for each time. As a consequence there is need to perform several runs (usually around 100) with different RF pulse length to obtain the detuning change in time. Of course, the presented method is invasive and cannot be used during the normal operation. It was an inspiration for developing a single pulse non-perturbing method of the detuning measurement.

3.5.2. Single pulse detuning measurement

The single pulse method base on the electromechanical model of the cavity presented in section 3.4. Rewriting the equation (3.10) it is possible to find the value of the detuning in respect to the amplitude and phase of the signal applied to the cavity (forward power) and the one measured inside it (probe signal). The formula for the detuning is given as:

$$\Delta\omega = -\frac{1}{2\pi} \left(\frac{d\phi_{probe}}{dt} - 2\omega_{1/2} \frac{|U_{for}|}{|U_{probe}|} \sin(\phi_{for} - \phi_{probe}) \right) \quad (3.14)$$

where U_{for} is a magnitude of forward power,

ϕ_{for} is a phase of forward power,

U_{probe} is a magnitude of probe signal,

ϕ_{probe} is a phase of probe signal,

Using the above equation, there is possibility to measure the detuning on-line. In case of algorithm presented in Chapter 6 it was implemented in MATLAB script. However, the algorithm might be easily implemented in FPGA chip [Jalmuzna 2006]. The board, which was used, is equipped with powerful programmable IC Virtex II Pro. Originally it is used for LLRF control purpose and only few percent of resources is used for presented algorithm. The results obtained with hardware implementation of algorithm are presented in Figure 3.15.

One of the important issues, which need to be solved for future usage of this method, is noise elimination. The presented method base on derivative of the phase, and as a consequence of that it is very sensitive to all changes of signal. The phase noise is visible as two glitches in the beginning and in the end of the flat top. There is need to use a smooth filter, but then the additional delay need to be taken into account.

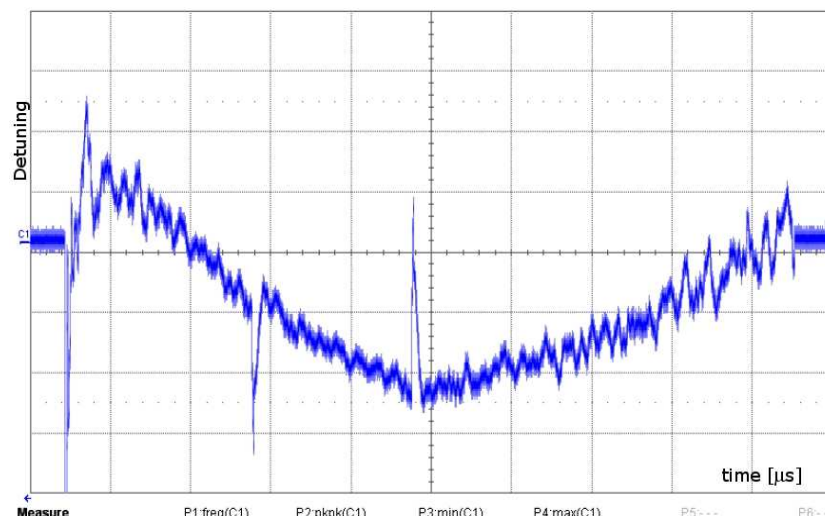


Figure 3.15 The cavity detuning measured using FPGA board. The scope screenshot [Jalmuzna 2006].

3.5.3. Comparison of single and multi-pulse detuning measurement

Both presented above methods – single and multi-pulse was compared to each other. The results are presented in Figure 3.16. There is need to note that they are shifted in time by $100\mu\text{s}$ because of the delay of ADC board.

The main difference between these two methods is the fact, that the multi-pulse method requires changing the pulse length, whereas the single pulse one is non invasive. As a consequence, it is possible to monitor the detuning all the time and what is more important it does not interfere with the experiment performed with the beam. Another advantage of the second method is possibility of implementation in FPGA-based system. As a result, the information about the detuning will be available on-line with a delay of hundreds ns. It means that the cavity frequency might be monitor

with 1 MHz, which is set as a main sample repetition for LLRF system. Such a promising outcome, allows compensating even the microphonics.

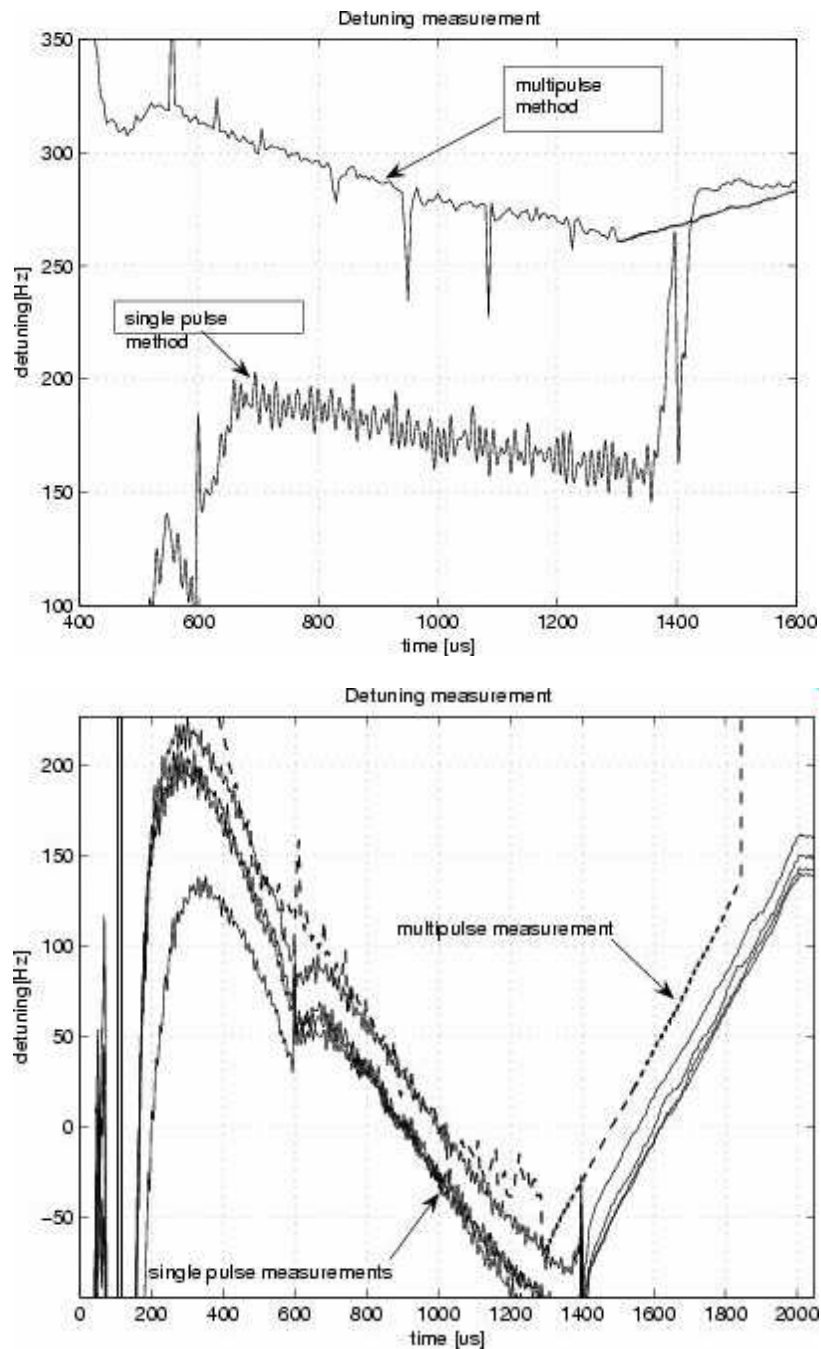


Figure 3.16 Comparison of single and multi-pulse detuning measurement method. FLASH, accelerating field gradient is set to 10.85 MV/m (left) and 15MV/m (right). LLRF feedback is switched off. A 100 μ s shift between the measurements is caused by DAC board delay.

3.6. Conclusion

In this chapter the information about detuning sources were presented. They were classified to two groups – to the periodic and predictive one, which are connected with Lorentz-force effect, and to

the stochastic one, which are caused by microphonics. The Lorentz-force phenomenon was described in details. Moreover, the mechanical study and electromechanical model of the superconducting TESLA type cavity were explained. The new method of detuning measurement, which base on the presented model, was described. At the end, it was compared to the previous method, which requires pulse length changing.

Using the knowledge presented in previous chapters it is possible to clearly define the requirements for the electromechanical system required for fast tuning. The actuator, used for this purpose, need to compensate the few microns of cavity length change. Moreover, the active elements must react at least with speed of $0.01 \mu\text{m}/\mu\text{s}$. The stiffness of the tuning system should be over $10 \mu\text{m}/\text{kN}$, whereas the blocking force of the actuator needs to be above 3 kN. Next chapter is dedicated to the active elements, which fulfils the above requirements and might be operated at 2 K in radiation environment without the damage.

Chapter 4. Smart materials

4.1. Introduction

Smart materials are ordinary name for wide group of different substances. The common feature of all of them is the fact that one or more properties might be dramatically altered under controlled condition. Most everyday materials have physical properties, which cannot be significantly changed, for example if oil is heated it will become a little thinner, whereas a smart material with variable viscosity may turn from a fluid which flows easily to a solid.

For the purpose of tuning system used for linear accelerator, there is need to use a material, which will change its length. The movement must be in range of several micrometers, but the resolution must be measured in teens of nanometres. The device must be also quick and strong enough – the slew rate of elongation should be over $0.01 \mu\text{m}/\mu\text{s}$ and the blocking force should be above 6 kN. One can imagine a mechanical apparatus, which could fulfil the above parameters, however the final system must work reliable for 10^{10} cycles in high vacuum, radioactive environment of temperature of 2K (below -270°C). That was the reason to explore different smart materials, which could be later used for tuner design.

As a consequence, two type of smart materials are investigated as an actuator for tuner purpose:

- piezoelectric stacks,
- magnetostrictive rods.

Both phenomena are well known and they are used for long time (piezoelectricity was discovered by Pierre and Jacques Curie in 1880, and the magnetostriction – by James Prescott Joule in 1840). Both of them exist as a direct and an inversed effect. Beside diverse material, in which given phenomenon exist; the main difference is the stimulus. The piezoelectric stacks are driven by electric fields supplied by metal plates, which are built in the stack, whereas the magnetostrictive rods are controlled by magnetic flux usually generated by the coil, which is assembled around the active element. As the result, from electrical circuit point of view, the first group is commonly treated as capacitors and are voltage driven components, whereas the second set of used smart materials are regarded as a current driven inductances (Figure 4.1).

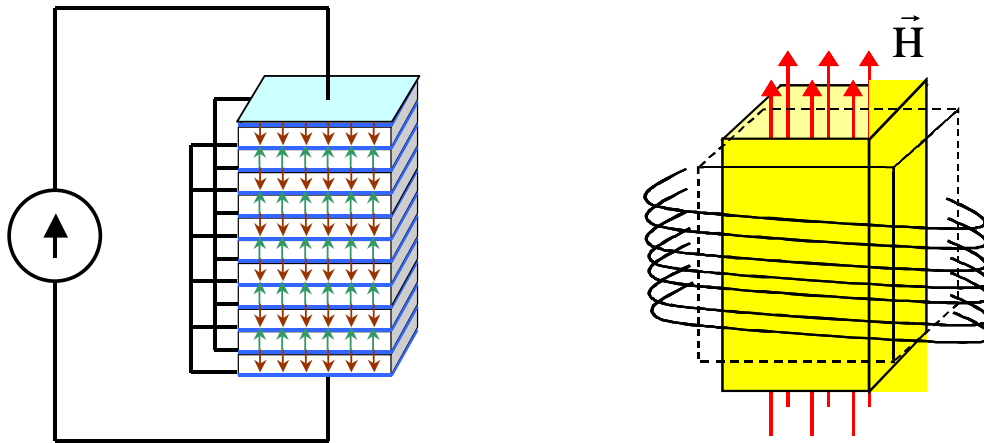


Figure 4.1 Piezoelectric stack and magnetostrictive rod principle of operation.

This chapter describes both types of smart materials in details. The parameters at room temperature and at cryogenic environment are presented. The elements are regarded as an actuator and sensor. The parameters with high importance for fast tuning purpose are underlined. In section 4.2 the piezoelectric stack from EPCOS, NOLIAC, Physical Instrumente (PI), PiezoJENA and Piezomechanik manufacturers are investigated. Section 4.3 is dedicated to magnetostrictive rods from ENERGEN and ETREMA.

4.2. Piezoelectric stacks

The piezoelectric elements have evaluated for more than 120 years. The Curie brothers discovered the direct piezoelectric effect in 1880. The name of the effect is a concatenation of two words “piezo”, which stands in Greek for pressure, and the “electricity”. It clearly defines that it is a generation of electricity from applied stress. The converse piezoelectric effect was deduced from fundamental thermodynamic principles by Lippmann in 1881 and was immediately confirmed by experiments. For next 20 years after the discovery, the core of piezoelectric applications science was established. In 1910 Voigt’s “Lehrbuch der Kristallphysik” was published which quickly became the standard reference for the future development. Nowadays, the main reference for piezoelectricity is publication of standards committee of the Institute of Electrical and Electronics Engineers [SC IEEE 1987]. It is the most widely recognized description of piezoelectric ceramic behaviour.

From physics of solids, it is known that piezoelectricity is very common effect. It exist in non-centrosymmetric crystal classes materials except the cubic class 432 [Soluch 1980]. All of them shows the dipole behavior. The reason of that is a charge separation between the positive and negative ions. Groups of dipoles with parallel orientation are called Weiss domains. In raw PZT material the Weiss domains are randomly oriented. However it is possible to align them. For this purpose the element is heated and the high electric field is applied (over 2 kV/mm). Under this

condition the material expands along the axis of the field and contracts perpendicular to that axis. Moreover, the electric dipoles align. Then, the piezoelement is cooled down, but the polarization of element remains (Figure 4.2).

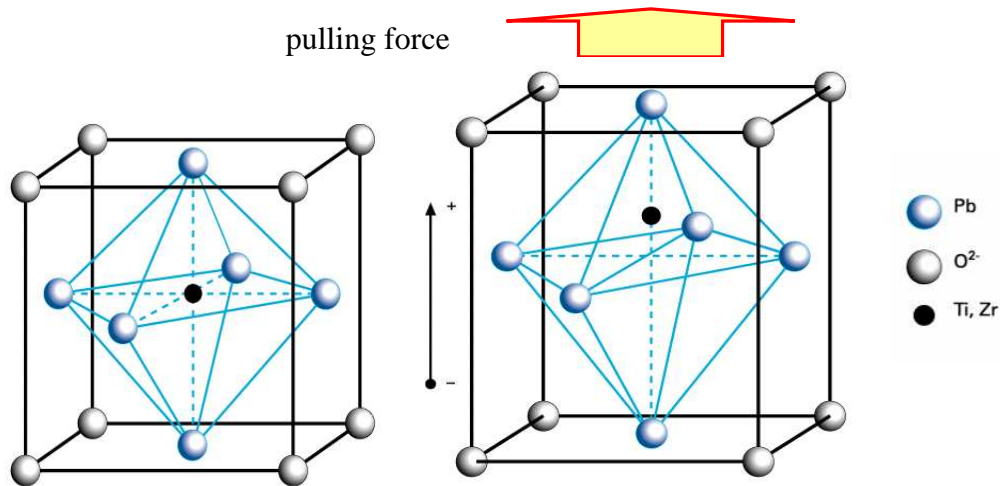


Figure 4.2 Single crystal of PZT before (left) and after (middle) pooling. On the right a legend of used atoms is presented.

The main equation, which describes behaviour of piezoelectric crystals, is given as:

$$D = \varepsilon \times E \quad (4.1)$$

where D is electric flux density
 ε is the permittivity matrix
 E is the electric field strength

The second equation, which is commonly used with the first one, is the Hooke's law, which describes the relation between strain, stress and compliance. In matrix notification there is possible to rewrite both equations to formula 4.2. The used parameters are usually given by manufacturers.

$$\begin{aligned}
 \begin{bmatrix} S_1 \\ S_2 \\ S_3 \\ S_4 \\ S_5 \\ S_6 \end{bmatrix} &= \begin{bmatrix} s_{11}^E & s_{12}^E & s_{13}^E & 0 & 0 & 0 \\ s_{12}^E & s_{11}^E & s_{13}^E & 0 & 0 & 0 \\ s_{13}^E & s_{13}^E & s_{33}^E & 0 & 0 & 0 \\ 0 & 0 & 0 & s_{44}^E & 0 & 0 \\ 0 & 0 & 0 & 0 & s_{44}^E & 0 \\ 0 & 0 & 0 & 0 & 0 & s_{66}^E \end{bmatrix} \begin{bmatrix} T_1 \\ T_2 \\ T_3 \\ T_4 \\ T_5 \\ T_6 \end{bmatrix} + \begin{bmatrix} 0 & 0 & d_{31} \\ 0 & 0 & d_{31} \\ 0 & 0 & d_{33} \\ 0 & d_{15} & 0 \\ d_{15} & 0 & 0 \\ 0 & 0 & 0 \end{bmatrix} \begin{bmatrix} E_1 \\ E_2 \\ E_3 \end{bmatrix} \\
 \begin{bmatrix} D_1 \\ D_2 \\ D_3 \end{bmatrix} &= \begin{bmatrix} 0 & 0 & 0 & 0 & d_{15} & 0 \\ 0 & 0 & 0 & d_{15} & 0 & 0 \\ d_{31} & d_{31} & d_{33} & 0 & 0 & 0 \end{bmatrix} \begin{bmatrix} T_1 \\ T_2 \\ T_3 \\ T_4 \\ T_5 \\ T_6 \end{bmatrix} + \begin{bmatrix} \epsilon_{11} & 0 & 0 \\ 0 & \epsilon_{11} & 0 \\ 0 & 0 & \epsilon_{33} \end{bmatrix} \begin{bmatrix} E_1 \\ E_2 \\ E_3 \end{bmatrix}
 \end{aligned} \tag{4.2}$$

where

S is a strain vector

s is a compliance matrix

T is a stress vector

d is a piezoelectric coefficient matrix

superscript E stands for measurement done at zero, or constant, electric field

$$s_{66}^E = 2(s_{11}^E - s_{12}^E)$$

Recent development in piezoelectric materials is focused on development of new materials, which will have higher piezoelectric coefficients. Simultaneously, the very thin layers of crystal (around 100 μm) are stacked together to improve the elongation of whole actuator. The electrode is inserted between the adjacent layers. As a consequence, electric field applied to the single layer is in range of few MV/m (100 V over 100 μm).

4.2.1. Piezoelement characterization and comparison

For purpose of FLASH a piezostack from EPCOS (LN 01/8002), Physik Instrumente (P-888.90 PIC255), Piezomechanik (PSt 150/10/60VS15 TT/UHV), and NOLIAC (SCMAS/S1/A/10/10/20/200/42/6000) were investigated (see Figure 4.3). All of them are the low voltage piezoelectric stacks, which might be operated up to 200 V. Only the Piezomechanik one was supplied with metal cover and it was initially preloaded.

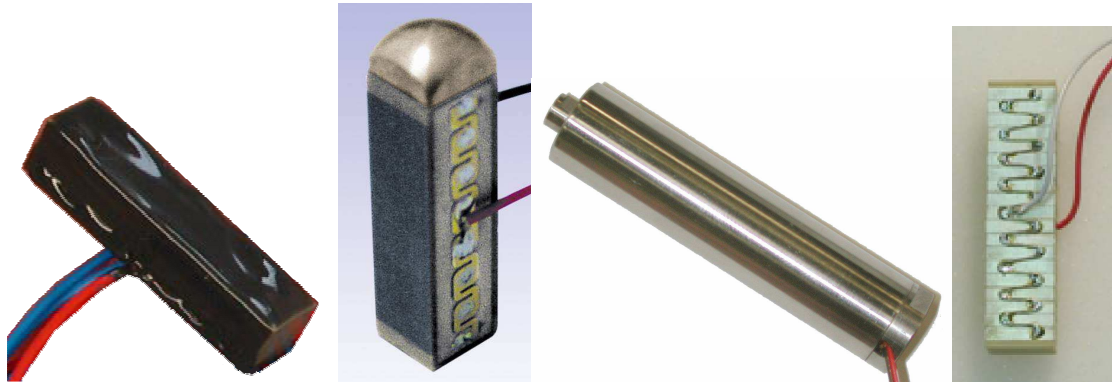


Figure 4.3 Photographs of used piezostacks. From left to right: EPCOS, PI, Piezomechanik, NOLIAC (not in scale).

The parameters of tested piezoelement are presented in Table 4.1. The one from EPCOS was used for FLASH tuner, however according to performed test two others – NOLIAC and PI should be taken under consideration for next development. The one from PiezoMechanik produces more failure than the previous ones and therefore were not investigated in details.

Table 4.1 Parameters of tested piezoelements

Parameter name	Units	EPCOS	NOLIAC	PI	Piezo-mechanik
Material		PZT-Nd34	PZT pz27	PZT 255	PZT 5H
Case/preload		no	no	No	yes/400N
Length	mm	30	30	36	55
Cross-section	mm ²	7 x 7	10 x 10	10 x 10	7.5 x 7.5
Young Module	kN/mm ²	51	45	48.3	55
Stroke (300K)	μm	40	42	35	60
Main resonance frequency	kHz		66	40	14
Stiffness	N/μm	83	150	105	56
Blocking force	kN	3.2	6.3	3.6	4
Density	kg/m ³			7800	
Minimum voltage @ 300K	V			-20	
Maximum voltage @ 300K	V	160	200	120	150
Slew rate	V/ms	1.6			
Load current	A	20			
Capacitance nominal (F _{load} =0N)	μF	2.1	5.7	12.4	13.4
Capacitance measured (F _{load} =0N)	μF	2.1	5.7	13.6	
Capacitance (F _{load} =850N)	μF	3.4			
Capacitance @10K	μF			3.4	1.43
Loss factor (tan δ)				0.015	

Initially the actuators were studied at room temperature of 300 K. Then the behaviours at LHe temperature range were investigated [Sekalski 2005c]. Sample of result is presented in the thesis. Full characterization will be covered in a detailed report, which will soon be published by the M. Fouaidy from IPN-Orsay.

In the Figure 4.4 displacement of PI piezostack at 300K is presented. The maximal elongation is over 40 μm for voltage of 120 V. The stroke of element dramatically decreases with the temperature, what is presented in Figure 4.5. For temperatures below 10K the element elongates only by 5 μm and drops more with temperature decreases. Therefore a reduction of stroke of 8 times is visible. It is important to remark that for purpose of FLASH the elongation of 3 μm at 2 K is required (red dashed line). As a result, there is need to use a piezostacks, which at room temperature have stroke at least equal to 40 μm .

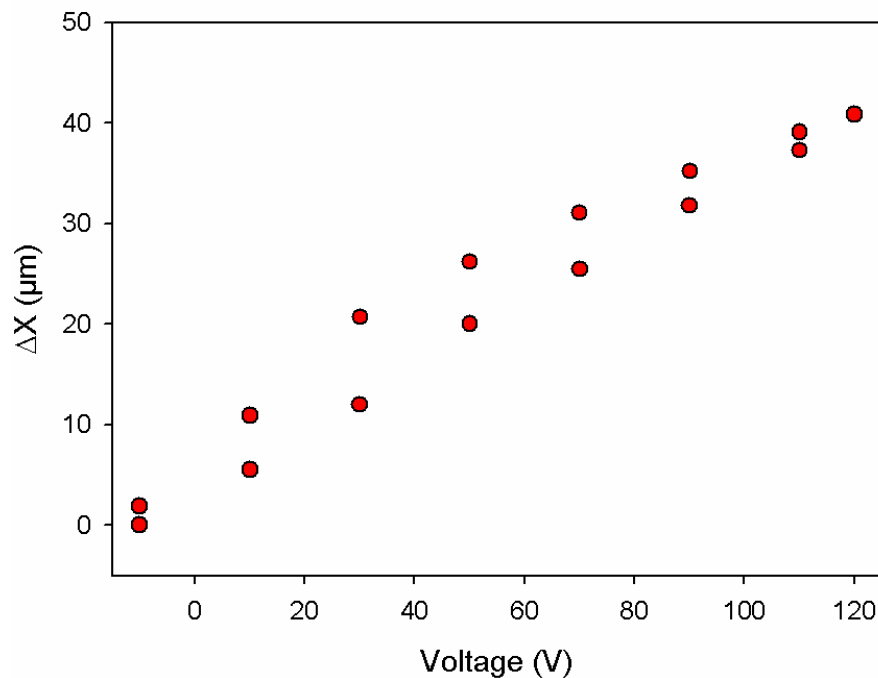


Figure 4.4 Displacement of PI piezoelement at 300K

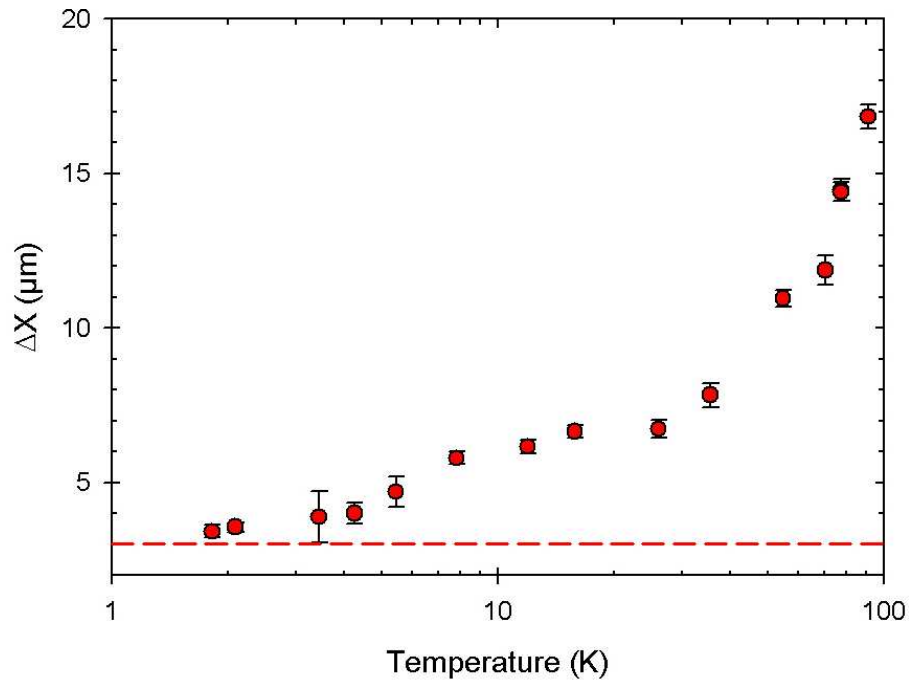


Figure 4.5 Maximum displacement (stroke) versus temperature (PI piezostack)

Another parameters, which were detailed investigated, are the magnitude and the phase of the piezoelement impedance. The sample of measurement is presented in Figure 4.6. The measurement was done using a LCR Agilent 4293 B. The impedance of the actuator decreases with the temperature whereas the phase remains almost constant (less than 1 degree).

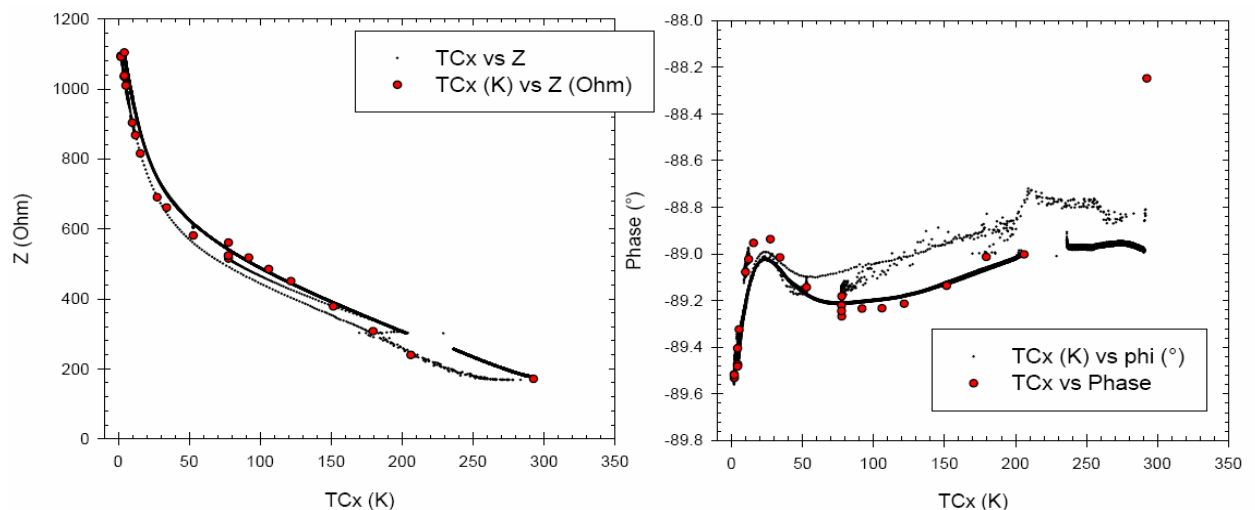


Figure 4.6 Magnitude and phase of impedance in function of temperature

The parallel capacitance and resistance of the PI piezoelectric stack in function of temperature is shown in Figure 4.7. The capacitance decreases by factor of 3÷4 when cooled down to LHe temperatures. It is due to the contraction of the element and, what is more important, it is due to the changing of properties of piezoelectric crystal itself. The piezoelectric stack at cryogenic

environment might be operated in wider range of voltages. Moreover, the so-called butterfly behavior of elongation in function of applied voltage, which is visible at room temperatures, becomes almost linear and as a result the actuator might be operated with bipolar voltages.

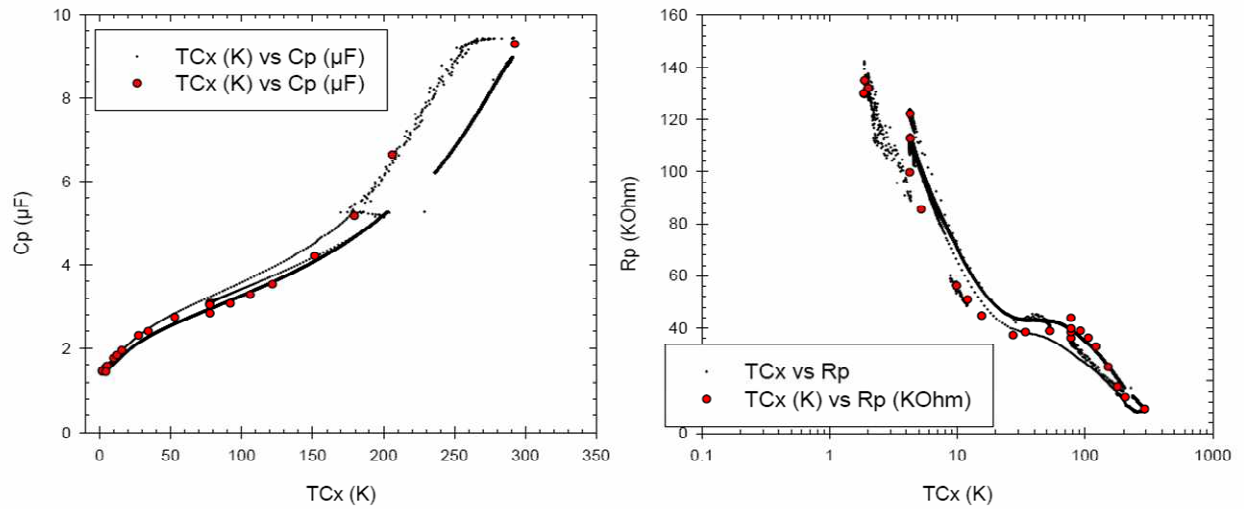


Figure 4.7 Parallel capacitance and resistance of piezoelement in function of temperature

The loss tangent was also studied during the piezoelement investigation. The sample of measurement done for PI piezoelement is presented in Figure 4.8.

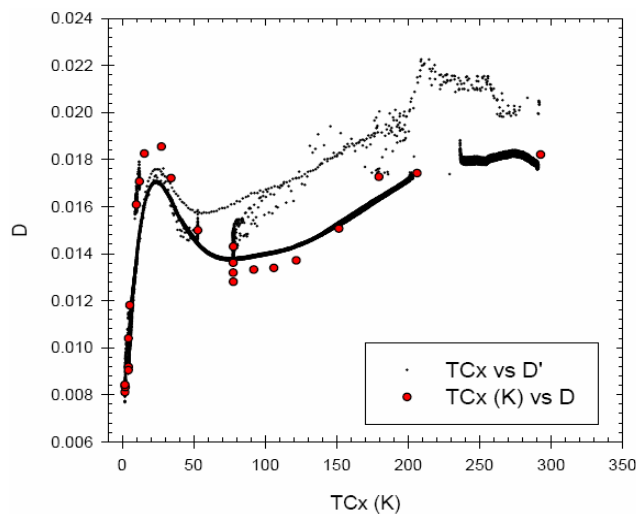


Figure 4.8 Loss tangent in function of temperature,

Another important issue, which was investigated, was a radiation hardness of the piezoelement. A special experiment to check the behaviour of irradiated actuator was performed at CERI – Orleans, France. The element was cooled down to 4.2 K and then exposed for 20h to the neutron radiation. The total acquired dose was calculated to $1.76 \div 3.09 \cdot 10^{14}$ n/cm². The only visible effect was the increasing the capacitance due to the heating caused by fast neutron beam.

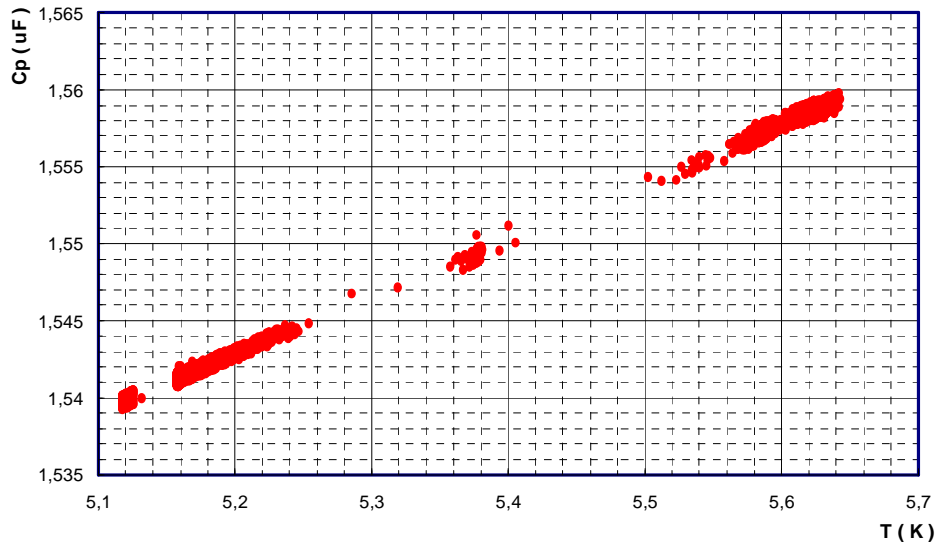


Figure 4.9 Capacitance in function of temperature during fast neutron beam test. (NOLIAC)

At the end of this chapter, there is need to mention that a long lifetime test of NOLIAC and PI actuator were performed at LN₂ temperature (77 K). The elements were pulsed by over 10⁹ cycles and no significant degradation was observed (see Figure 4.10) [Bosotti 2005d]. However there is need to mention that preload force was set to optimal value of 1.2 kN (one third of the blocking force).

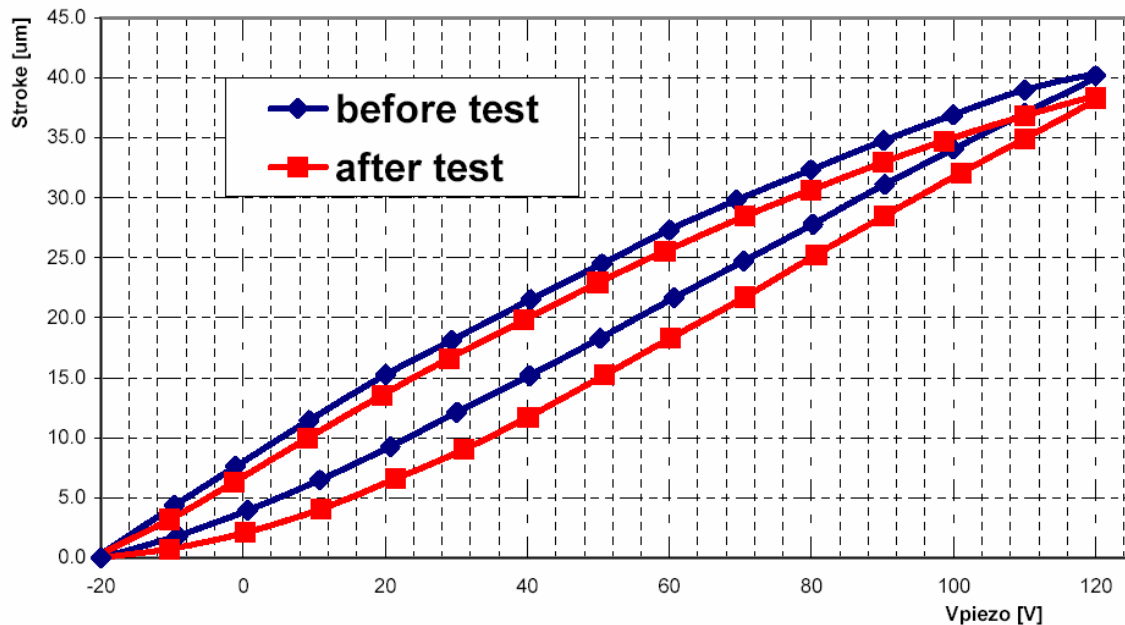


Figure 4.10 Stroke in function of applied load before and after lifetime test.

According to the literature [Zickgraf 1995] and [PI web] the lifetime of the piezoelectric stack strongly depends on the static force applied to the actuator. Higher preload causes a mechanical fatigue of material and significantly reduces the MTBF factor. Therefore, correct preload of one

third of the blocking force is necessary for long operation of fast tuning system. Thus, the Chapter 5 is dedicated to static force measurement at LHe environment.

The presented above issue is important especially for the tuners in which the active element is assembled inside the cryomodule and therefore cannot be easily replaced with the new one. Depending on the repetition rate the lifetime of the actuator should be above 10^{10} cycles (20 Hz for 10 years of operation).

4.3. Magnetostrictive rods

At the current state two types of magnetostrictive elements seem to fulfil above requirements - one of them is fabricated by ENERGEN INC, the other by ETREMA. Material from first company is called KELVIN ALL®, the other GalFeNOL. There is need to use special materials because the ones commonly used at room temperature i.e. Terfenol-D does not work correctly at LHe environment (see Figure 4.11). The others like TbDyZn are extremely expensive (even 5÷10 times more than Kelvin All). In general the magnetostrictive rods are twice or three times more expensive than piezoelectric stack of the same properties.

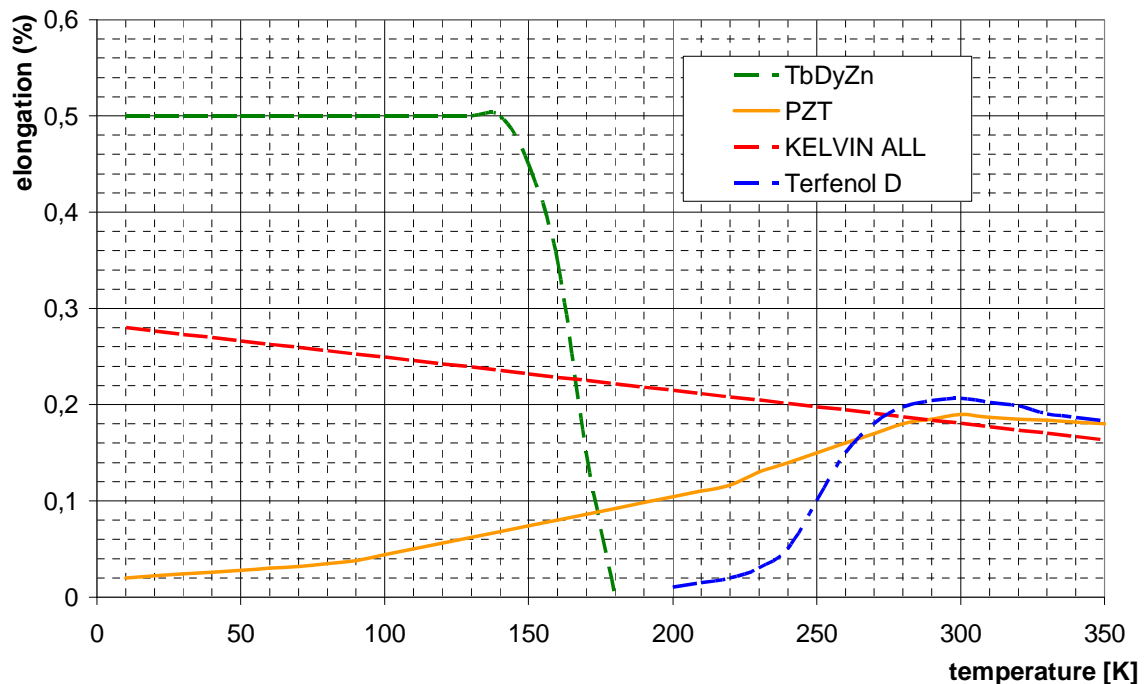


Figure 4.11 Elongation of different materials in function of temperature [Mavanur 2003]

First of the magnetostrictive element rod is made of material called KELVIN All®. Its magnetostriction is range of thousands of ppm (see Figure 4.11) [Energen 2003]. Manufacturer claims that the 18 mm length rod has a stroke around 20 μm . The full-length elongation takes only 250 μs , which stands for control speed of 0.08 $\mu\text{m}/\mu\text{s}$. It may operate in radioactive, high vacuum

environment. However, currently there is no data about degradation in time caused by radiation. Assumed lifetime is higher than 10^{10} , but a proper test needs to be performed to verify this statement.

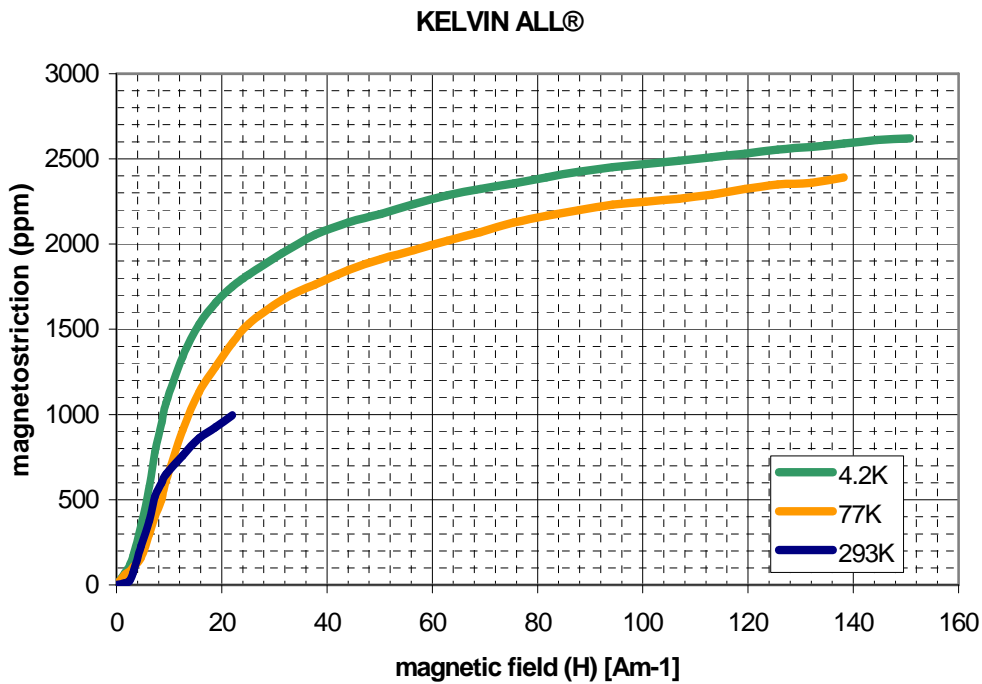


Figure 4.12 Magnetostriction of KELVIN ALL® material (courtesy of ENERGEN)

The company ENERGEN, INC provide a tuner with magnetostrictive rod inside. The draft view with dimensions and its photo are presented in Figure 4.13. The details of magnetostrictive tuner are shown in Figure 4.14.

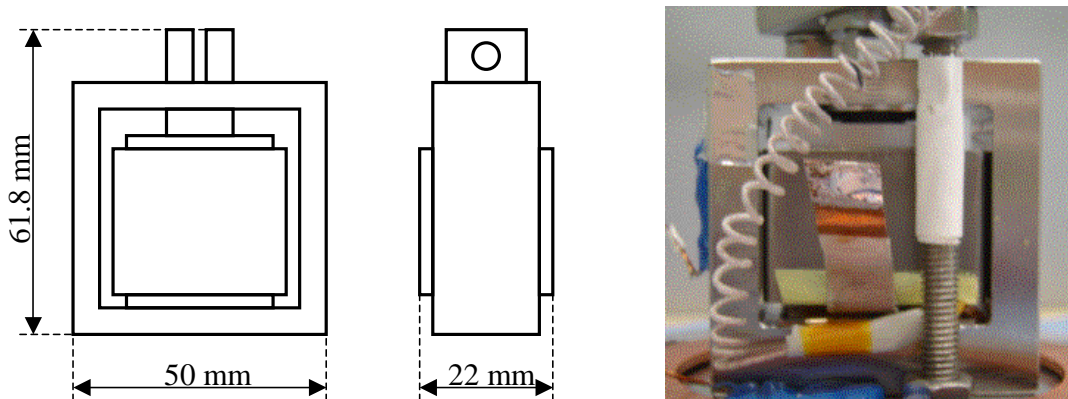


Figure 4.13 Magnetostrictive element with metal frame – the draft view with dimensions (left) and its photo (right).

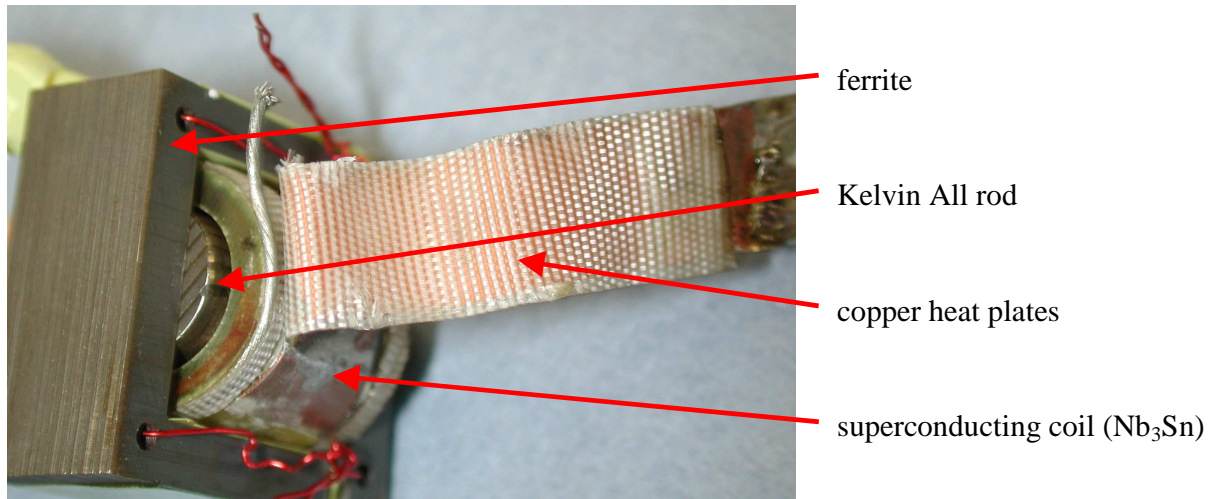


Figure 4.14 At the bottom a magnetostrictive rod with Nb_3Sn coil and ferrite ring is presented.

The tuner was validated in the vertical cryostat [Sekalski 2005b]. A special insert was designed, which consist of a frame in which, two active elements were assembled in series: the piezoelectric one from NOLIAC, which works as a sensor, and the magnetostrictive one from ENERGEN as an actuator (see Figure 4.15). The special screw mounted on top allows adjusting the system compression. The preload force was set at room temperature to 1.2 kN.

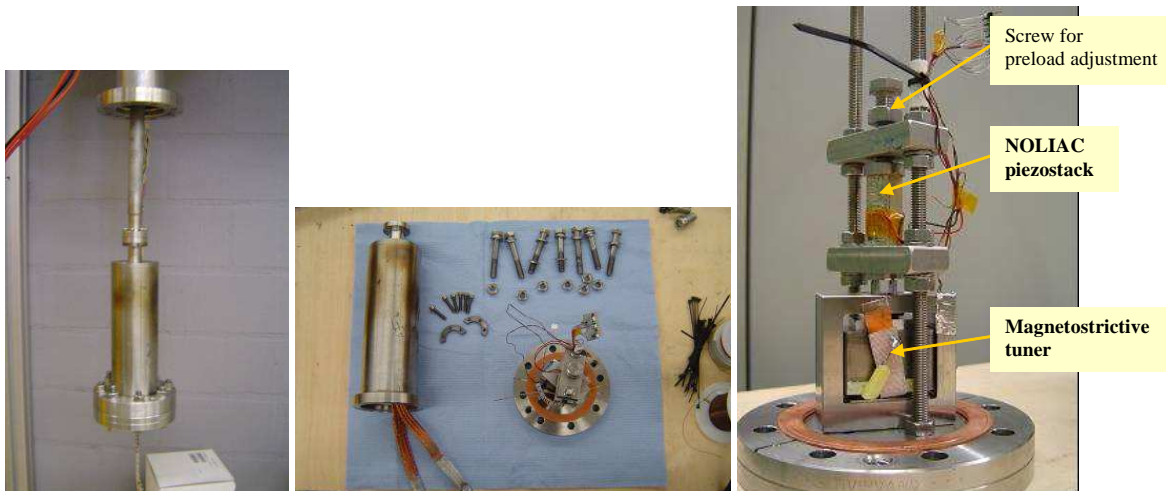


Figure 4.15 Photos of insert for the vertical cryostat.

Three temperature sensors were glued to base, to magnetostrictive tuner frame, and to metal block close to piezoelectric sensor. They allow controlling heat flow through the system during experiment. Additionally, they indicate if the insert is well thermal stabilized. The whole system was cooled down to 4 K. The coil was thermally stabilized by two thermal cooper connectors, which were attached to the metal cover (Figure 4.15 – in the middle). It allows keeping the superconducting coil made of Nb_3Sn below critical temperature.

To superconducting coil was driven by voltage to current transducer (device base on APEX PA93 linear power amplifier). The maximum output current is slightly over 8 Amps. Over this value the amplifier saturates. Remarkable is fact, that the inductance of the coil is 2.4 mH, therefore also high voltage is necessary to reload coil with frequency of 1 kHz. Due to the heat dissipation, the transducer might work only in pulse mode. The input signal is set in Rhode & Schwartz function generator.

The magnetic field inside the coil elongates the magnetostrictive rod. Noliac's piezoelement acts as a displacement sensor. When pressed it generates voltage, which was registered on the scope. Similar experiment with two Noliac piezostacks was performed previously. At that time, one piezostack acted as a sensor, the second as an actuator.

Comparing the results from both experiments, the elongation of magnetostrictive tuner was calculated [Sekalski 2005b]. The results is presented in Figure 4.16. The coil was supplied by half-sine current wave. The current amplitude was changed from 0.4 to 8.3 Amps.

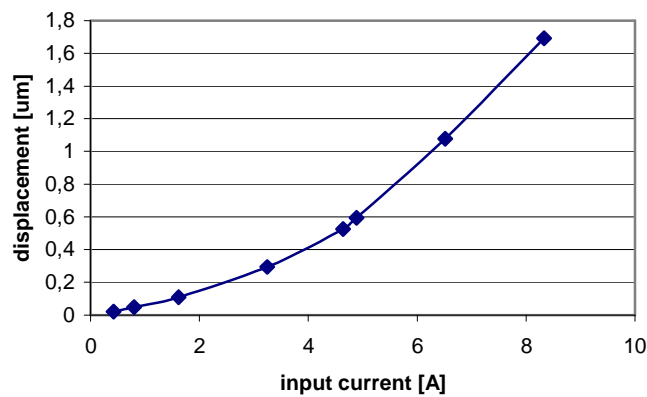


Figure 4.16 Calculated displacement of magnetostrictive rod versus applied current.

First of all, the experiment indicates that KELVIN ALL material works at 4K. Nevertheless, the elongation of the magnetostrictive rod is smaller than presented in datasheet ($4 \mu\text{m}$ for 8 A). However, it might happen that the preload force was not well controlled and it was higher than 1kN, because stiffness of fixture was unknown.



Figure 4.17 Photo of GalFeNOL rod of cross-section of 7x7 mm and length of 18 mm.

The second set of actuators is made of GalFeNOL (see Figure 4.17). It is a composition of gal, iron and rare earth minerals. Its dimensions are 6x6x20mm. It has smaller magnetostriction than KELVIN ALL® by factor of 2÷3. Moreover, it has no lamination to reduce the edgy current, as the previous one. On the other hand, it is at least twice cheaper than ENERGEN solution. According to the manufacturer, it will fulfil the requirement list, but till now it was tested only in liquid nitrogen. The precise characterization of GalFeNOL rods at LHe environment will be done in the nearest future.

4.4. Conclusion

Two types of smart materials have been investigated as an actuator for fast tuning system for TESLA type cavities. The piezoelectric stacks are used for longer time and therefore their behaviour is better understanding. The influences of temperature and neutron radiation were studied in details. As well, the lifetime issues were taken under consideration. As a result two stacks – one from NOLIAC, the other from PI – were chosen for further validation. Both of them fulfils requirement for fast tuning components. The one important remark which need to be stressed is the fact, that both element must be correctly preloaded to guarantee the required lifetime. It is a reason of study presented in next chapter, in which a different method of static force measurement at LHe environment is investigated.

The alternative solution base on the magnetostrictive tuner. However, the research on these devices is not as well advanced as on the piezoelectric one. Nevertheless, the magnetostrictive rods were successfully operated at cryogenic temperatures (4 K) and the stroke was in the required range of 2 µm. In the nearest future, a test with cavity in horizontal cryostat is planed.

Chapter 5. Force measurement

5.1. Introduction

One of the most important parameter, which needs to be taken under consideration, is the static force applied to the piezostack, when it is cooled down to the desired temperature. It not only indicates the stroke of the actuator as it is described in Chapter 4.2. But also according to the literature it also changes the lifetime of the actuator [Zickgraf 1995].

The active elements are assembled in the cryomodule at room temperature. After that, the structure is closed and then it is pumped to gain a high vacuum in the module. The tank is filled up with helium. Due to the pressure difference the force distribution is modified. Moreover, the system is also cooled down to the desired operation temperature of 1.8 K. The temperature coefficient of expansion (TCE) of materials used for cryomodule insert construction is diverse; therefore shared stresses are generated when temperature is varying. As a consequence, both processes lead to shift of the force applied to piezostack.

If the displacement of the internal elements of cryomodule is huge it may happen that the piezostack will be completely released and, in the worst case, it may fall out from the fixture. It was the reason to design special holdings for active element, which have four fingers. Moreover, the metal handle helps to arrange the actuator in correct position during assembling process. In contrary, if the piezostack are preloaded too much the stroke is reduced. At the limit, if the preload force is higher than blocking force, the element no longer elongates.

There is possible to roughly estimate the preload force, but due to the complexity of the system the error could be enormous. That is the reason to introduce the force sensor. The commercial solutions are either too big to fit into the tuner or they are too expensive. In this chapter different method developed by authors and CARE project co-workers are presented. Part of the measurements was done at IPN Orsay, France and INFN Milan, Italy. Three types of method are presented. There is possibility to use a strain gauge sensor, as it is describe in section 5.2. However it is more convenient to use one of the two other methods, which do not require additional sensor and base only on the piezostack itself. The first method, developed by author, which base on shift of resonance on the impedance curve is described in section 5.3³. The second one, showed in section 5.4, bases on the capacitance change in function of applied force. This method is developed in IPN Orsay and arises as the consequence of the first one.

³ For this invention the author gained a Gold Medal on 54th The World Exhibition of Innovation, Research and New Technologies, "BRUSSELS EUREKA 2005" and prize of Ministry of Education and Science in Poland.

5.2. Strain gauge

Strain gauge is a well-known device whose electrical resistance varies in proportion to the amount of strain in the device. One of the most widely used gauges is the bonded metallic strain gauge. The metallic strain gauge consists of a thin wire arranged in a grid pattern or, what is more often nowadays, the metallic foil is used. To improve the sensor response, the amount of metallic wire or foil subject to strain in the parallel direction is improved, whereas the cross-section of single wire is minimized to reduce the effect of shear strain and Poisson Strain. The whole grid structure is tied to the thin carrier, which is attached directly to the element on which stress is measured (see Figure 5.1). To increase the range of measured force it is possible to use as a basement a metallic structure of known stiffness – in example a membrane or cantilever. Whole strain experienced by the test specimen is transferred directly to the strain gauge, which responds with a linear change in electrical resistance. The sensors available commercially have nominal resistance in range of few hundreds to few thousand of Ohms.

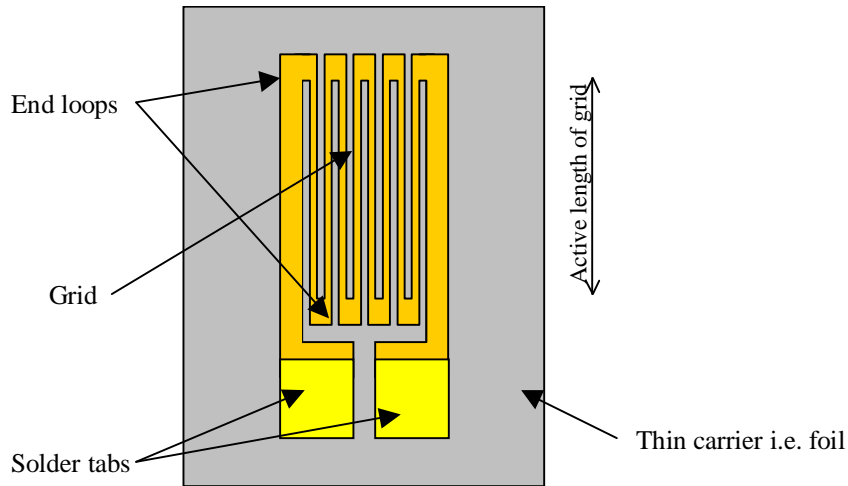


Figure 5.1 Overview of metallic strain gauge sensor

One of the most important parameters of strain gauges is gauge factor (GF). It is the ratio of fractional change in electrical resistance to the fractional change in length (strain), what is written as:

$$GF = \frac{\Delta R / R}{\Delta L / L} = \frac{\Delta R / R}{\varepsilon} \quad (5.1)$$

where ε is a strain

The gauge factor of typical metallic strain gauges varies from 1 to 5 and it is relatively low in comparison to the semiconductor-based one in which gauge factor due to the piezoresistive effect is usually above 100. The piezoresistive effect besides the advantages has several negative attributes. First of all, it is a nonlinear thus the output signal is not direct proportional to the strain. It is also

very dependent to the temperature. Another disadvantage is the semiconductor itself, which usually is very fragile and therefore it might be exposed to relatively limited strain range (typically 3000 to 10,000 microstrain units compared to the 100,000 microstrain units for a metallic resistance gauge).

The Wheatstone bridge configuration is used to increase the sensor sensibility (see Figure 5.2). There are at least three types of possible configuration: quarter, half and full bridge. The output voltage versus supplied voltage is given by formula:

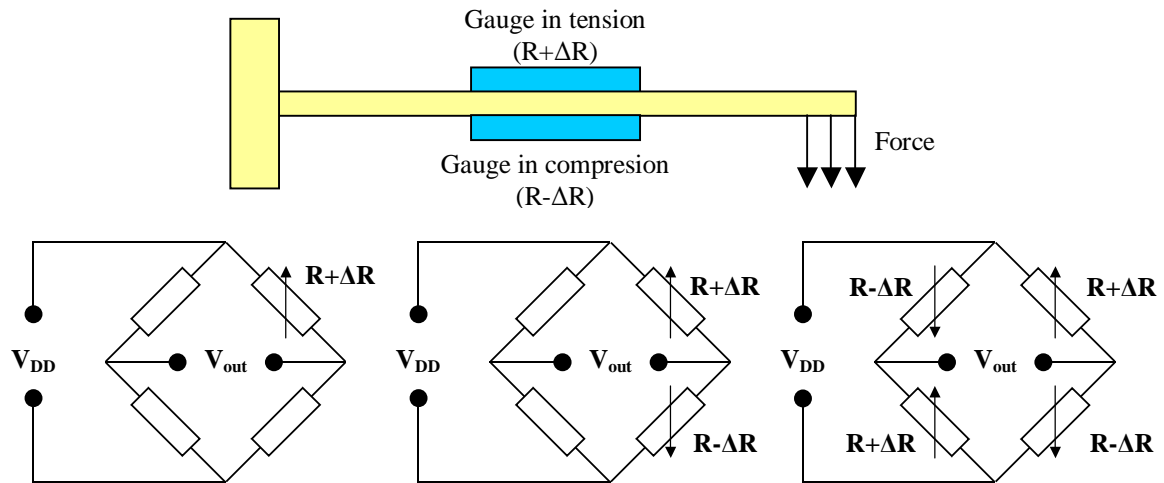


Figure 5.2 Gauge placement on measured plate (top) and configuration of strain gauges (bottom) - quarter (left), half (center) and full Wheatstone bridge circuit (right)

for quarter bridge circuit configuration:

$$\frac{V_{out}}{V_{DD}} = -\frac{GF * \varepsilon}{4} \left(\frac{1}{1 + GF * \frac{1}{2} \varepsilon} \right) \quad (5.2)$$

for half bridge circuit configuration:

$$\frac{V_{out}}{V_{DD}} = -\frac{GF * \varepsilon}{2} \quad (5.3)$$

for full bridge circuit configuration:

$$\frac{V_{out}}{V_{DD}} = -GF * \varepsilon \quad (5.4)$$

It is important to locate the strain gauges in places where strain is maximal. Moreover, if a full bridge or half bridge configuration is used, some gauges must work in tension whereas the other must work in compression to unbalance the bridge (see Figure 5.2).

Another important issue, which need to be taken under consideration when strain gauges are operated, is a thermal compensation of the sensor. Commonly used technique bases on the placement on the inflexible area the second set of Wheatstone bridge of the same type of gauges.

As the consequence, the temperature change acts on both sets of bridges, but only one of them is affected by applied stress. The final signal proportional only to applied stress is calculated as a difference of response of both bridges.

During the research, both types of strain gauge were investigated – metallic and semiconductor ones. The metallic foil type gauges from FLEX company were tested in the beginning. These small and cheap sensors have high sensitivity for low applied forces (see Figure 5.3), but unfortunately they were too fragile for our purpose. The static force, which is applied to piezostack, might be equal even up to 6 kN. For this strength the foil was deformed permanently. This is the reason to use a metal support on which gauges was glued. These types of devices are more complex and as a consequence more expensive but allow operating with higher preloads.

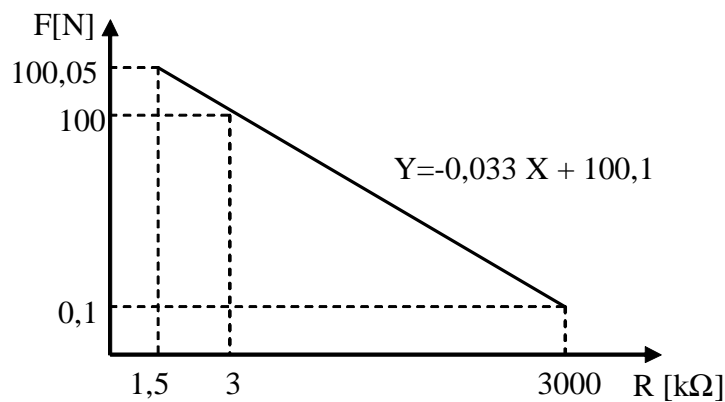


Figure 5.3 Resistance change of FLEX strain gauge sensor in function of applied force.

The commercial available sensors are designed for room temperature and the materials used for their construction were unstable at LHe environment (i.e. the glue crystallizes and crumbles). The test of standard load cell from BURSTER manufacturer 8415-6002 at LHe temperature were performed at DESY-Hamburg and at INFN Milan independently. The output signal was unstable and was not repeatable. The main problems were the plastic deformations of the glue and the choice of the strain gauges. In further research, a custom load cell has been realized and tested in order to verify the performances of cryogenic devices. The tests made in LHe on the prototype have been successful and proved that this load cell can work in cryogenic environment with good sensitivity and repeatability (see Figure 5.4) [Bosotti 2005b].

The presented force sensor has a linear response in whole applied load range. Due to the cryostat limitation higher loads could not be measured. Several performed run shows that the sensitivity is constant and equal to 0.02 mV/kg (~0.2 mV/N). Moreover, what is also important the same sensitivity is for room temperature and only offset value varies with temperature.

One of the main disadvantages of the sensor is its size. The cell presented in Figure 5.4 has a diameter of 10 cm and will not fit to current design of PTS or CTS tuner. The smaller device is under design and will be available in the mid of 2006.

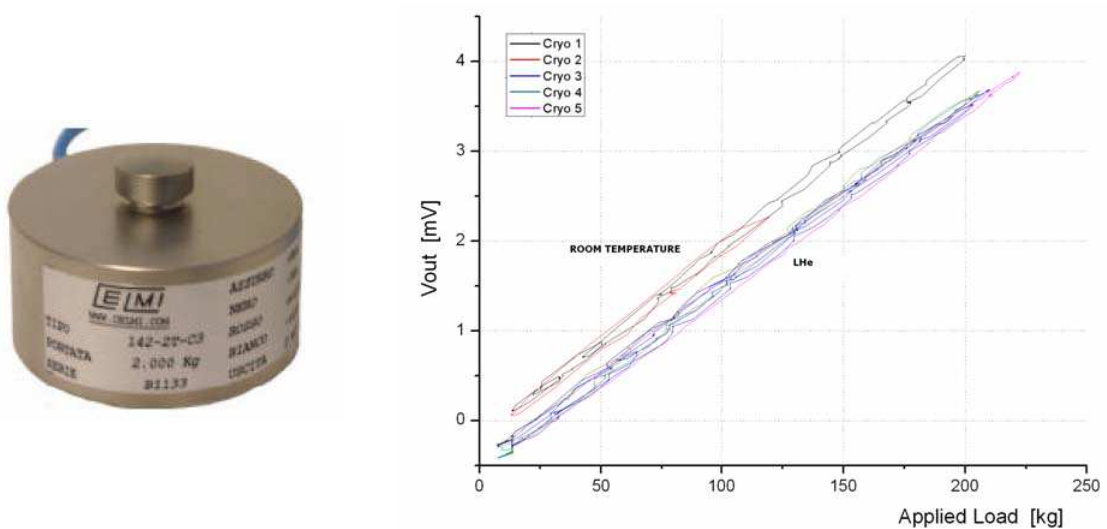


Figure 5.4 Load cell developed for cryogenic operation and its transfer characteristics.

[Bosotti 2005b]

One of the disadvantages of strain gauge sensor beside its price is an offset voltage, which needs to be annulling. Since now, two samples of load cell for LHe temperature operation have been manufactured. First measurements performed at 4 K shows that the output voltage is linear in function of applied force (above 300 N), but the offset of both devices is different (see Figure 5.5). As a consequence, the independent characterization of each force sensor is highly recommended.

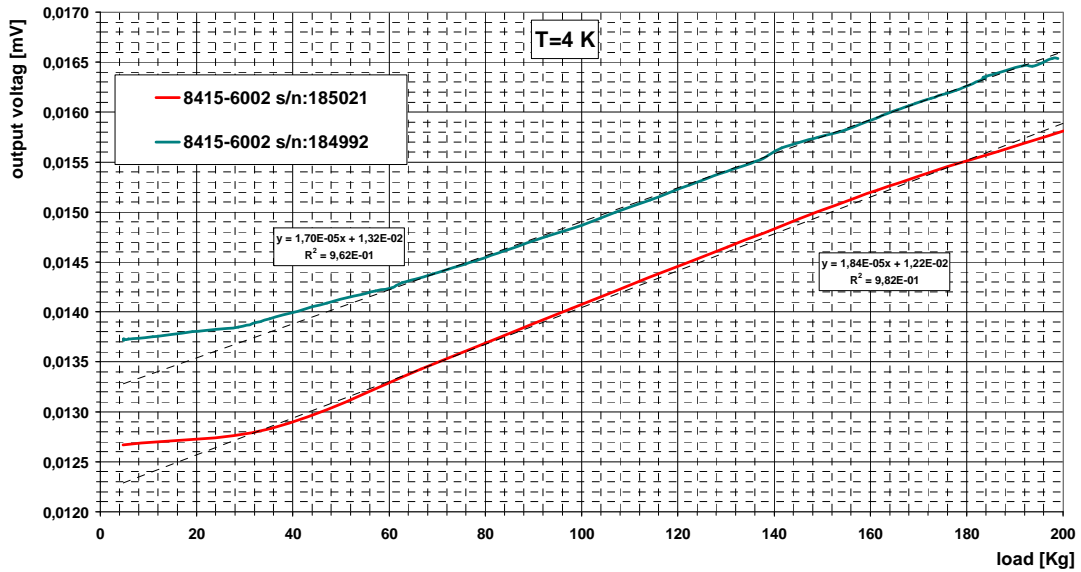


Figure 5.5 Output voltage of two samples of strain gauge sensor dedicated for LHe temperature operation. [Bosotti 2005b]

5.3. Shift of piezoelectric stack resonant frequency

Another method of measurement of static force applied to piezostack is the investigation of characteristic parameters of actuator itself. As it was described in chapter 4.2 the piezoelement is a dynamic force sensor. Thus, it might measure only a relatively fast change of applied load and cannot be used for static force evaluation. The mechanical energy of stress is transferred to electrical energy because of positive and negative charges centre shifts (refer to Chapter 4). Unfortunately, due to the measurement and the actuator itself, the charges are dissipated, and the voltage decays to zero value. The relaxation time depends on the size and material of actuator (which determines the capacitance) and the resistance of external circuit and parasitic resistance of sensor. When piezostack is connected to the scope (few $M\Omega$ of input resistance), the charge on piezoelectric plates remains only for few seconds. One of the solutions to improve the time is using a MOS transistor. The piezostack output voltage drives the gate of transistor. The resistance of MOS channel is proportional to the gate voltage; therefore it might be used for force estimation. Due to the fact that the leakage current between gate and source is very low, then the setup, presented in Figure 5.6, might be used even for quasi-static measurement.

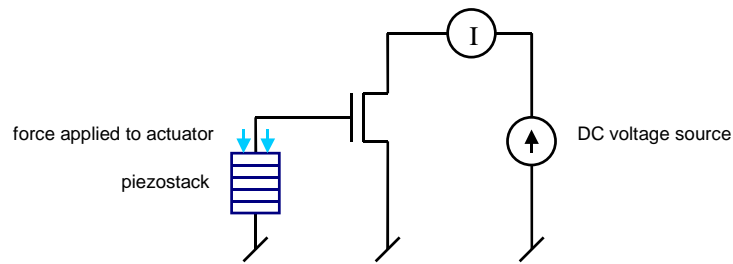


Figure 5.6 Overview of circuit configuration for quasi-static force measurement using the piezostack.

However, the above-presented solution cannot be used for the case of FLASH. The actuator are assembled into the cryomodule in room temperature, then the module is placed in the line with the others, cooled down, and at least the stepper motor are used to tune the cavity to desired 1.3GHz. Whole process is extremely long and takes few weeks. In this time the charge generated by force applied to piezostack dissipates. Moreover, the properties of piezoactuator are changing with temperature so the output signal will be influenced. That is the reason to search for other techniques of static force measurement.

According to the literature the piezoelectric element has two resonances – parallel and series one (see Figure 5.7). The frequencies are commonly called resonance (f_r) and anti-resonance (f_a). However, according to the performed measurement, the multilayer piezostack has several pairs of the resonances. The typical measured impedance curves of NOLIAC, EPCOS and PI active elements are presented in Figure 5.8. It is worth to notice that the resonances observed by author are well below the main resonance of piezostack, which usually appears in range of few hundreds kHz (depends on material, size and construction of actuator).

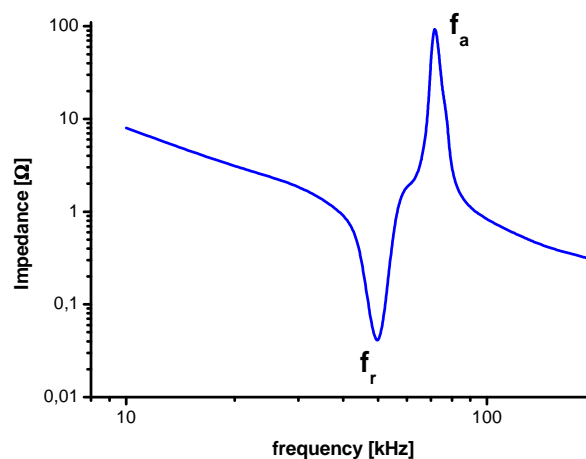


Figure 5.7 Typical example of an impedance-versus-frequency plot for piezoelement that indicates the resonance frequency (f_r) and the antiresonance frequency (f_a).

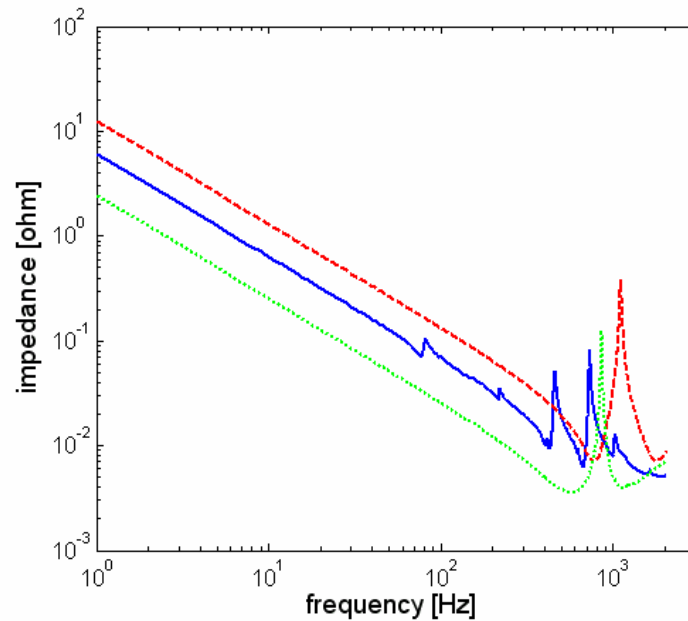


Figure 5.8 Multilayer piezostacks impedances. EPCOS (blue line), PICMA (green dotted line) and NOLIAC (red dashed line).

The method, developed by author, permit to use a piezostack as a static force sensor. During the measurement, it was observed that the impedance curve is changing in function of applied force. Especially, the position and amplitude of resonances were varying. The precise measurement performed at room and cryogenic temperature proved that this method might be used for case of FLASH. The results are presented in next subsections.

5.3.1. Measurement at room temperature

The effect was initially observed at room temperature (300 K), during the piezoelement classification. At that time, the impedance was one of the parameters, which was investigated. Each piezoelement was examined individually. The experimental setup is presented in Figure 5.9. The active element was assembled in series with piezoresistive force sensor – model 8415-6002 from BURSTER Company. At the top of the fixture, the screw for force adjustment was mounted. The stiffness of the fixture is well above the stiffness of the actuator and force sensor therefore it is possible to assume that all force generated by the screw is transferred to the DUT (device under test).

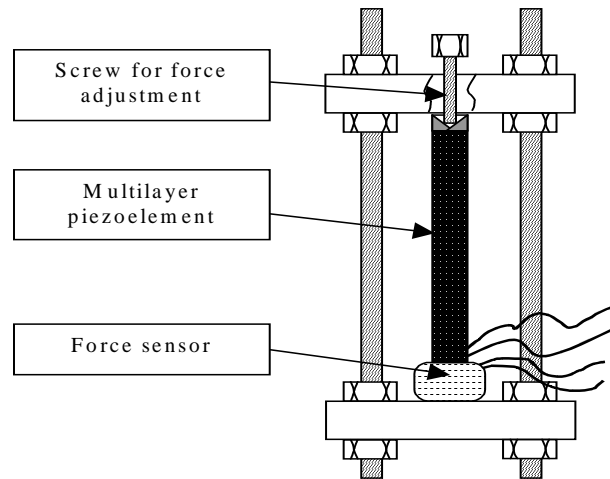


Figure 5.9 Setup for impedance change measurement

The actuator impedance was measured using Signal Analyzer SR785 for frequency range from 50 Hz up to 100 kHz. The voltage amplitude applied to piezostack was constant and equal to 1 V. The elongation of actuator and the force generated due to the 1 V applied to active device was neglected. The current flow was measured on resistance of 50 Ohms connected in series to actuator. The static force applied to piezostack was varying from 0N to 2 kN.

The example of impedance curve of two EPCOS piezostack is presented in Figure 5.10. The colour represents different preload force in BGR notification (blue smallest values of force – 0 N, green-middle, red-large values – up to 2 kN). Several resonances are visible, which are shifting right (to higher frequencies) when the preload is increasing. The behaviours of resonances are also changing. Some of them decrease in amplitude whereas the other increases. From performed experiments, the author found that the frequency of resonance is shifting in function of applied force. Figure 5.11 illustrates behaviour of two resonances – one around 30 kHz and the second around 65 kHz, in function of preload.

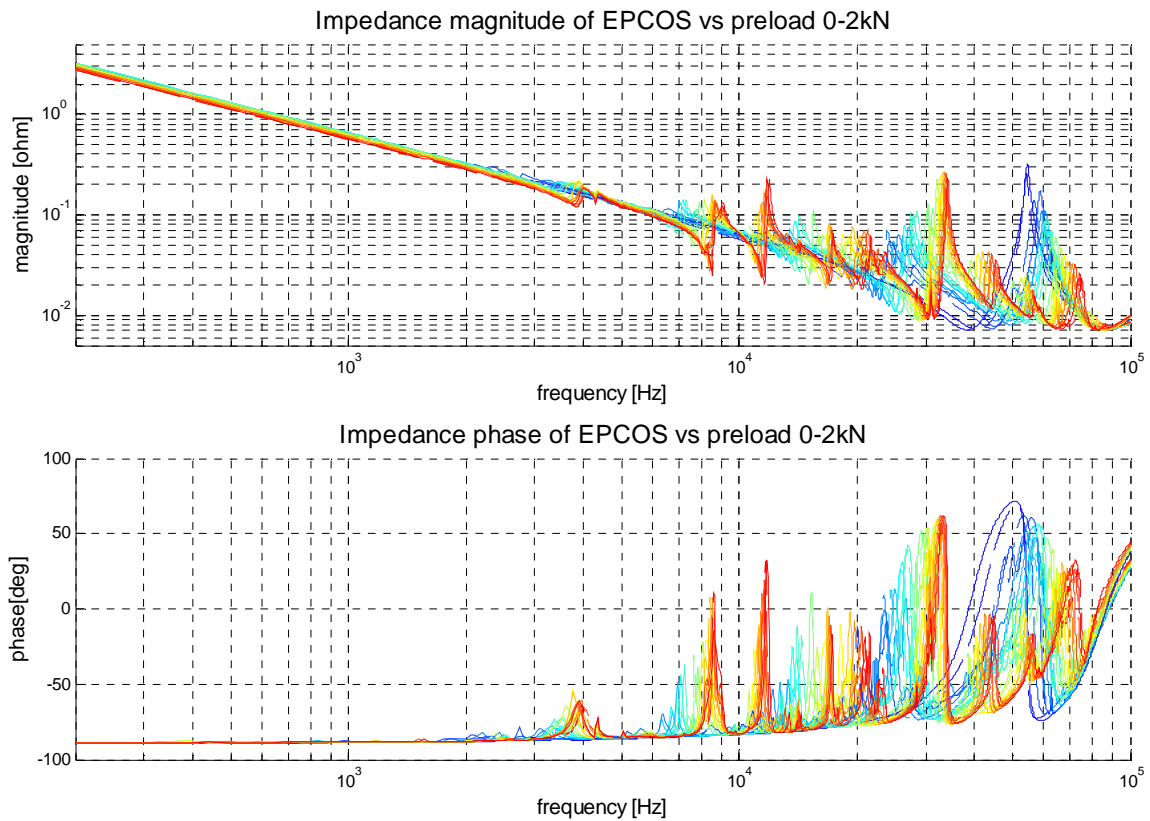


Figure 5.10 Impedance of two EPCOS piezostacks (dashed and solid lines) in function of preload from 0 N (blue) to 2kN (red). Measurements performed at room temperature.

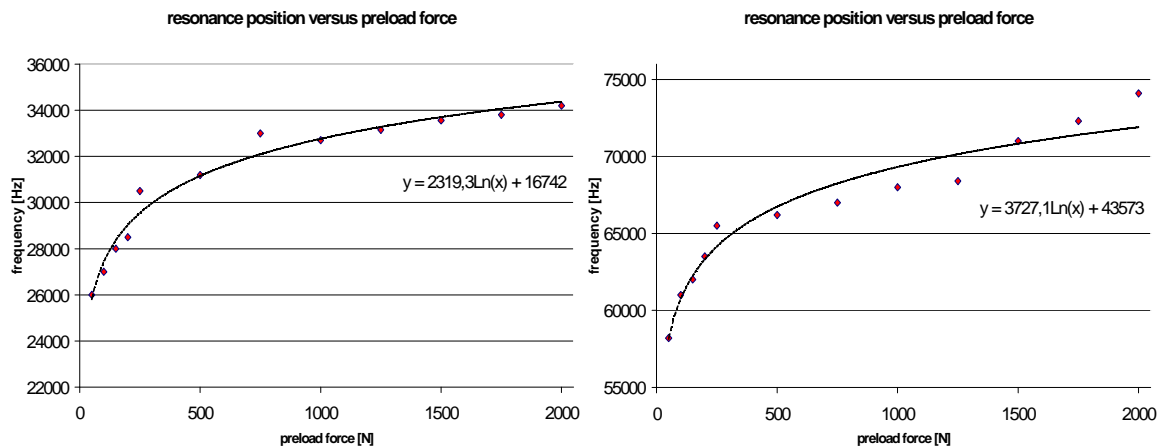


Figure 5.11 Resonance frequencies shift in function of preload for EPCOS piezostack- left figure for the resonance around 30kHz, the right for the resonance around 65kHz.

Both presented resonance shift shows the logarithmic dependency to the force applied to the piezostack. However, the coefficients of approximation are different for both resonances, what indicates that the higher resonance is not a first harmonic of the lower one. Moreover, several performed run shows that the resonance frequencies are shifting in the same manner with no respect of the fact that the element was stressed or relaxed.

Another advantage of this method is the information that for piezoelements from the same manufacturer line the shift of resonance remains constant. The proper test was performed for PI piezostack from ch0201 (3 samples), ch0214 (2 samples) and ch0215 (3 samples) series. It is obvious that because of different element type the positions of resonance are different than for EPCOS piezoelement (around 30 kHz and 60 kHz respectively). However, for known manufacturer the resonance shift is similar in function of applied force and vary for given preload by 2 kHz. The estimation of force is even more precise when the same manufacturer line of active element is used. Then the spread of resonance frequencies remains below few hundreds of Hertz what corresponds to force estimation error below 100 N.

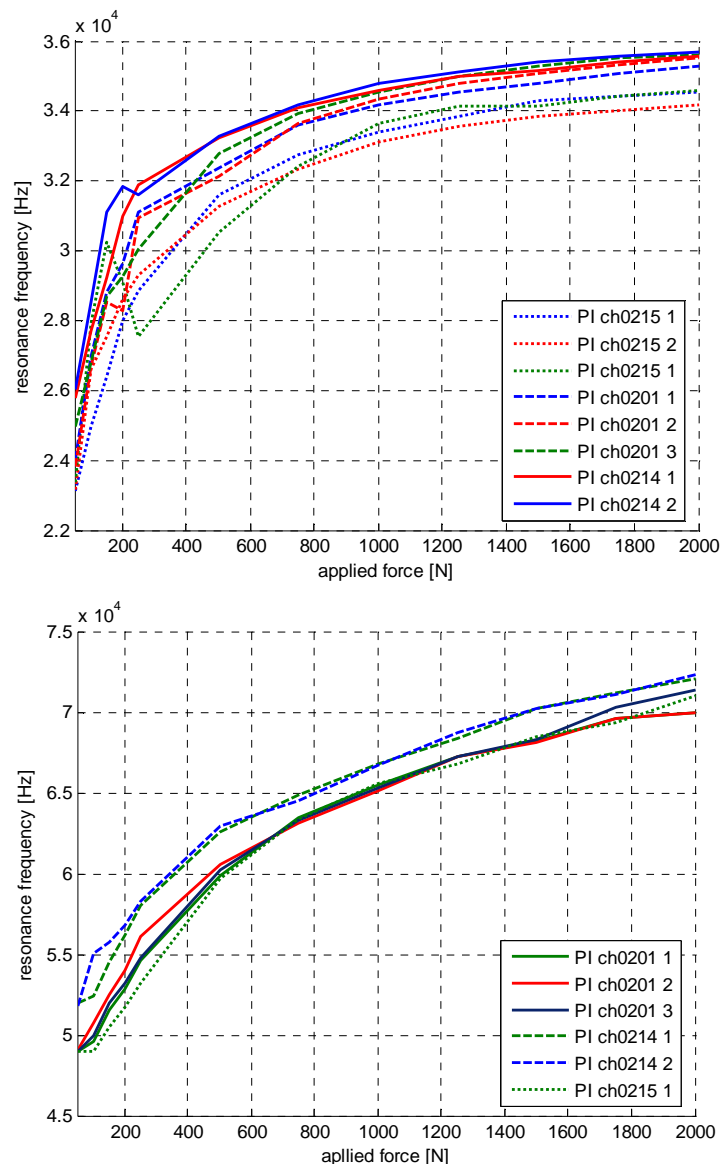


Figure 5.12 Resonance frequency shift in function of applied force for PI piezostack from ch0201, ch0214 and ch0215 series. Top figure shows resonance around 30kHz, bottom figure presents resonance shift around 60kHz.

One of the most interesting questions, which appear, is the one about the source of the described phenomenon. The author considers that the resonances, which are visible in multilayer piezoelements, are caused by acoustic waves [Bah 1992]. Applied force changes the boundary condition of each layer and thus it interacts with these waves. The effect is visible as a shift of resonances. Moreover, the amplitude of resonances are changing due the fact that wave reflection coefficient is strongly depended on the boundary condition of actuator volume. When element is relaxed at the end there is a loop of the wave, whereas when the end of element is fixed there is the node.

5.3.2. Measurement at LHe temperature

Next step for the estimation of force applied to the piezoelectric element inserted into the fixture assembled in tuner for FLASH is characterization of resonance shift at desired temperature. According to performed test, it is possible to conclude that the phenomenon does not disappear with decrease of temperature but due to change of parameters of active elements the position of resonances are different.

The experiment at LHe temperature might be divided in two parts. First of all, there is need to characterize the piezoelement in function of different preload, and then, it is possible to perform the test ‘in-situ’ of the actuators assembled in tuners. For the first part, a special cryostat was design at INFN Milan, Italy to characterize the piezostack. Using it, there is possible to cool down the actuator to desired 4K and then apply preload from outside of cryostat.

Basically the insert grants the possibility to exert a known force on the piezostack, keeping it in cryogenic conditions. This is achieved via an external device, placed at the top of the insert, in which spring-washers are coupled to a screwed ring to generate the test force (up to 2.5 kN). This force is transferred, by a long steel & G10 rod, to the device under test (DUT). A calibrated load cell, working at room temperature, is assembled in series. It is used for generated force measurement.

The insert for a vertical cryostat has been realized to host measurements in liquid helium environment. This insert hosts the DUT (in this case – the piezoelectric element) in a box under isolation vacuum. The box is immersed in liquid He in order to bring and keep the DUT at the temperature of 4.18 K. This satisfactory value can be considered as a good approximation of the real operating temperature of the piezoelement (almost 2 K, super fluid He condition), at least for what concerns electro-mechanical properties of the piezostack itself.

For piezostack impedance measurements, each piezoelement to be tested is hosted in a properly shaped aluminium support to avoid any non-vertical force component on the ceramic element; the

support element is then fixed inside the cold box. The thermal contact between the DUT and the LHe bath is also provided by four copper strings, which connect it to the bottom of the box.

The results of experiment are presented in Figure 5.13. It represents the resonance position of EPCOS piezostack at 4 K in function of applied force. However, the axes of figure are swapped. It allows to using this curve for estimation of force applied to piezoelement in CHECHIA stand test.

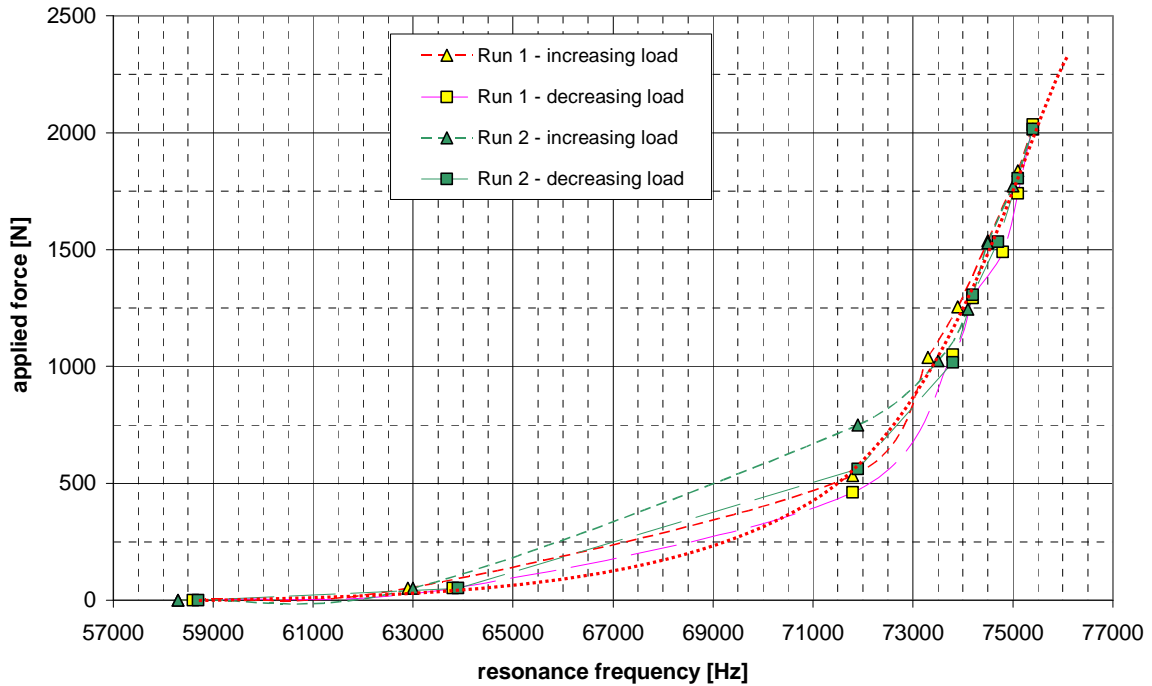


Figure 5.13 Resonance shift of EPCOS piezostack at 4K in function of applied force. [Bosotti 2005a]

The previous measurement allows estimating the force applied to piezostack, which are located in fixture of cavity tuner assembled in CHECHIA cryostat (see Figure 5.14). As previously, the EPCOS piezostack was used. There was a possibility to change the preload force by moving the position of stepper motor (used for so called slow tuner). The stepper motor might be moved from 0 up to 1 million of steps. The resonance position was monitored in function of location of stepper motor. The shift of resonance around 70 kHz is presented in Figure 5.15.

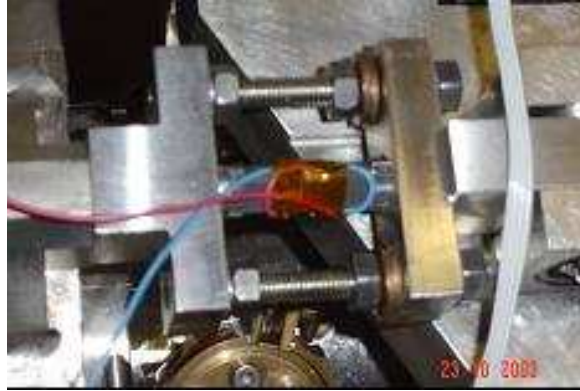


Figure 5.14 Photo of single fixture with EPCOS piezostack. The fixture is assembled to the cavity tuner in CHECHIA cryostat.

A comparison of the result from Figure 5.13 and Figure 5.15 allows estimating of preload change. Proper calculation is illustrated in Figure 5.16. As a result one can judge that the force applied to piezostack was changed from almost 850 N down to 30 N. Further movement of stepper motor was dangerous because the piezoelement could fall out from the fixture.

The presented above method is not very precise one, but it allows to roughly estimating the force applied to piezoelement. It does not require any additional sensor assembled inside the test stand but relays only on parameters of the piezostack. Furthermore, it do not requires an expensive lifetime test for static force sensor, which are should be performed in case of using the strain gauge device. It is worth to remind that the whole tuner will be mounted to cavity and closed inside the cryomodule. Any part might be exchanged or replaced during the module operation, which is planed for at least ten years.

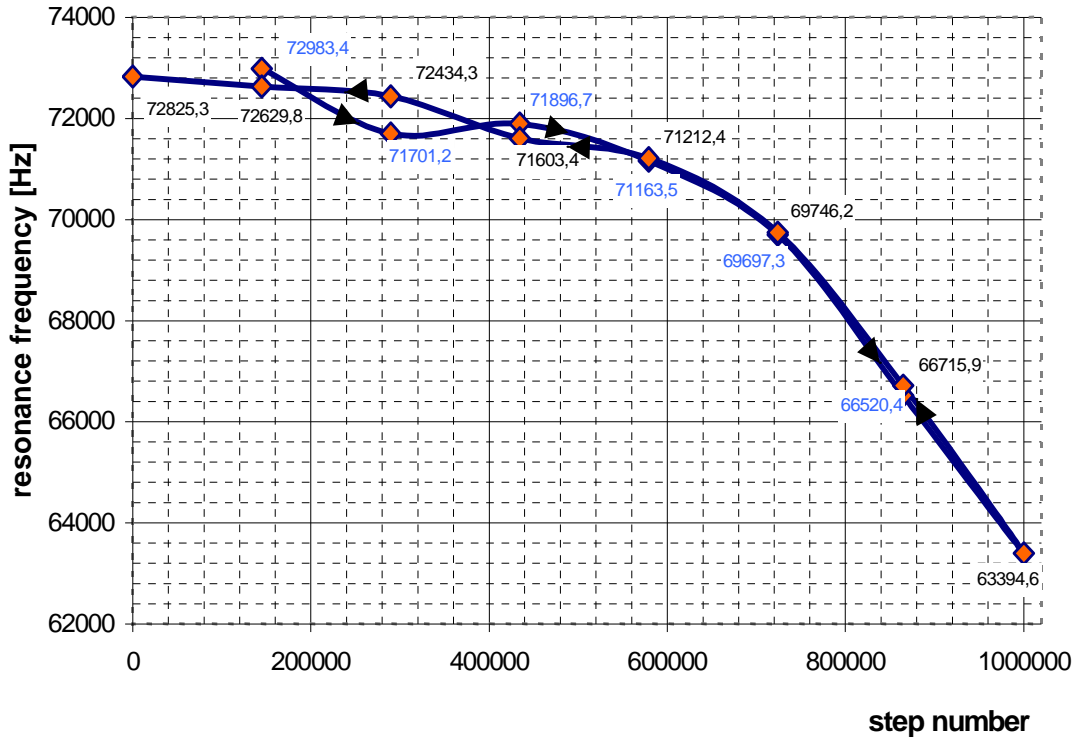


Figure 5.15 EPCOS piezostack resonance shift in function of position of stepper motor. Test done in CHECHIA. Resonance around 70kHz.

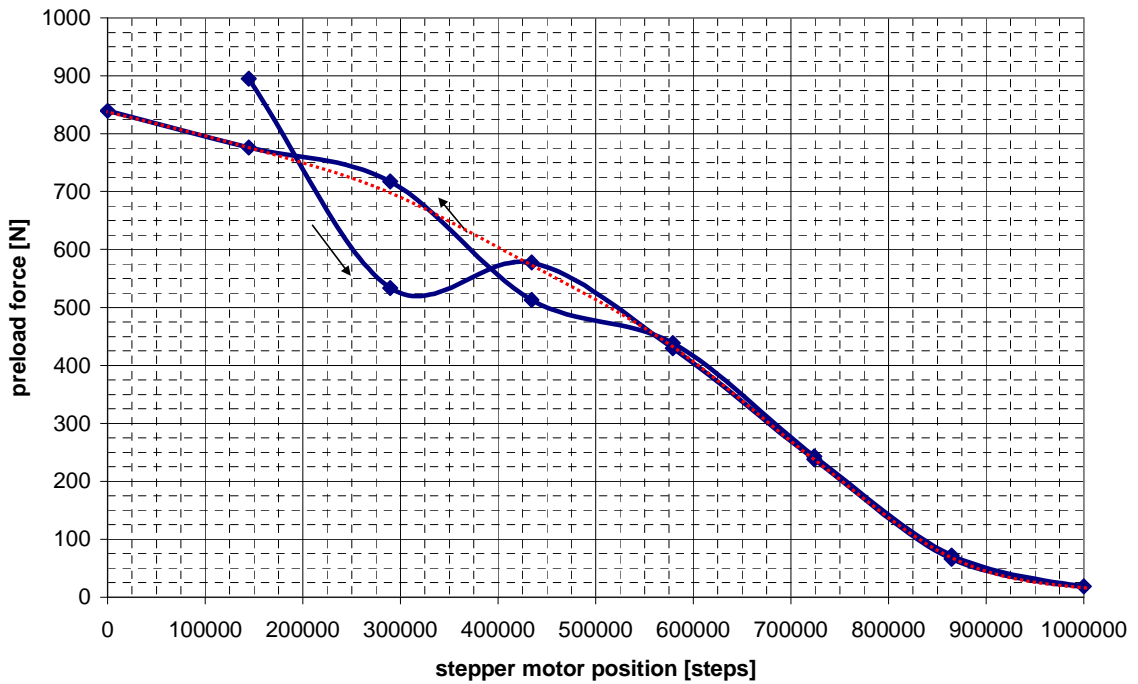


Figure 5.16 Change of force applied to piezostack in function of position of stepper motor (CHECHIA stand test) when motor moved upward and downward. Red dotted line is smoothed estimation of force.

Simultaneously, the measurement of resonance frequency of the cavity was performed for different position of stepper motor. The curve presented in Figure 5.17 is a result of this test. The dependency between cavity resonance frequency and stepper movement is fully linear (R^2 is equal to 0.9998). There is need to move stepper motor by 1343 steps for 1 kHz change of cavity frequency. This information will be also used for design of multi-pulse algorithm for Lorentz force compensation described in chapter 6.4.2.

From the same figure it is possible to find that for proper pre-tuning in which cavity should reach desired 1.3 GHz frequency, the force applied to piezostack is equal to 378 N. These value comes from information covered in Figure 5.17, where 1.3 GHz corresponds to 617982 steps. The results is finding by applying this value to the data presented in Figure 5.16.

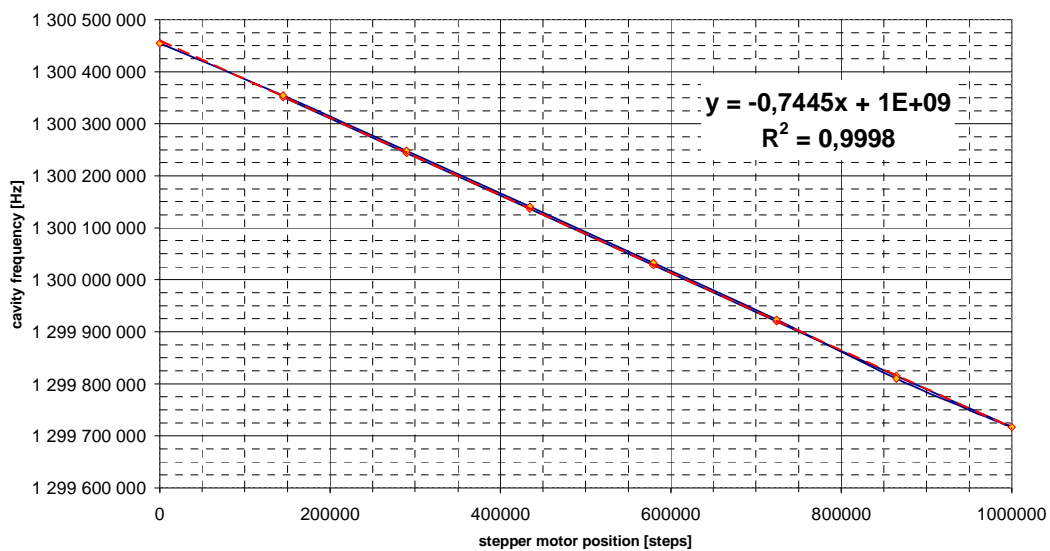


Figure 5.17 Resonance frequency of cavity in function of position of stepper motor.

It seems that piezoelement was not enough preloaded. According to manufacturers the preload force should be set to one third of the blocking force to ensure maximal lifetime. The blocking force in case of used piezostack is 3.2 kN, thus the preload should be slightly over 1 kN.

5.4. Capacitance change

As it was mention at the beginning the impedance was only one of the parameter, which was investigated. One of the other parameters was the capacitance of the piezostack. From electrical point of view it is a key element of the impedance. Proper measurement of capacitance change versus applied force at 4 K was performed in IN2P3 Orsay, France. As it was expected, the preliminary results done with Piezo JENA (#9222) stack shows that, the capacitance is also changing versus the piezostack preload (see Figure 5.18). The behaviour of change is exponential, the same manner as it was with impedance resonance shift. The main disadvantage of this method

is small change of capacitance (0.71 nF / 1 N) caused by applied force in comparison to capacitance of the active element (4 μ F). During measurement there is need to minimize all noises.

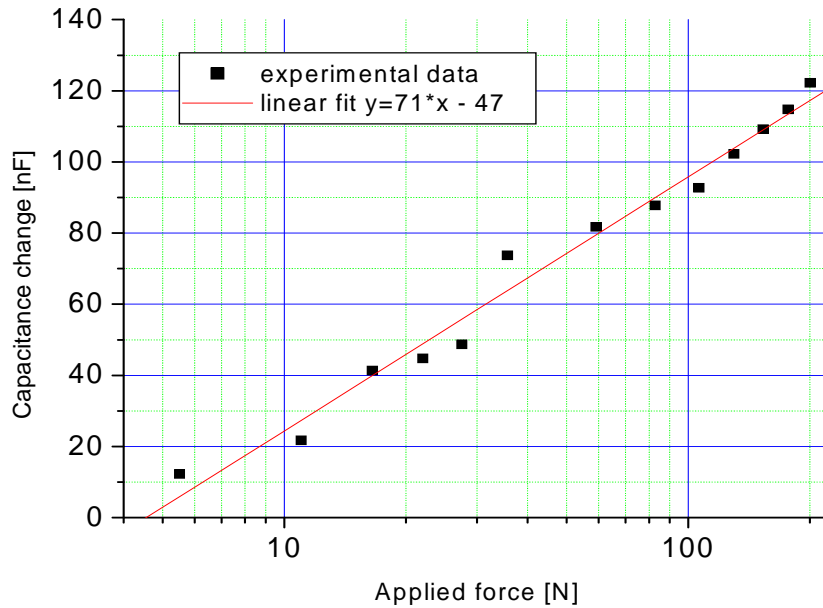


Figure 5.18 The change of capacitance of Piezo JENA (9222) versus applied force at RT.

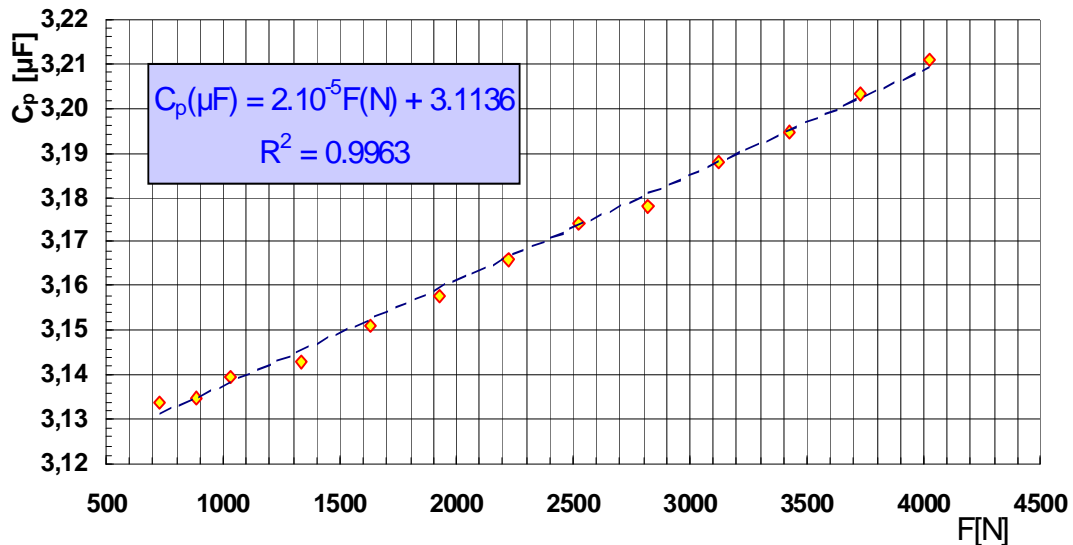


Figure 5.19 Capacitance of PICMA piezoelectric actuator versus preloading force at $T=4.4$ K, vacuum pressure 10^{-5} mBar. Test performed at IPN-Orsay in July 2005. [Fouaidy 2005]

The sensitivity of capacitance change to applied force ($\Delta C_p / \Delta F$) of the PICMA piezoelectric actuator was measured in the wide temperature range from 1.68 K up to 300 K. As it was expected the $\Delta C_p / \Delta F$ decreases monotonously with temperature. The maximal value is for room temperature and is equal to 426 nF/kN @ $T=295$ K, whereas the minimum is for $T=1.7$ K and is equal to 16nF/kN. The change of sensitivity is presented in Figure 5.20.

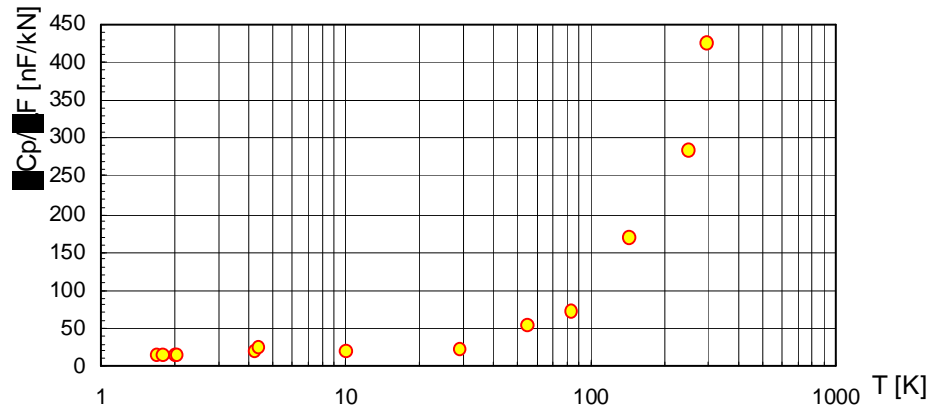


Figure 5.20 Sensitivity of piezoelectric actuator to preload force versus temperature

5.5. Conclusion

In the chapter different methods of static force measurement was presented. The standard solution, which base on strain gauges demands additional wiring. Moreover, the device, which will hold this sensor, needs some additional place. Furthermore, the sensor needs to be tested to check its lifetime. At least, additional element requires extra cost. It is a reason to use presented solution, which base on characterization of piezoelectric stack itself. Two methods were described – resonant frequency shift on the impedance curve and capacitance change. Both methods might be used in parallel to guarantee proper measurement. Preliminary results show that the sensibility is sufficient for case of preload determination and allows to measure the force with resolution of hundreds of Newtons. As a consequence, it is possible to apply the correct – optimal – preload to piezostack and therefore it is possibly to increase the lifetime of the actuator.

Chapter 6. Fast tuning system

6.1. Introduction

As it was proven in previous chapters (2 and 4), a fast tuning system to counteract Lorentz force and microphonics is necessary to operate cavities at high field. The system must be fully integrated with existing slow tuner used for pre-tuning purpose. Authors propose to use a smart material based actuator. Multilayer piezoelectric stacks, which are described in Chapter 4 are suitable for fast tuning function. These devices are reliable enough, might work at required hard environment and what is the most important they fulfil design requirements.

Depending on the maximal gradient the different actuators might be used. For example, for FLASH purpose (for gradient up to 20 MV/m \Leftrightarrow <200 Hz of detuning) an EPCOS's piezoelement of cross-section of 8x8 mm is sufficient. However, for higher gradients there is need to use active devices, which have higher stroke. In example for X-FEL linac a 35 MV/m cavities are planned, therefore a 600÷800 Hz of detuning is expected. For this purpose a piezoelement with higher cross-section and higher blocking force, as the ones from PI or Noliac (cross-section of 10x10 mm), are needed. Nevertheless, the main concept for compensation remains the same. In this chapter a detailed description of electromechanical tuning system is given.

The overview of the system is presented in Figure 6.1. It can be divided into three main parts. One of them is a software part, which consists of GUI interface, MATLAB script including all functions, as well as implemented algorithms and finally DOOCS servers dedicated for electronic device control (drivers). This part is described in subchapter 6.4.

The middle part of control system is an electronic hardware part. It consist of a function generator (D/A converter), a filter, PZD and PZM amplifiers, A/D converters and probes antennas. It is presented in details in subchapter 6.3. The piezostack which is driven by PZD amplifier is inserted into the fixture, which is internal part of mechanical tuner. In the Figure 6.1 the piezostack is connected directly to the cavity, but there is need to keep in mind that there is a complex mechanical system of tuner itself and the whole cavity environment assembled in cryomodule. More details might be found in next subchapter (6.2).

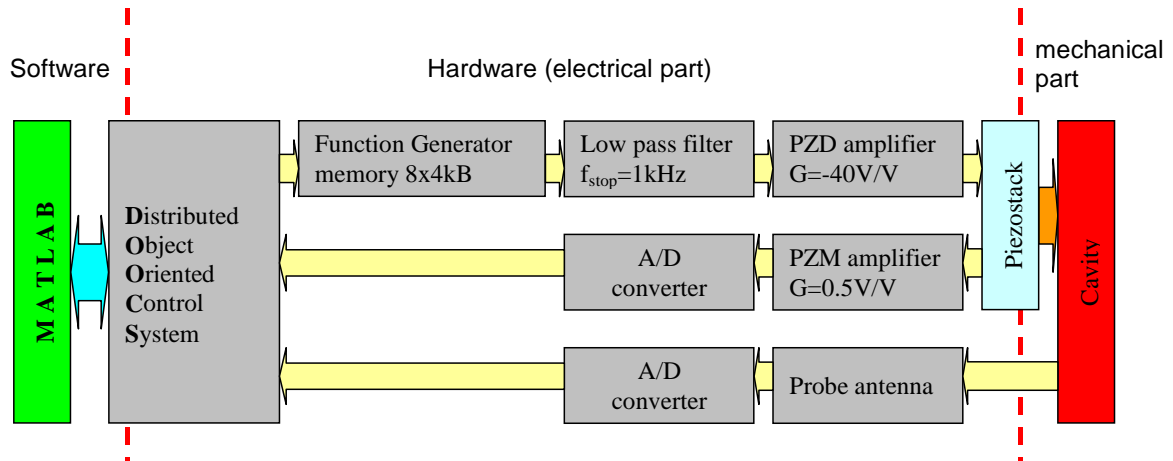


Figure 6.1 Overview of control system

At the end of Chapter 6 two experiments with single pulse and multi-pulse compensation are presented. Moreover, a feed forward control algorithm used for automatic operation is described in subchapter 6.4. The results of the performed experiments with exhaustive description are collected in next chapter.

6.2. Mechanical part – Cold Tuning System

During the research, the author has an opportunity to cooperate with Commissariat à l’Energie Atomique (CEA) from Saclay, France. The laboratory is involved mainly in mechanical design of the tuners. They developed and produced the Cold Tuner System (CTS) used in module ACC1 in FLASH accelerator.

Initially, the CTS was able to work only as a slow tuner. For this purpose a double lever system with ratio 1 to 17 was designed (see Figure 6.2). To move the arms a stepper motor from PHYTRON with harmonic drive gearbox is used. One arm of tuner is attached to helium tank with three anchors. The second one is attached to cavity flange. The cavity is attached to helium tank at the opposite side to the tuner. When stepper motor is stimulated then depending on the direction of movement the cavity is pushed or pulled. The theoretical resolution of system is 1.5 nm/step but due to the mechanical backlash system might be operated with teens of steps. The maximal displacement is ± 5 mm, what corresponds to ± 2.6 MHz of frequency change.

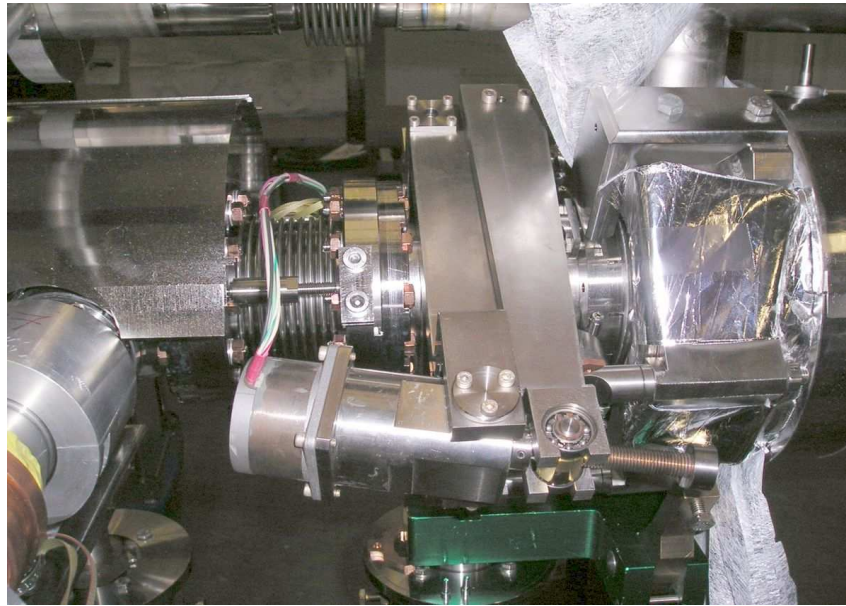


Figure 6.2 Photograph of CTS tuning system attached to the cavity.

The presented system proved its functionality as a slow tuner. Nowadays, each FLASH cavity is equipped with such a device, which allows adjustment of resonance frequency to desired 1.3 GHz. However, the stepper motor is too slow to use it during the RF pulse and it cannot be used for Lorentz force compensation. That is the reason to implement the active element build of smart materials. The principle idea of fast tuner is showed in Figure 6.3. The piezoelement is assembled between the helium tank and the slow tuner mechanism. In the original design there was one of three anchors, which hold a tuner at right position. Depending on the type of fixture it can hold one or two piezoelements. There is also a possibility to replace it by the magnetostrictive tuner.

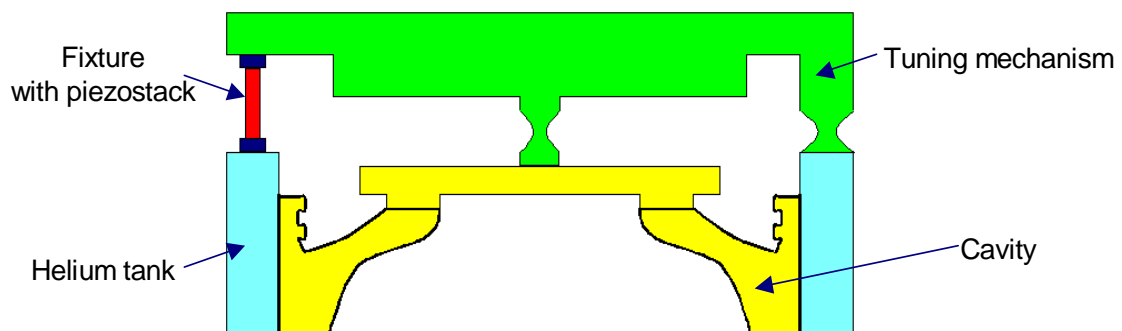


Figure 6.3 The idea of fast tuner based on piezoelectric stack

The same laboratory is also responsible for the new design of Piezo Tuner System (PTS) [Bosland 2005]. The fast and slow tuners are fully integrated and problems with the previous version of device (CTS) are solved. The test of the tuner is scheduled for beginning of 2006 year.

Piezoelectric devices assembled either in CTS or PTS might be connected to the same electronic control system. Its detailed description is presented in next subchapter.

6.3. *Electronic part*

The hardware (electronic) part might be separated in two subsystems. One of them is used for signal generation; the other one is dedicated for reading of system response. The first one consists of the function generator, low pass filter and PZD amplifier; the second one is a readout system, which includes PZM amplifier, probe antennas and A/D converters.

The function generator FG is a D/A converter [Rehlich 1999]. It is compatible with VME standard and might be controlled via DOOCS system. It has two separate output channels. Each of them might store up to 32 kB of 16 bits words (8 banks of 4 kB for each channel). The data might be loaded through DOOCS system i.e. from MATLAB. There is a possibility to load each bank separately or to upload all banks at once. In our solution, the second method was chosen to eliminate any error values, which might appear during operation.

The system is connected to clock signal of 9 MHz (maximal clock frequency up to 10 MHz). To slow down the system, there is a possibility to use a build-in clock divider. In the presented tuning control system, the value of the divider is set by MATLAB script in the initialization stage. It depends on the repetition rate of RF system. The FG is triggered with the RF field (from 1 to 10 Hz). Thus, the period of clock signal multiplied by number of words stored in memory and the value of divider must be always higher than the time between two pulses. It is due the fact that the pulse applied to the piezostack is generated before the RF system trigger. As a consequence, the function calculated in MATLAB is written usually to the last and first bank of FG in such a way that the last value of last memory bank must exactly match the first value of first bank. It is a weak point of the presented solution, however the repetition rate is very stable and the deviation of time is much below 100 μ s. As a consequence, the low pass filter will eliminate the noise caused by this misalignment.

Another disadvantage of FG is a quantization of output voltage. If the FG has been connected directly to piezostack through PZD amplifier, the current peaks would appear. It is due the fact that actuators used in the current solution might be regarded as capacitors, which need to be reloaded in very short time and consume current. The value of peak current might be calculated. The parallel capacitance of the active element at LHe temperature varies from 1.5 μ F to 3.3 μ F (refer to Chapter 4.2.1). The FG might store one of 65536 values (16 bits). The output voltage might be in range ± 5 V. The signal is then amplified by PZD with gain -40 V/V. The quantization step is then around 6.1 mV. If we assume that the rise time of clock is 100 times shorter than its width, the peak current might be in range of 100 Amps. That is the reason to implement a low pass filter.

The bandwidth of low pass active filter is set to be a 1kHz. From mechanical simulation and experiment, one can find that higher modes do not have a strong impact on the cavity behaviour.

The filter is inserted between the output of FG and input of PZD amplifier. The input and output impedance are adjusted in such a way that the gain is equal to 1V/V.

Next element of the control system is a PZD transducer. The device base on APEX power booster PB-58a. The gain of amplifier is -40 V/V. The output voltage might vary from -60 V to 160 V. The current is limited to 2 Amps for up to 5 ms period. The rise and fall time (full scale) is slightly over 200 μ s for 1 μ F load. The device was initially designed to work with capacitance load up to 3 μ F. Such a parameters of piezostack driver allows to operate the piezostack presented in Chapter 4 and to obtain a slew rate of elongation higher than required value of 1 μ m/100 μ s.

Between the output of PZD transducer and the cryomodule, there is a distance of around 120 m. A pair of coaxial cables with common shields is used for differential signal transmissions to reduce noise and signal degradation. A special feed-through connector is used to send signal into the cryomodules. Inside the module a standard low temperature tolerance Teflon wires are used to connect piezostack with feed-through connector.

The read-out part of electronic system consists of devices used commonly at FLASH. The probe signal antenna measures the accelerating field gradient inside the cavity. Moreover, forward and reflected power antennas are used. All three are connected to A/D converters assembled in VME crate and might be operated through DOOCS.

In addition, especially if the tuner holds two piezoelements, there is possibility to connect one of active device as a sensor. The adjust impedance a PZM transducer is used. The gain of the device is 0.5 V/V. The output of PZM might be connected to the ADCs.

All signals are accessible from DOOCS system and might be observed from *rpc panel* (it is a build in software for DOOCS server investigations and property changing). The addresses of servers depend on the location of devices. It is possible to read from and write to given device using a MATLAB. The description of software part is presented in next subchapter.

6.4. Software part

The control system for piezostacks must be reliable and easy to operate for end-user. It is the reason that during the research the author decided to use MATLAB environment. It not only allows building a Graphical User Interface GUI using built-in GUIDE, but also permits easy communication with DOOCS system, which is commonly used at DESY for operation of FLASH accelerator. However, the main reason of choosing MATLAB environment was flexibility of algorithms design and model description.

Thanks to the GUI the end-user might easily operate the control system dedicated for fast tuning. Clicking on the button invoke functions written in *.m* file. The used solutions help to build a

modular script in which sets of separate functions are collected. The main window of Piezo Control Panel (PCP) is presented in Figure 6.4.

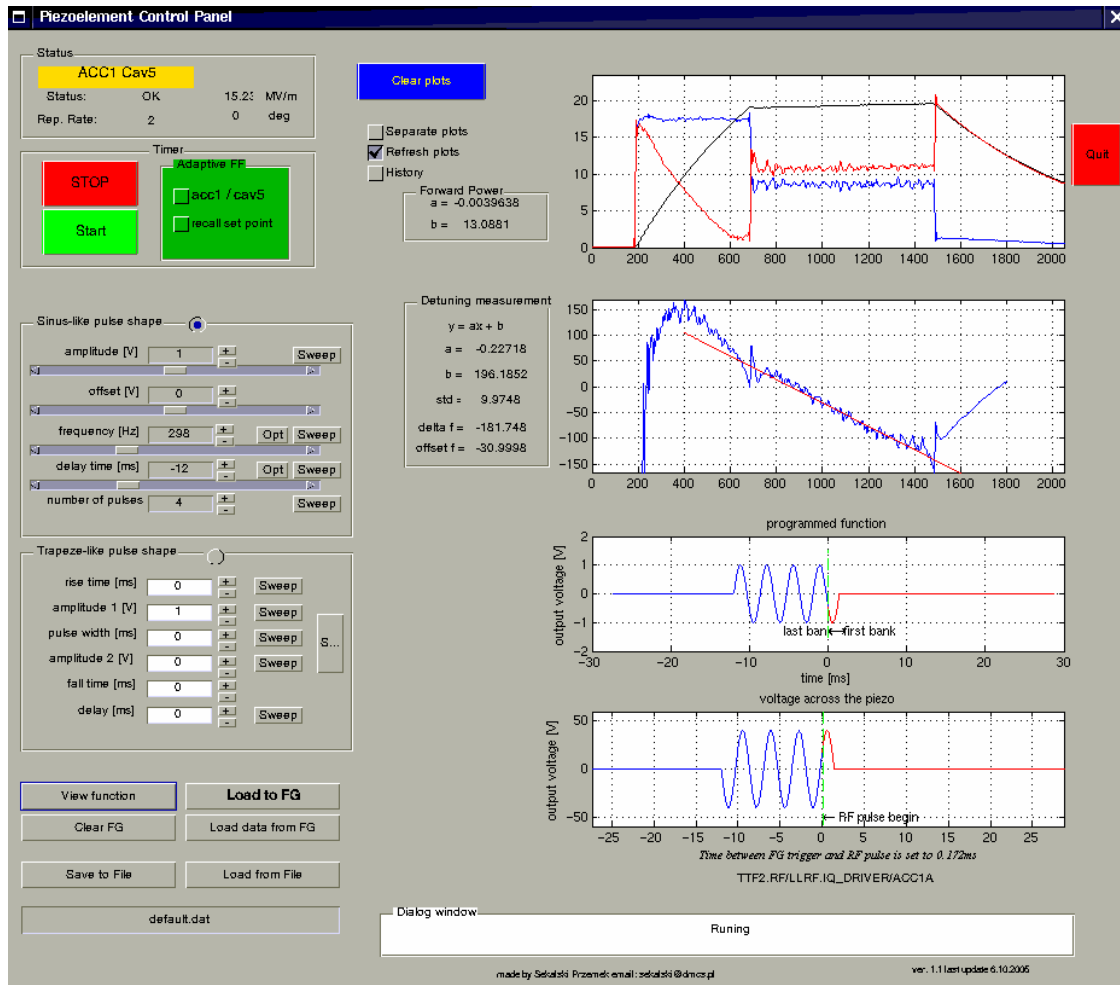


Figure 6.4 Panel for piezoelectric devices control

The PCP allows to measure the forward and reflected power as well as probe signal within given cavity (top right subplot in Figure 6.4). Using these parameters the detuning is calculated according to the algorithm described in Chapter 2 (a blue curve on the second subplot). The detuning is linearly approximated during the flat-top of RF pulse. The coefficients are written on the left side of the subfigure. Moreover, a standard deviation between the measurement and approximation is calculated. To simplify the interpretation of the polynomial values, detuning during pulse duration and offset of detuning in the middle of a pulse are shown in Hertz. The two bottom subplots show a signal stored in the memory of the function generator and the one applied to piezostack after amplification.

The PCP communicates with the function generator, and ADCs through dedicated DOOCS servers. Two MatLab functions are used: to read (*ttfr*) and to write (*ttfw*) the properties to/from servers. The names of the servers depend on the location.

During the PCP initialization, the repetition rate of RF pulses is checked and the divider in FG is set to proper value (refer to 6.3). The detailed description of PCP functionality is presented in Appendix A. The experiments, which helped to develop the feed forward algorithm, are presented in next two subchapters, but the algorithm itself is described separately in chapter 6.4.3.

6.4.1. Single pulse compensation method

The easiest way to compensate detuning caused by Lorentz Force is to find a transfer function between voltage applied to piezostack and detuning caused by this action. Unfortunately, due to the fact that the system might work only in pulse mode, it is very hard to perform such an experiment. As a consequence, the author decided to investigate the influence of different shapes of the pulse to the detuning compensation. At the beginning a single pulse method has been chosen. A piecewise linear function was used. The following parameters have been examined: rise time (t_{rise}), fall time (t_{fall}), the shift time between the beginning of the piezo signal and the RF pulse (t_{delay}), width of the pulse and two amplitudes $A1$ and $A2$ (see Figure 6.5). Each parameter has been varied independently and the coefficients of linearization were observed. Moreover, a standard deviation between linear approximation and measurement has been calculated. This parameter has been used to find if the estimate used for the purpose is sufficient enough.

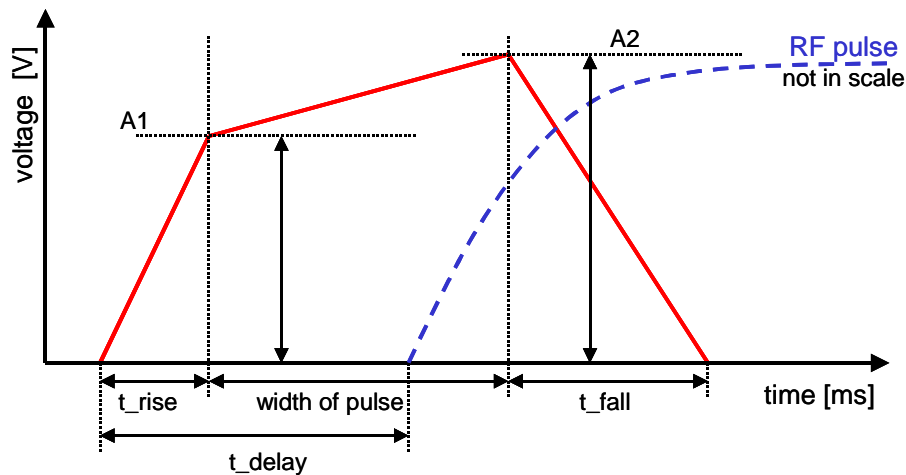


Figure 6.5 Shape of the pulse with variable parameters.

At the beginning the both amplitudes of signal ($A1$ and $A2$) were set to 80 V. The rise time was the same as the fall time and was equal to 0.1ms. The width of the pulse was set to 1ms. The delay time between the beginning of the signal applied to piezostack and RF pulse was varying from -1.2 ms to $+1.3$ ms. The coefficients of the linearization of detuning during flat-top in function of delay time are presented in Figure 6.6.

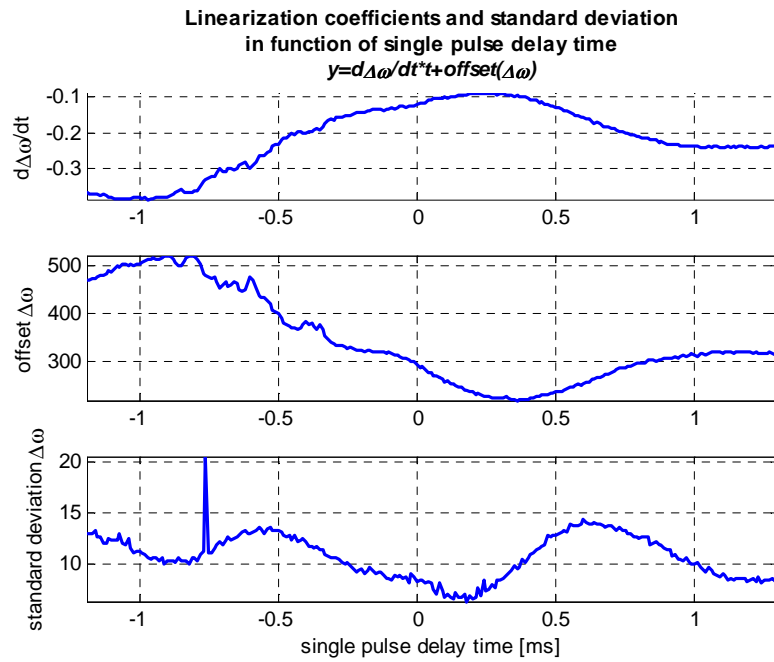


Figure 6.6 Coefficients of detuning linearization and standard deviation from measurement in function of delay time between beginnings of RF pulse and piezostack signal.

One can find that the value of slope is the highest ($-0.089 \Leftrightarrow 75$ Hz of detuning during the $800\mu\text{s}$ RF pulse duration) when the delay time is equal to 0.27 ms. For further investigation the delay time was set to this value. Then, the offset and standard deviation is close to the minimum value (223 Hz and 8 Hz respectively).

Next a width of the pulse was investigated. It was changed from 0.1 ms to 1.1 ms. The amplitudes of signal (A1 and A2), rise and fall times were set as previously. The result of sweeping is presented in Figure 6.7. The peak in standard deviation curve around 0.9ms is caused by measurement error.

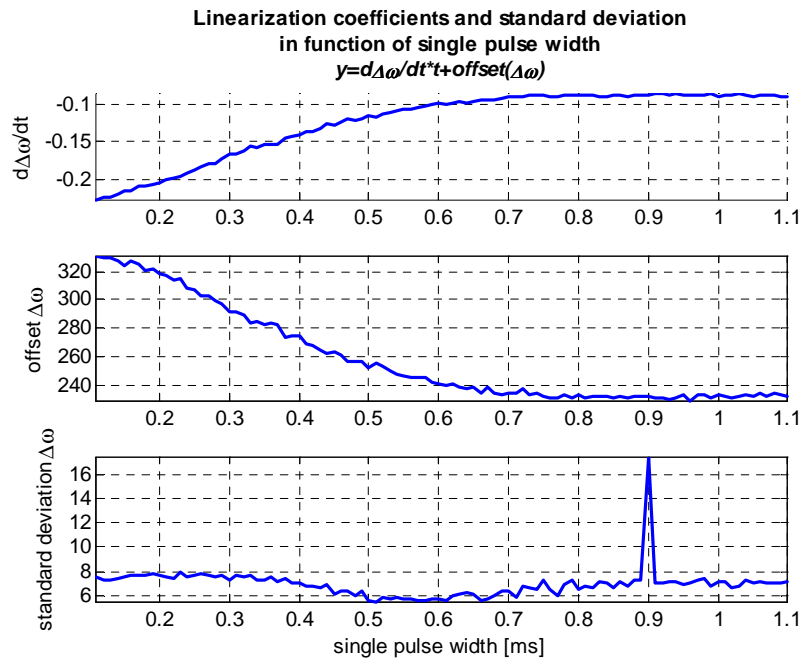


Figure 6.7 Coefficients of detuning linearization and standard deviation from measurement in function of width of the piezostack signal.

From these measurements one can find that the longer pulse the more reduced the Lorentz force effect. However, the saturation appears when the pulse is too long. It is easy to explain this behaviour because the length of RF pulse is only 0.8 ms. In other words it means that the pulse applied to piezostack lasts longer than RF pulse itself. Another effect that needs to be taken into account is the fact that the piezostack work in a dynamic mode. As a consequence, the constant voltage does not mean that the piezo keeps its elongation, but it means that it starts shrinking. For further investigation a width of the pulse was set to 0.8 ms.

After that, the rise time of the signal was investigated. The rise time was varying from 0.1 ms to 1.1 ms. The point when the pulse reaches the amplitude A_1 was fixed. The result of sweeping is showed in Figure 6.8. From this measurement one can find that the shortest rising time the stronger piezoelectric stack action (it is also a proof that piezostack really works in dynamic mode). It is due to the fact, that piezos are driven by the electric charges accumulated on plates inside the actuator. For further investigation the rise time was set to 0.1 ms. There is no reason to use shorter time because the amplifier and the filter will not transmit the signal.

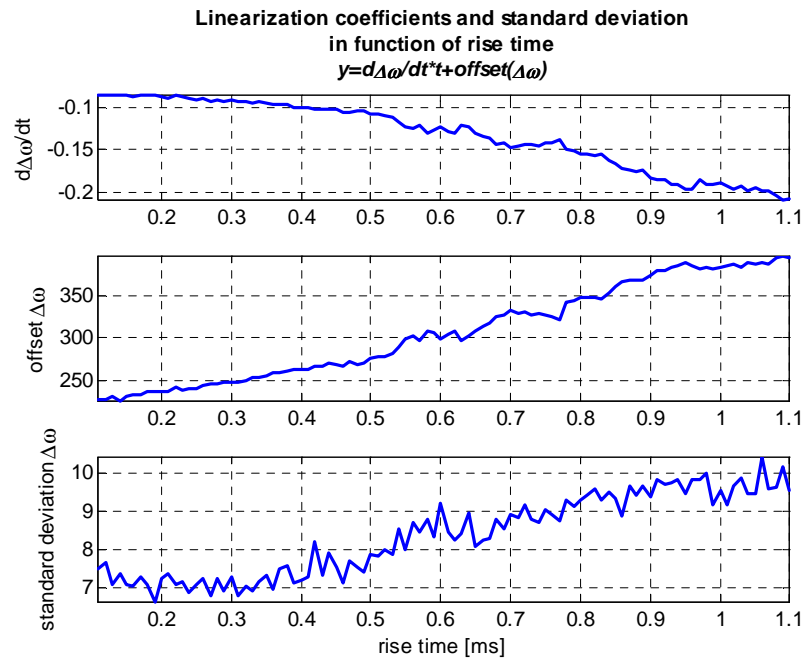


Figure 6.8 Coefficients of detuning linearization and standard deviation from measurement in function of rise time of the piezostack signal.

Further, the amplitude of signal applied to piezostacks was altered from 20 V to 120 V. The A2 was constant and equal to 80 V. The result is shown in Figure 6.9a. The experiment was performed twice because during measurement the settings was changed, what is visible as a step around 93 V (red dashed curve). However, reproduction of experiment proofs that the piezostack behaves in the same manner. Nevertheless, the most important thing, which can be driven from the test, is the fact that even for value of 120 V the first linearization coefficient stays below the zero. It means that even if piezostack is supplied by maximal voltage the action is too weak to compensate the detuning caused by Lorentz force. The similar effect was observed when the A1 amplitude was constant (80 V) and A2 was varying from 20 V to 120 V (see Figure 6.9b).

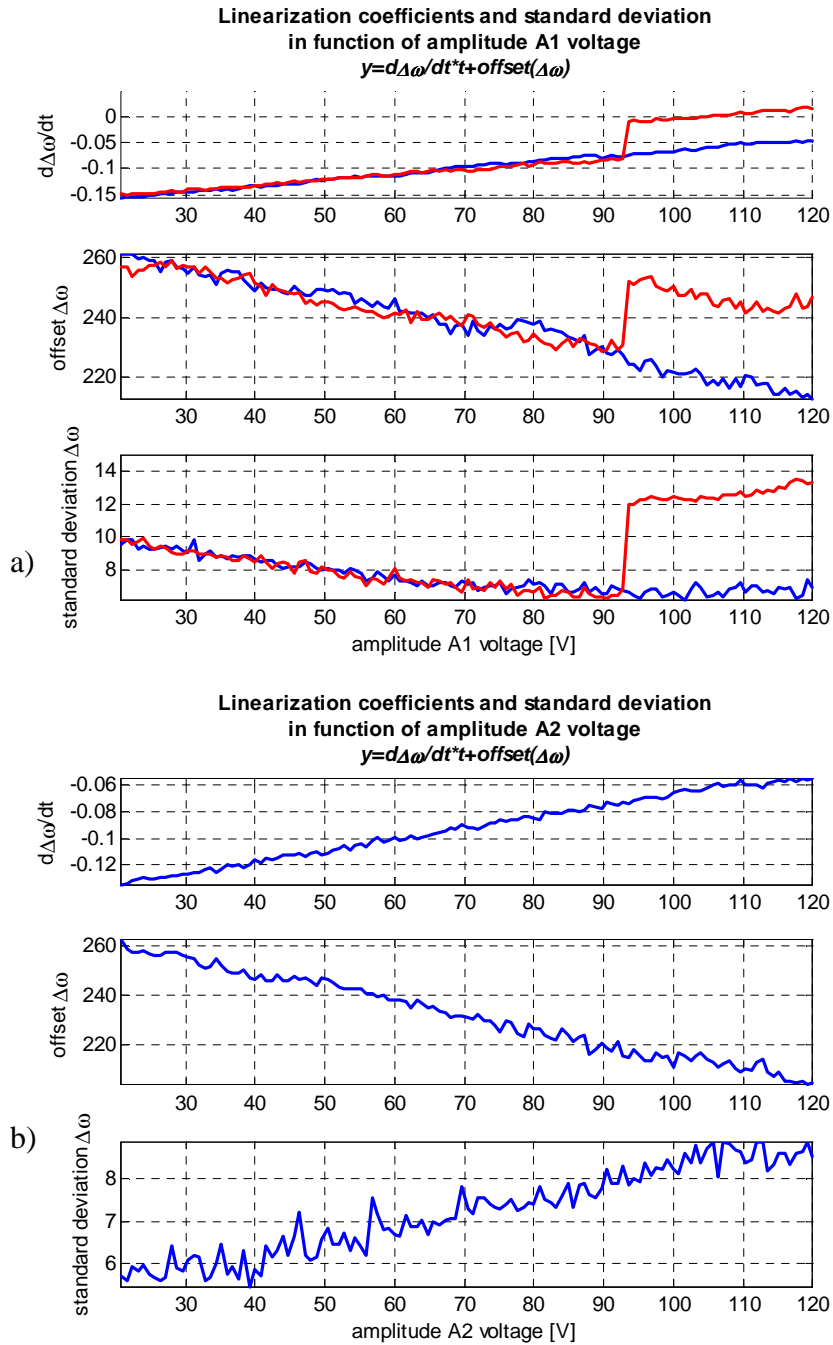


Figure 6.9 Coefficients of detuning linearization and standard deviation from measurement in function of amplitude A1 (a) and A2 (b) of the piezostack signal, when changed independently.

To allow a full compensation one should apply over 200 V to the EPCOS piezostack. The actuator is assembled in FLASH therefore the authors preferred to stay far from the limits not to destroy the active element. Another option to increase the piezostack influence is to increase both voltages simultaneously. For given parameters of pulse founded in previous test (rise time=fall time=0.1 ms, width of pulse=0.8 ms and delay time=0.27 ms) and varying amplitude of both A1 and A2 parameters the measurement of detuning was done. The results are shown in Figure 6.10.

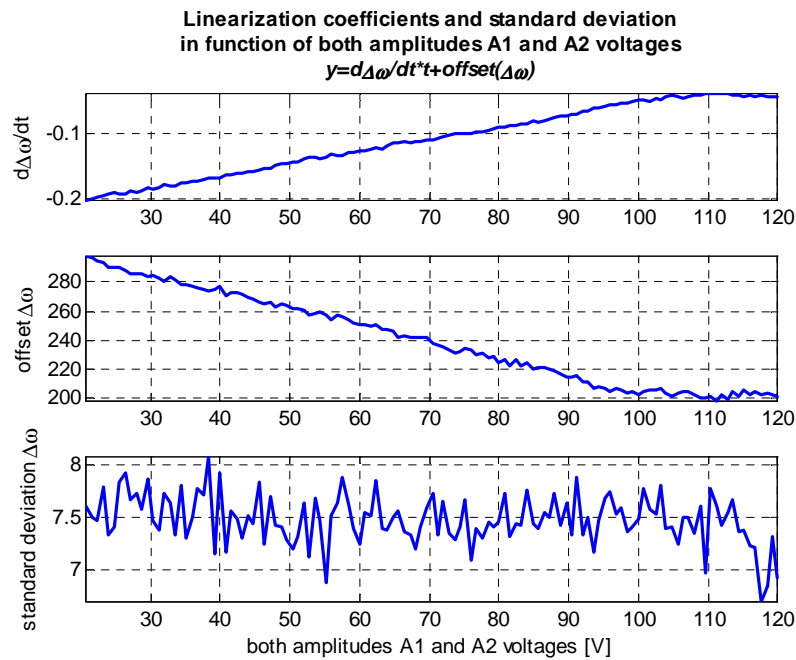


Figure 6.10 Coefficients of detuning linearization and standard deviation from measurement in function of amplitude A1 and A2 increased simultaneously.

On the top subfigure, above 110V the saturation appears. It is due to the amplifier limitation. The piezostack behaves as a capacitor. The capacitance is in range of 2 μF . When a voltage arises too quickly (over 100 V/1 μs), the needed current to reload piezostack is over 2 Amps. To reduce the heat dissipation the PZT driver has an internal limitation of current set to 2 Amps.

As a consequence, one can find that using a single pulse method there is a need to use either a stronger piezostack or higher power amplifier. However, the authors propose to use another method, called multi-pulse, for which current setup is sufficient. The proposed algorithm is presented in next subchapter.

6.4.2. Multi-pulse compensation method

Another method proposed by Authors is to use a repetitive stimulus. In this case if a proper signal frequency is used a mechanical vibration will arise. As a consequence, smaller voltage applied to piezoelement might have a stronger influence. The proper tests to prove this method are presented in this subchapter.

As previously a set of parameters was investigated. To simplify the study a sinusoid function has been chosen. Its frequency, amplitude, number of pulses and the delay time between the beginning of the signal applied to piezostack and the RF pulse (see Figure 6.11) are the variables.

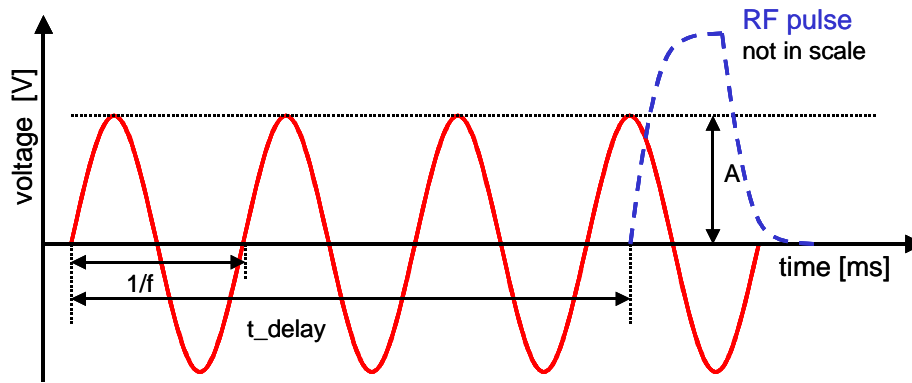


Figure 6.11 Shape of the pulse with variable parameters

Similar to single pulse research, also here each parameter was studied individually. The accelerating field gradient at cavity 5 in ACC1 module was set to maximal value 15.6 MV/m. At the beginning 4 pulses of frequency of 294 Hz and amplitude of 42 V has been used. The delay time has been varying from -12.5 ms to -11.5 ms. The other settings came from experience of the authors. The results are shown in Figure 6.12.

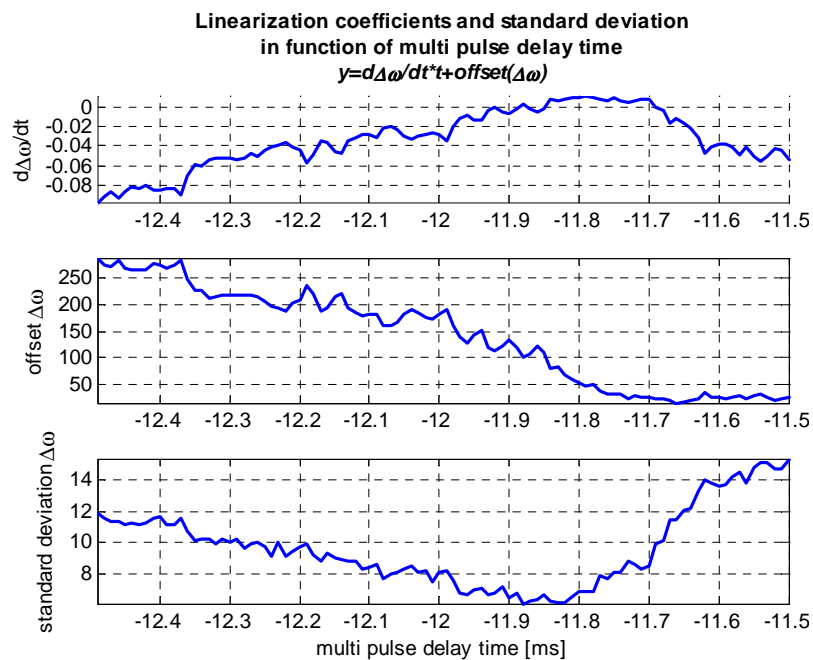


Figure 6.12 Coefficients of detuning linearization and standard deviation from measurement in function of delay time.

It is visible that the maximum of slope of detuning is for the delay time equal to $-11,85$ ms. The offset detuning and standard deviation from linear approximation are then the smallest ones. One more thing is also remarkable – the slope coefficient is higher than zero what indicates that the system is overcompensated. In other words, it proves that the system is able to compensate a Lorentz Force detuning caused by accelerating field gradient of 20 MV/m.

According to the previous measurement a delay time has been set to the -11.85 ms and an investigation of varying amplitude has been made. The amplitude has been changed from 30 V to 50 V (see Figure 6.13). From the test one can find that the slope equal to 0 (the linear approximation of detuning during the flat-top is really plane) is when the $A=40.8$ V. The peak around the 39.5 V is due to the fact that function generator was reset, when detuning measurement has been performed.

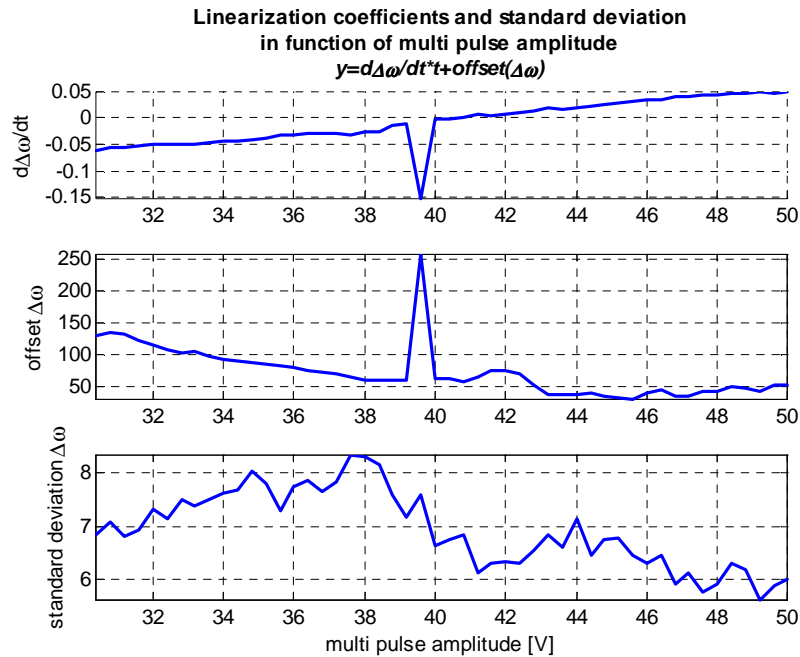


Figure 6.13 Coefficients of detuning linearization and standard deviation from measurement in function of amplitude of multi-pulse signal.

Further investigation was dedicated to optimization of frequency of the signal. For previous test, it was set to 294 Hz. This value was found during the previous experiments, which were fully manual ones. To check if the assumption was correct two measurements have been done. In the first of them the end of the 4 pulses was fixed and the frequency was varying from 100 Hz to 500 Hz (Figure 6.14). Two maximums are visible; the first one is around 285 Hz and the second around 430 Hz. For these values also the offset and standard deviation go to the minimum value (below 100 Hz and 8 Hz respectively).

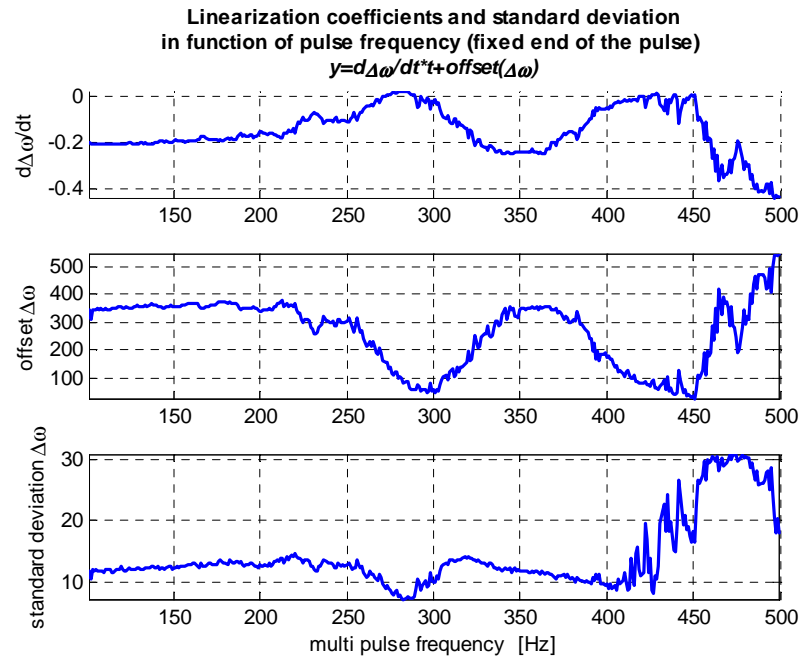


Figure 6.14 Coefficients of detuning linearization and standard deviation from measurement in function of frequency of multi-pulse signal. The end of the 4 pulses is fixed.

Furthermore, the experiment was performed once again with the difference of the fixed point. Instead of holding the end of the pulse, the point after 3.5 periods was rigid. In the other words, the beginning of the last quarter part of the last pulse was constant in respect to the beginning of the RF pulse (see Figure 6.15). As previously a frequency was changed from 100 Hz to 500 Hz and the adequate parameters were measured. The results are presented in Figure 6.16.

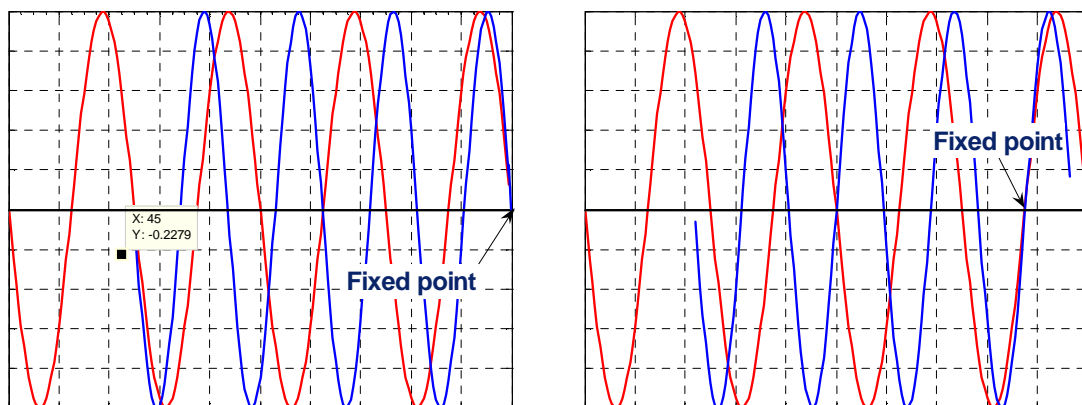


Figure 6.15 Illustration of difference in fixing point. Left figure present situation when end of the pulse is fixed in respect to RF pulse (not shown). Right figure present situation when signal applied to piezostack is fixed in respect to RF pulse after 3.5 periods.

From the zoom figures one can find that the deviation is smaller than 8 Hz (for peaks around 281 Hz and 427 Hz), whereas the value of slope of linearized detuning are zero or positive

(overcompensation). The offset does not reach the minimal value, however the stepper motor used for slow tuning might it easily compensate.

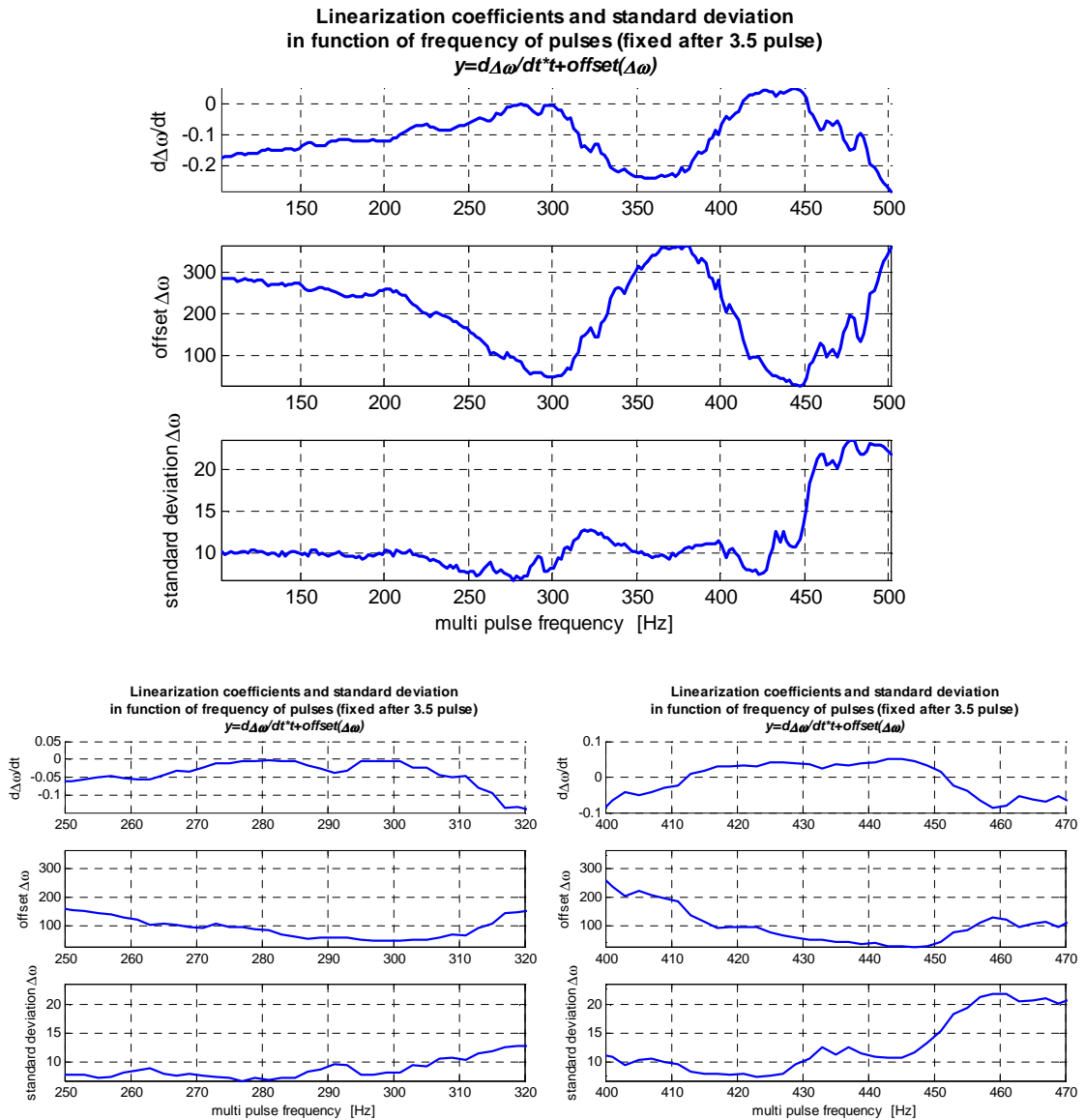


Figure 6.16 Coefficients of detuning linearization and standard deviation from measurement in function of frequency of multi-pulse signal. The point after 3.5 pulses is fixed. Bottom plots are the zoom of the top figure around 285 and 435 Hz respectively.

To summarize, a multi-pulse compensation permits to compensate the detuning caused by Lorentz force for accelerating field gradients up to 15.6MV/m (according to the DSP settings, the measured value of probe signal was around 20MV/m). The next step was to find the correlation between the field gradient and the amplitude of signal applied to piezostack, to dump the Lorentz force to minimum value. The proper experiment is presented in Appendix B The optimal amplitude of voltage applied to piezostack to reduce the Lorentz force in function of accelerating field gradient

is shown in Figure 6.17. The measured points are marked as red dots. The red curve is a quadratic approximation of measured data:

$$y = 0.2718x^2 - 2.632x + 15.06 \quad (6.1)$$

The green lines illustrate the 95% confidence. However, for lower gradients it is better to use a cubic approximation (see Appendix B).

Using the given formula, it is possible to predict the maximal gradient, for which a Lorentz force effect might be compensated (see Figure 6.18). For gradient of 35MV/m, the amplitude is slightly above 250V, which is much more than the limit of piezostack voltage. However, it is possible to reduce the amplitude by increasing the number of used pulses.

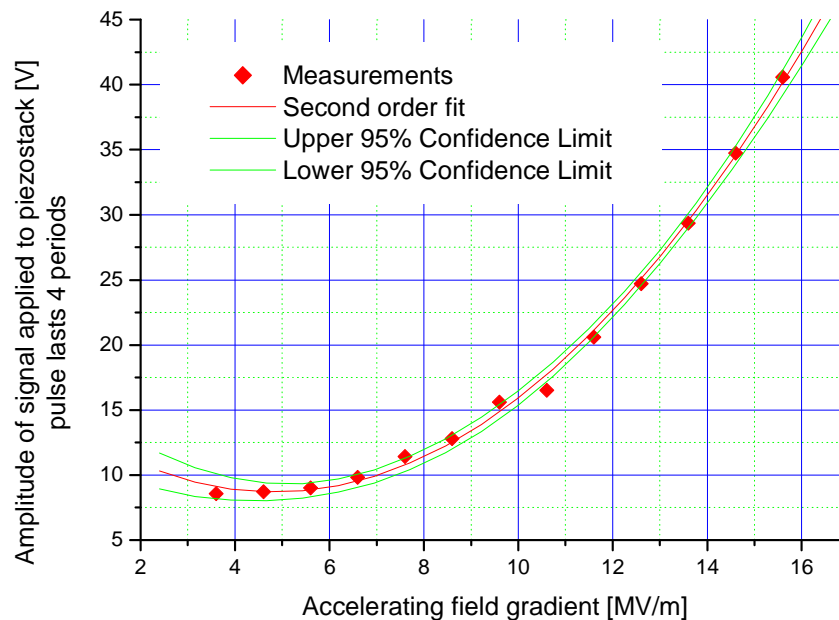


Figure 6.17 Measured amplitude of signal applied to piezostack needed for optimal compensation of Lorentz force in function of accelerating field gradient.

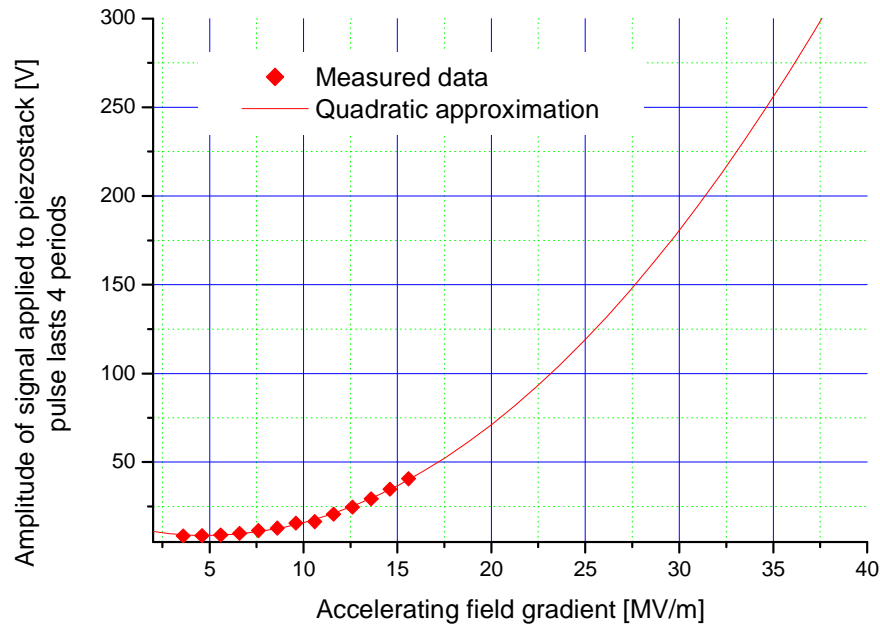


Figure 6.18 Prediction of amplitude of signal applied to piezostack needed for optimal compensation of Lorentz force in function of accelerating field gradient.

6.4.3. Feed forward algorithm for Lorentz force compensation

The experiments presented in subchapters 6.4.1 and 6.4.2 was used for the design of the automatic method for Lorentz force compensation. The developed method base on the adaptive feed forward algorithm. It is possible to predict a distortion because Lorentz force depends on the accelerating field gradients and the properties of the system. The second set of parameters is constant, therefore it is possible to develop algorithm, which will rely only on the measurement of the field gradient. This idea was proved in previous chapters.

The multi-pulse compensation is used. Four sine-wave pulses of frequency of 284Hz are used. The offset is equal to 0V. The delay time between beginnings of RF pulse and signal applied to piezostack is constant and equal to -11.84ms . The initial setting for amplitude of sine signal is taken from the preset table depending on the accelerating gradient settings in DSP. The value of the table represents the function shown in Figure 6.17 with step of 1MV/m.

The signal is applied to piezostack and the measurement of detuning is done. Usually, due to the imperfections the detuning curve is not really horizontal during the RF flat-top. As a consequence, a fine-tuning is needed, which will cancel these small errors. In the algorithm presented by authors, the data obtained from experiment described in Appendix B are used. One can find, that close to the optimal compensation the amplitude of piezostack signal might be assumed as a linear function. The slope of this line is almost constant for different gradient ($0.0048 \div 0.0083 \text{ V*Hz/s}$). As a

consequence, the fine-tuning relies on this phenomena. If the slope is different from zero, then an amplitude correction is calculated. The value of the adjustment ΔA is given by the formula:

$$\Delta A = \Delta\omega/\Delta t * 0.0050 \quad (6.2)$$

where $\Delta\omega/\Delta t$ is the slope of the linearized detuning

Then, in next iteration a new signal is applied and new detuning is measured during RF pulse. If the error is smaller than previous then new settings are stored in the preset table. If the error still exists then a further correction is calculated and signal is properly modified. The last step is iterated.

The presented algorithm was tested in ACC1 cavity 5 with success. The detuning for accelerating field gradient above 15MV/m, which if uncompensated is around 180Hz, was usually reduced to below 10Hz in 2 or 3 iterations. The results are shown in subchapter 6.5.

Moreover, the presented algorithm tracks the changes of accelerating field gradient. It also follows the parameter change i.e. beam current or stepper motor position. Another advantage of the

The main advantage of presented algorithm, beside of the fact that it suppress the Lorentz force effect, is its simplicity. As a consequence, it would be quite easy to implement the presented algorithm in the low-level radio frequency control (LLRF) system realized either in DSP or FPGA.

6.5. Measurements and results

The system presented in previous subchapter was tested on cavity 5 mounted in cryomodule ACC1 which is part of FLASH accelerator. The cavity was power with RF field gradient of 20 MV/m. The measurement of the detuning when system was switched off and on is shown Figure 6.19. The detuning without the piezoelectric stack action was around 180 Hz. When the fast tuner was switched on the detuning was compensated and remains below 10 Hz in average. The offset of 50 Hz might be compensated by stepper motor.

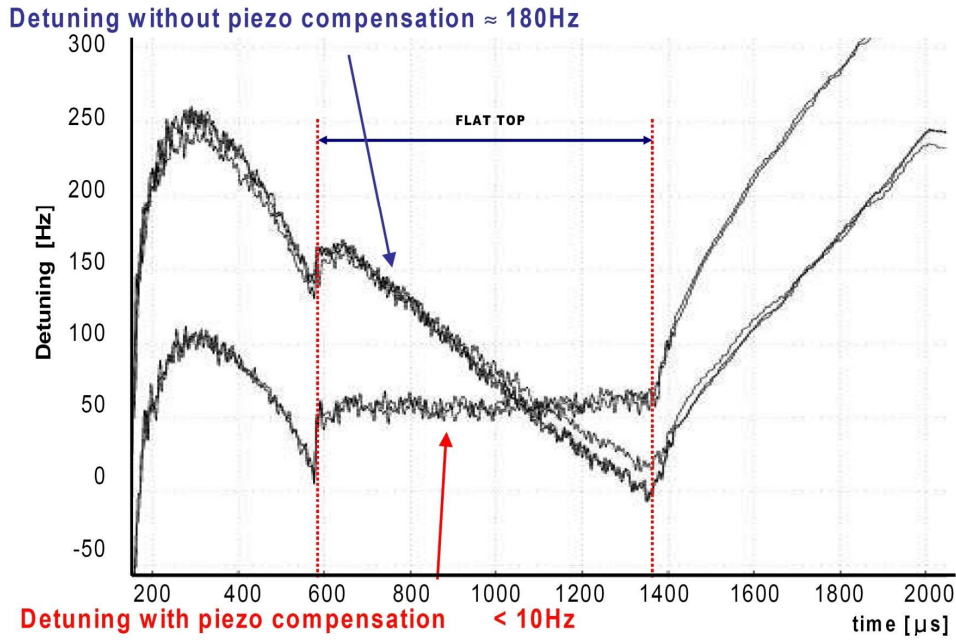


Figure 6.19 Cavity detuning with and without piezostack-based system measured in cav5, ACC1, FLASH accelerator. The accelerating field gradient is 20MV/m.

The presented experiment was performed several times for different accelerating field gradient settings. The algorithm of detuning compensation adapts in 4÷6 steps, and after that the detuning was below 10Hz. It is important to mark that after the first step the detuning was below 20 Hz.

Moreover, the influence of the fast tuner on the beam was tested. The mean energy of the beam might be monitored after the first module using the Bunch Compressor. The readout from the device is presented in Figure 6.20. The total energy gain in ACC1 module is 123 MeV. According to performed measurement the beam gained additional 600 keV when the fast tuner was activated. It is caused by the fact that the cavity 5, which is equipped with the tuner, was operated on the resonance and therefore the energy transfer from RF field to the beam was higher. It is easy to calculate that using the fast tuner with only a single cavity there is possibly to acquire 0.5% of total energy.

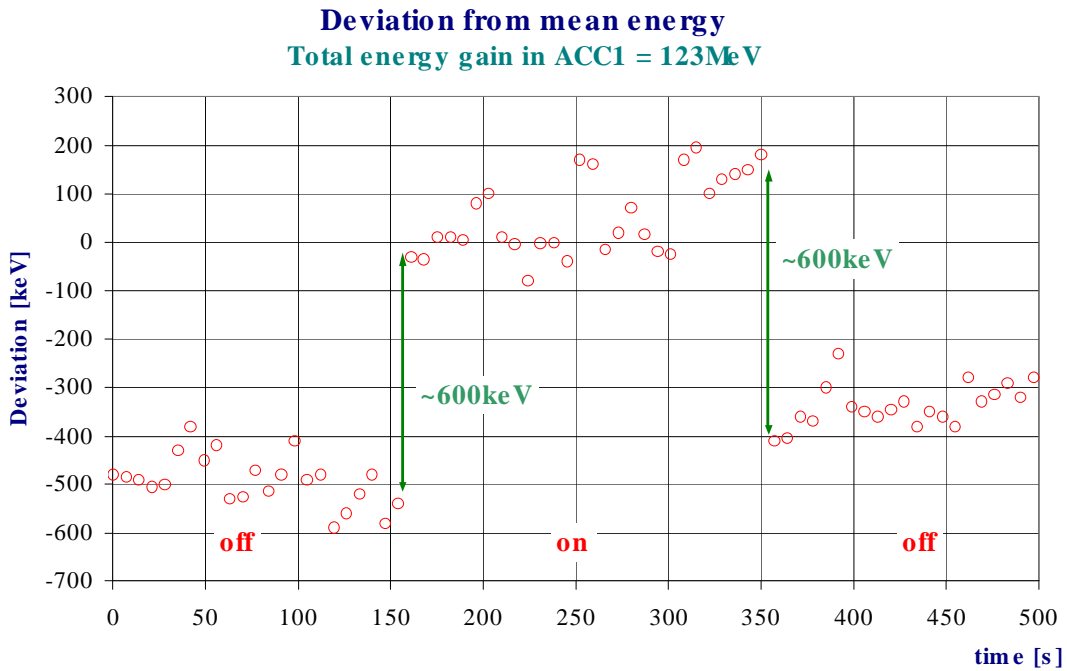


Figure 6.20 Beam energy deviation from mean value in function of time measured after the ACC1 module. The fast piezostack-based tuner was switched on after 160 s and switched off after 350 s.

There is need to take under consideration that in case of higher accelerating field gradients the advantage of fast tuning will be higher because the Lorentz force effect is proportional to the square of the field gradient. Some preliminary results with higher gradients were performed at CHECHIA cryostat [Sekalski 2004c]. The performed test indicates that there is possible to use a current piezostack with resonant excitation algorithms to compensate the detuning of 500Hz. For higher detuning compensation, there is need to use a PI or NOLIAC piezostacks, which were described in chapter 4.2.

The amplitude and phase of the accelerating field is presented in Figure 6.21. It is visible that the gradient during the flat-top stabilizes when the fast tuner is switched on.

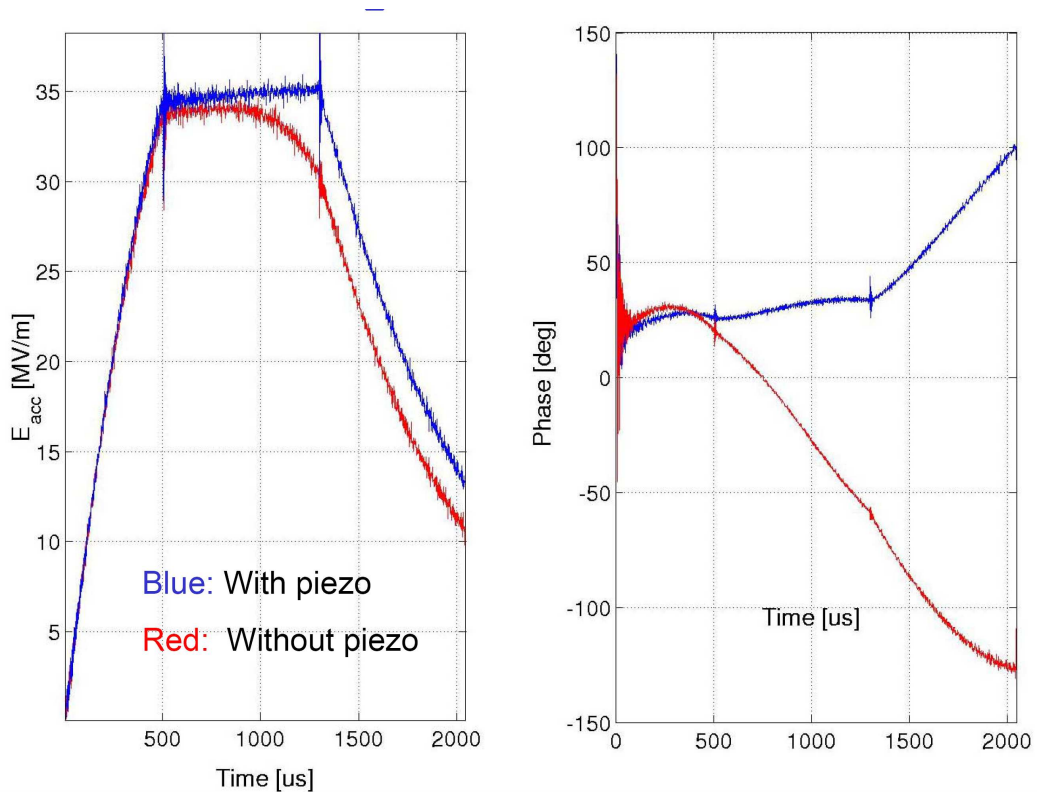


Figure 6.21 Amplitude and phase of accelerating field gradient. CHECHIA horizontal cryostat, 35MV/m.

Chapter 7. Summary and conclusion

During the last decade the TESLA superconducting technology significantly evaluates and nowadays is the one of the most advanced. A few accelerators, which base on the nine-cells niobium cavities were constructed and tested in practice. The most recent construction called Free Electron Laser in Hamburg – FLASH (previously named Vacuum Ultra Violet Free Electron Laser) is nowadays operated by the end users who perform sophisticated experiments in the biology, the medicine and the crystallography fields. During the summer 2006, it was operated with laser wavelength of 13 nm. This is the shortest wavelength which can be reached with the present maximum energy of the accelerator.

Meanwhile, the same machine is used for technology development by the engineers in framework of CARE programme supported by the European Community. The main aim of these common efforts is to establish the technology for the next generation of linear colliders. One of the projects – the XFEL – has been actually approved and will be constructed between 2008 and 2012 in Hamburg. It is a free-electron-accelerator based laser which will be operated with X- ray regime. The solutions and results, which are presented in this dissertation, will be used in this machine.

Since, the full system is extremely complicated therefore the studies presented in this dissertation focuses only on the one of subsystems, which is the fast tuner. This electromechanical device, equipped with the smart materials based actuators and sensors, is able to change the length of the niobium cavity, which is cooled down to 1.8 degree of Kelvin, within few hundreds of microseconds. The tuner motion is extremely small in comparison to the full length of the cavity. The stroke is below 4 microns whereas the cavity length is slightly above 1 meter. As a result, there is need to control with high precision these extremely small action performed by the smart-material-based actuators in order to compensate the Lorentz force effect. The Lorentz force phenomenon is presented in detail in Chapter 3.

As it was proposed previously by M. Liepe, the author uses piezoelectric stacks as an actuator to counteract the Lorentz force generated by the accelerating field. The thesis covers characterization and comparisons of several different types of piezoelements. All of them were tested in cryogenic operation. After preliminary test, two types: PI and NOLIAC elements were selected as the best candidates for future developments. Then, more sophisticated experiments as neutron irradiation and lifetime test were done. Both types of elements satisfactory passed the test. Moreover, the magnetostrictive actuators were tested with success in cryogenic operation. These researches, described in Chapter 4, were performed by the authors within collaboration with IPN – Orsay (France), INFN – Milan (Italy) and of course DESY-Hamburg (Germany).

One of the important issues which were investigated in the thesis is a measurement of preload force applied to the active element. This pre-stress force determines the lifetime of the piezoelectric actuator and the operation range. According to the performed experiments and calculation the initial load should be kept in quite narrow range around 1.2 kN. As a result there was a need to develop the method of force measurement in cryogenic, high vacuum environment. The standard solution, which base on strain gauges, requires additional wiring, space and of course funds. Two other methods, developed by the author, are presented in the dissertation. Both of them allow to estimate the static force applied to the piezoelectric actuator. The first of them base on resonant frequency shift on the impedance curve. In the second one, the capacitance variation in function of applied load is investigated. Both methods were checked in real system. Moreover, both methods might be used in parallel to guarantee better measurement. Preliminary results show that the sensibility of both techniques is sufficient for case of preload determination and allows measuring the force with resolution of hundreds of Newtons. As a consequence, it is possible to apply the optimal preload to piezostack and therefore it is possibly to increase the lifetime of the actuator.

Another topic, which is covered in the dissertation, is connected with Lorentz force compensation algorithms. The author proposes to use a self-developed feed-forward based method which allows reducing the detuning by 90%. The results, which are presented in previous chapter indicates that the system not only fulfils strict requirements, but also might be successfully used for large scale production. The presented solution allows automatically applying correct settings to the piezoelectric stack in order to reduce the detuning below 10 Hz. The system was successfully tested in FLASH accelerator.

Moreover, the presented resonant excitation method permits to reduce the magnitude of applied voltage to the value below 50 V. It is important for the lifetime of the piezostack, because the element is no longer excited to the limit (120÷200 V, depending on the piezostack). Such compensation applied to only one cavity allows to improve the energy gain of whole module by 600 keV (it is half percent of total energy of module ACC1 equipped with 8 cavities operated with mean gradient of 15 MV/m).

Promising results was also obtained in CHECHIA test stand. It is a facility, which can hold only one niobium cavity which might be operated with high gradients (depending on the cavity) but without the beam. During the test, in which cavity accelerating field gradient was reached 35 MV/m, the phase decay was reduced from more than 100 degrees to below 15 degrees. This experiment demonstrated the power of proposed solution. Nevertheless, further investigation is needed. Such an opportunity will be accessible when the new stand test will be finished. It will consist of full module equipped with eight high power cavities which will be operated at gradients

above 30 MV/m. The fast tuners with active elements proposed by the author will be attached to all cavities instead to only one (as it is at the moment).

Additionally, the new stand test allows to investigate the crosstalk between the cavities. The proposed resonant excitation method might cause interaction between the nearest cavities. This topic is in the interest of the author and the detailed study of this phenomenon will be performed in the future. Additionally, each tuner in this new installation will be equipped with two piezostacks. As a consequence, it allows performing more studies on mechanical behaviour of the cavity.

Two identical active elements mounted in one fixture of fast tuner significantly increases the lifetime of device. In case of failure of any of them, the second one can be normally operated as it is happened at this moment. However, without the breakdown the piezoelectric element might be operated as a sensor. This actuator-sensor system might be used to compensate not only the Lorentz force effect but also to compensate the microphonics. These small vibrations caused by the environment are reasonably low (the detuning caused by the microphonics is below 10 Hz) but they are unpredictable. In case of system which will be soon operated there will be a possibility to close the feedback loop.

In perfect case, both Lorentz force and microphonics compensation should be combined together and the detuning during the pulse should be zero. Moreover, the fast and slow tuning methods should be joined as well in order to operate the cavity always on resonance. Since, the research presented in the dissertation helps to become closer to the ideal case, there is still a room for further development of next technologies.

Bibliography

With author contribution

- [A Bosland 2004] P. Bosland, C. Pagani, A. Bosotti, M. Liepe, P. Sekalski, Hervé Saugnac, M. Fouaidy, R. Lange, S. Simrock, L. Lilje, ITRP meeting, April 2004, poster
- [A Napieralski 2005a] A. Napieralski, M. Grecki, P. Sękalski, D. Makowski, M. Wójtowski, W. Cichalewski, B. Kosęda, B. Świercz; "Przegląd prac Politechniki Łódzkiej realizowanych w programie CARE", Elektronika 2/2005, ISSN 0033-2089
- [A Napieralski 2005b] A. Napieralski, P. Sękalski; "Application of multilayer piezoelectric elements for resonant cavity deformation in VUV-FEL DESY accelerator", IMAPS Darłówek 2005, pp. 41-47, ISBN 83-917701-2-5 *invited paper*
- [Sekalski 2003] P. Sekalski, "EPCOS Piezostack impedance measurement", DESY, internal report, 2003-1
- [Sekalski 2004a] P. Sekalski, A. Napieralski, S. Simrock, L.Lilje, A. Bosotti, R. Paparella, F. Puricelli, M. Fouaidy: "Static absolute force measurement for preloaded piezoelements used for active Lorentz force detuning system", LINAC 2004, pp. 486-488, Lübeck, Germany,
- [Sekalski 2004b] P. Sękalski; "Siła Lorentza oraz drgania mechaniczne jako główne czynniki powodujące odstrojenie od częstotliwości rezonansowej w nadprzewodzących wnękach rezonansowych stosowanych w technologii TESLA", MIKROELEKTRONIKA I INFORMATYKA, pp. 196-178, ISBN: 83-919289-5-0
- [Sekalski 2004c] P. Sękalski, S. Simrock, L. Lilje, C. Albrecht; „Lorentz Force Detuning System for Accelerating Field Gradients Up to 35 MV/m for Superconducting XFEL and Tesla Nine-Cell Cavities”, 11th International Conference MIXDES 2004, pp. 398-402, ISBN 83-919289-7-7
- [Sekalski 2005a] P. Sękalski; „Systemy elektromechaniczne do kompensacji odkształcenia wnęk rezonansowych stosowanych w technologii TESLA”, Elektronika 7/2005, pp. 21-26, ISSN 0033-2089

- [Sekalski 2005b] P. Sękalski M. Grecki, C. Albrecht; “Performance of Magnetostrictive Elements at LHe Environment” 12th International Conference MIXDES 2005, Kraków, 22-25 June 2005, pp. 799-802, ISBN 83-919289-9-3
- [Sekalski 2005c] M. Fouaidy, G. Martinet, N. Hammoudi, F. Chatelet, N. Gandolfo, H. Sagnac, S. Bousson, P. Bosland, Bo Wu, P. Sekalski, “Static and dynamic properties of piezoelectric actuators at low temperature and integration in SRF cavities cold tuning systems”, 12th International Conference MIXDES 2005, Kraków, 22-25 June 2005, CARE session
- [Sekalski 2006a] P. Sekalski, A. Napieralski, S. Simrock, “Electromechanical System For Lorentz Force Compensation”, NSTI-Nanotech 2006, pp. 393-396, ISBN 0-9767985-8-1 Vol. 3, 2006,
- [Sekalski 2006b] P. Sekalski et all, “Smart Materials Based System Operated At 2K Used As A Superconducting Cavity Tuner For VUV-FEL Purpose”, ACTUATOR 2006, pp. 948-951, ISBN-3-93333-08-1
- [Sekalski 2006c] P. Sekalski, A. Napieralski, S. Simrock, „Automatic, resonant excitation based, system for Lorentz Force compensation for VUV-FEL”, EPAC 2006, to be published
- [Sekalski 2006d] P. Sekalski, A. Napieralski, M. Fouaidy, A. Bosotti, R. Paparella, “Measurement of static force in liquid helium temperature”, Measurement Science and Technology IOP Journal, to be published

Other authors

- [Aune 2000] B. Aune et al., “Superconducting TESLA cavities”, Physical Review Special Topics – Accelerators And Beams, Volume 3, 092001 (2000)
- [Bah 1992] S. Bah, G. Quezel, Ph. Benech, L.Ngalamou and J. F. Legrand, “Effect Of Compressive Stress On A Composite Resonator Based On PVF2”, 1992 ULTRASONICS SYMPOSIUM, pp. 973-975, 1051-0117/92/0000-0
- [Benesch 1997] J. F. Benesch and M. Wiseman, “Tests of a Prototype Magnetostrictive Tuner for Superconducting Cavities”, IEEE Transactions On Applied Superconductivity, VOL. 7, NO. 2, JUNE 1997, pp. 375-377

- [Bosland 2005] P. Bosland, Bo Wu; “Mechanical study of the Saclay Piezo Tuner PTS (Piezo Tuning System)”, CEA-Saclay, Dapnia, 2005, DAPNIA-05-38, CARE-Note-2005-004-SRF
- [Bosotti 2005a] A. Bosotti, R. Paparella, F. Puricelli; “Piezo Impedance Measurements”, Internal note, INFN Milan, Italy, 2005,
- [Bosotti 2005b] A. Bosotti, P. Pierinia, P. Michelatoa, C. Paganib, R. Paparella, N. Panzeria, L. Monaco, R. Paulona, M. Novatia; “CARE activities on superconducting RF cavities at INFN Milano” INFN-Milan, Italy, internal report, 2005, CARE-Conf-05-047-SRF
- [Bosotti 2005c] A. Bosotti et all, “Report on Fast Piezo Blade Tuner (UMI) for SCRF Resonators Design and Fabrication”, CARE-Note-2005-021-SRF
- [Bosotti 2005d] A. Bosotti et all, “PI piezo lifetime test report”, INFN Milan, Italy, internal report, CARE-Note-2005-020-SRF
- [Bousson 2000] S. Bousson, M. Fouaidy, H. Gassot, T. Junquera, J-C. Le Scornet, J. Lesrel, “Cavity Stiffening By Thermal Spraying”, Proceedings of EPAC 2000, Vienna, Austria
- [Brinkmann 2001] R. Brinkmann, K. Flöttmann, J. Rossbach, P. Schmüser, N. Walker, H. Weise, “TESLA Technical Design Report Part II: The Accelerator”, DESY 2001-011, ECFA 2001-209, 2001.
- [Brinkmann 2002] R. Brinkmann, et all “TESLA XFEL, Technical Design Report Supplement”, DESY 2002-167, 2002.
- [Claeyssen 2002] F. Claeyssen, N. LHermet, T. Maillard, “Magnetostrictive Actuators Compared to Piezoelectric Actuators” ASSET, European Workshop on Smart Structures in Engineering and Technology, France, 2002, ISSN 0277-786X and 2003, ISSU 4763, pages 194-200
- [Chao 1999] A. W. Chao, M. Tigner, “Handbook of Accelerator Physics and Engineering”, World Scientific, Singapore, 1999.
- [Davis 2003] G. K. Davis, J. R. Delayen, “Piezoelectric Tuner Compensation of Lorentz Detuning in Superconducting Cavities”, Proceedings of the 2003 Particle Accelerator Conference, pp. 1383-1385
- [Delayen 2001] J.R. Delayen, “Electronics Damping of Microphonics in Superconducting Cavities”, Proceedings of the 2001 Particle Accelerator Conference, Chicago, JLAB-ACT-01-11

- [Doleans 2003a] M. Doleans, “Studies in reduced-beta elliptical superconducting cavities”, PhD thesis, University Paris 7 – Denis Diderot, 2003
- [Doleans 2003b] M. Doleans, “Insights in The Physics of the Dynamic Detuning in SRF Cavities and its Active Compensation”, Proceedings of the 2003 Particle Accelerator Conference, pp. 1599-1601
- [Gassot 2001] H. Gassot, “Etudes de la stabilité mécanique des cavités supraconductrices et de la méthode de rigidification par projection thermique de cuivre”, PhD thesis, Université Paris Sud – Paris XI, 2001
- [Energen 2003] Magnetostrictive tuner datasheet, ENERGEN, INC
- [Fouaidy 2003] M. Fouaidy, N. Hammoudi, ”Characterization of Piezoelectric Actuators Used for SRF Cavities Active Tuning at Low Temperature”, SRF Workshop, 2003.
- [Fouaidy 2005] M. Fouaidy, G. Martinet, N. Hammoudi, F. Chatelet, S. Blivet, A. Olivier, H. Saugnac “Electromechanical, Thermal Properties and Radiation Hardness Tests of Piezoelectric Actuators at Low Temperature”, SRF Workshop 2005 Ithaca, USA
- [Jalmuzna 2006] W. Jalmuzna, “Design And Implementation Of Universal Mathematical Library Supporting Algorithm Development For FPGA Based Systems In High Energy Physics Experiments”, master thesis, Warsaw University of Technology, 2006
- [Lilje 2002] L. Lilje, S. Simrock, D. Kostin, M. Fouaidy, “Characteristics of a fast Piezo-Tuning Mechanism for Superconducting Cavities”, Proceedings of EPAC 2002, Paris, France.
- [Lilje 2004a] L. Lilje, E. Kako, D. Kostin, A. Matheisen, W.-D. Moeller, D. Proch, D. Reschke, K. Saito, P. Schmueser, S. Simrock, T. Suzuki, K. Twarowski, “Achievement of 35 MV/m in the Superconducting Nine-Cell Cavities for TESLA”, Nucl. Inst. Meth. A (DOI: 10.1016/j.nima.2004.01.045), DESY 04-018, TESLA 2004-05
- [Lilje 2004b] L. Lilje, “Achievement of 35 MV/m in The Tesla Superconducting Cavities Using Electropolishing As A Surface Treatment”, Proceedings of EPAC 2004, Lucerne, Switzerland, pp. 129-131

- [Liepe 2001a] M. Liepe, W.D.-Moeller, S.N. Simrock, "Dynamic Lorentz Force Compensation with a Fast Piezoelectric Tuner", Proceedings of the 2001 Particle Accelerator Conference, Chicago, USA, pp. 1074-1076
- [Liepe 2001b] M. Liepe; "Superconducting multicell cavities for linear colliders", PhD thesis, University of Hamburg, DESY-THESIS-2001-045, 2001.
- [Liepe 2005] M. Liepe, S. Noguchi, Report on current status for ILC tuner development, Workgroup 5, Snowmass 2005, *to be published*
- [Loew 1996] G.A. Loew, "Review of Electron-Positron Linear Colliders", LINAC 1996
- [Mavanur 2003] A. Mavanur, C-Y Tai, C. H. Joshi, "Magnetostrictive tuner for SRF cavities", Proceedings of the 2003 Particle Accelerator Conference, pp. 1407-1409
- [Padamsee 1998] H. Padamsee, J. Knobloch, T. Hays, "RF Superconductivity for Accelerators", John Wiley & Sons, New York, USA, 1998.
- [Padamsee 2001] H. Padamsee, "The Science and Technology of Superconducting Cavities for Accelerators", Supercond. Sci. Technol. 14 (2001), pp. R28-R51
- [Pagani 2005] C. Pagani, A. Bosotti, P. Michelato, N. Panzeri, R. Paparella, P. Pierini, "The Fast Piezo-Blade Tuner For SCRF Resonators", CARE-Conf-05-051-SRF
- [Paparella 2005] R. Paparella, "Sviluppo Di Un Sistema Attivo Di Controllo Delle Vibrazioni Indotte In Cavità Superconduttive Ad Alto Campo Per Acceleratori Di Particelle", master thesis, INFN Milan, Italy
- [PI web] Physic Instrumente web site, <http://www.physikinstrumente.com>
- [Rehlich 1999] K. Rehlich, P. Shevtsov, Y. Tschernoousko; "Two Channel Functional Generator Board and Its Server", MVP group, DESY, Internal report, 1999
- [Saito 2005] K. Saito, "ILC High Gradient Cavity Development Status", Asia Video meeting on 4 Aug 2005
- [SC IEEE 1987] Standards Committee of the IEEE Ultrasonics, Ferroelectrics, and Frequency Control Society, An American National Standard: IEEE Standard on Piezoelectricity, The Institute of Electrical and Electronics Engineers, 1987, ANSUIEIEEE Std 176-1987, New York.

- [Schilcher 1998] T. Schilcher, “Vector Sum Control of Pulsed Accelerating Field in Lorentz Force Detuned Superconducting Cavities“, PhD thesis, Hamburg 1998
- [Schmueser 2002] P. Schmueser, “Superconductivity in High Energy Particle Accelerators”, Progress in Particle and Nuclear Physics, Volume 49, Number 1, 2002, pp. 155-244(90)
- [Schmueser 2003] P. Schmueser, “Basic Principles of RF Superconductivity and Superconducting Cavities”, CERN Accelerator School 2003
- [Simrock 2002] S. Simrock, “Lorentz Force Compensation of Pulsed SRF Cavities”, Proceedings of LINAC 2002, Gyeongju, Korea, pp. 556-560
- [Simrock 2003] S. Simrock, G. Petrosyan, A. Facco, V. Zviagintsev, S. Andreoli, R. Paparella, “First Demonstration Of Microphonic Control of a Superconducting Cavity with a Fast Piezoelectric Tuner”, Proceedings of the 2003 Particle Accelerator Conference, pp. 470-472
- [Simrock 2004] S. Simrock, V. Ayvazyan, “Dynamic Lorentz Force Detuning Studies in TESLA cavities”, EPAC 2004, pp. 993-996
- [Simrock 2005] S. Simrock, “Review of Fast and Slow Tuners”, SRF Workshop 2005, Ithaca, USA
- [Soluch 1980] W. Soluch et all, „Wstęp do piezoelektroniki”, WKŁ, Warszawa, 1980
- [Stuchechnikov 1991] V. M. Stuchechnikov; “SOS Strain Gauge Sensors For Force And Pressure Transducers”, Sensors and Actuators, 1991, v.28, No 3, pp. 207-213
- [Slater 1950] J.C. SLATER, Microwave Electronics, D. Van Nostrand Company, Inc. Princeton, New Jersey, USA, 1950
- [Voigt 1910] W. Voigt, “Lerhbuch der Kristallphysics”, Leipzig, Berlin, B.G. Teubner, 1910
- [Zickgraf 1995] B. Zickgraf, et all “Fatigue Behaviour of Multilayer Piezoelectric Actuators”, Applications of Ferroelectrics, 1994. ISAF '94, pp. 325-328

Index of figures

Figure 2.1	Nine-cell cavity used at FLASH. [Brinkmann 2001]	9
Figure 2.2	Overview of VUV-FEL localization. [DESY web]	10
Figure 2.3	Dimension of single cell used in TESLA technology	12
Figure 2.4	Structure of pulse used in VUV-FEL accelerator. [Schilcher 1998]	13
Figure 2.5	Fixture for two piezoelements attached instead of old tuner support.	15
Figure 2.6	Photographs of cavity tuner.	15
Figure 2.7	Drawing and photo of new design of CEA-Saclay - PTS tuner. [Bosland 2005]	18
Figure 2.8	Drawing and photo of INFN blade coaxial tuner [Pagani 2005]	18
Figure 2.9	KEK tuners - coaxial ball screw tuner (left) and slide jack tuner (right).[Liepe 2005]	19
Figure 2.10	TJNAF tuner [Liepe 2005]	20
Figure 3.1	Single cell deformation due to the internal electromagnetic forces (left side) and the volume change caused by Lorentz force ΔV (right side).	22
Figure 3.2	Static Lorentz force detuning and Lorentz force coefficient. [Schilcher 1998]	23
Figure 3.3	Detuning caused by Lorentz force for different accelerating field gradients	24
Figure 3.4	Noise measured in cavity and distribution of frequency caused by microphonics. The cavity was operated in cw mode in CHECHIA cryostat [Liepe 2001b].	25
Figure 3.5	Spectrum of piezostack output voltage. Data from CHECHIA stand test. Figure shows the response in cw mode [Liepe 2001]	26
Figure 3.6	Spectrum of piezostack output voltage. Data from CHECHIA stand test. Figure shows the response to RF field, accelerating field gradient 30 MV/m.	26
Figure 3.7	The cavity detuning obtained from FEM simulation done using CAST3M [Gassot 2001].	27
Figure 3.8	The cavity detuning obtained from measurement done at DESY.	28
Figure 3.9	Output voltage of piezostack inserted in CHECHIA stand test. (red line represents the RF field, blue line is a piezostack response).	28
Figure 3.10	The measurement of transfer function between two piezoelements and piezoelement and the RF field. [from L. Lilje]	29
Figure 3.11	Spectrum of pulse response. A half-sine wave signal of frequency of 800Hz was used as an input pulse.	30
Figure 3.12	The model of cavity connected to a RF generator by coupler and transmission lines [Schilcher 1998]	31
Figure 3.13	The simplified model of cavity circuit.	31
Figure 3.14	Principle of detuning measurement in multi-pulse method [Schilcher 1998].	35
Figure 3.15	The cavity detuning measured using FPGA board. The scope screenshot [Jalmuzna 2006].	36
Figure 3.16	Comparison of single and multi-pulse detuning measurement method. FLASH, accelerating field gradient is set to 10.85 MV/m (left) and 15MV/m (right). LLRF feedback is switched off. A 100 μ s shift between the measurements is caused by DAC board delay.	37

Figure 4.1	Piezoelectric stack and magnetostrictive rod principle of operation.	40
Figure 4.2	Single crystal of PZT before (left) and after (middle) pooling. On the right a legend of used atoms is presented.	41
Figure 4.3	Photographs of used piezostacks. From left to right: EPCOS, PI, Piezomechanik, NOLIAC (not in scale).	43
Figure 4.4	Displacement of PI piezoelement at 300K	44
Figure 4.5	Maximum displacement (stroke) versus temperature (PI piezostack)	45
Figure 4.6	Magnitude and phase of impedance in function of temperature	45
Figure 4.7	Parallel capacitance and resistance of piezoelement in function of temperature	46
Figure 4.8	Loss tangent in function of temperature,	46
Figure 4.9	Capacitance in function of temperature during fast neutron beam test. (NOLIAC)	47
Figure 4.10	Stroke in function of applied load before and after lifetime test.	47
Figure 4.11	Elongation of different materials in function of temperature [Mavanur 2003]	48
Figure 4.12	Magnetostriction of KELVIN ALL® material (courtesy of ENERGEN)	49
Figure 4.13	Magnetostrictive element with metal frame – the draft view with dimensions (left) and its photo (right).	49
Figure 4.14	At the bottom a magnetostrictive rod with Nb ₃ Sn coil and ferrite ring is presented.	50
Figure 4.15	Photos of insert for the vertical cryostat.	50
Figure 4.16	Calculated displacement of magnetostrictive rod versus applied current.	51
Figure 4.17	Photo of GaFeNOL rod of cross-section of 7x7 mm and length of 18 mm.	51
Figure 5.1	Overview of metallic strain gauge sensor	54
Figure 5.2	Gauge placement on measured plate (top) and configuration of strain gauges (bottom) - quarter (left), half (center) and full Wheatstone bridge circuit (right)	55
Figure 5.3	Resistance change of FLEX strain gauge sensor in function of applied force.	56
Figure 5.4	Load cell developed for cryogenic operation and its transfer characteristics. [Bosotti 2005b]	57
Figure 5.5	Output voltage of two samples of strain gauge sensor dedicated for LHe temperature operation. [Bosotti 2005b]	57
Figure 5.6	Overview of circuit configuration for quasi-static force measurement using the piezostack.	58
Figure 5.7	Typical example of an impedance-versus-frequency plot for piezoelement that indicates the resonance frequency (f_r) and the antiresonance frequency (f_a).	59
Figure 5.8	Multilayer piezostacks impedances. EPCOS (blue line), PICMA (green dotted line) and NOLIAC (red dashed line).	59
Figure 5.9	Setup for impedance change measurement	60
Figure 5.10	Impedance of two EPCOS piezostacks (dashed and solid lines) in function of preload from 0 N (blue) to 2kN (red). Measurements performed at room temperature.	61
Figure 5.11	Resonance frequencies shift in function of preload for EPCOS piezostack- left figure for the resonance around 30kHz, the right for the resonance around 65kHz.	61

Figure 5.12	Resonance frequency shift in function of applied force for PI piezostack from ch0201, ch0214 and ch0215 series. Top figure shows resonance around 30kHz, bottom figure presents resonance shift around 60kHz.	62
Figure 5.13	Resonance shift of EPCOS piezostack at 4K in function of applied force. [Bosotti 2005a]	64
Figure 5.14	Photo of single fixture with EPCOS piezostack. The fixture is assembled to the cavity tuner in CHECHIA cryostat.	65
Figure 5.15	EPCOS piezostack resonance shift in function of position of stepper motor. Test done in CHECHIA. Resonance around 70kHz.	66
Figure 5.16	Change of force applied to piezostack in function of position of stepper motor (CHECHIA stand test) when motor moved upward and downward. Red dotted line is smoothed estimation of force.	66
Figure 5.17	Resonance frequency of cavity in function of position of stepper motor.	67
Figure 5.18	The change of capacitance of Piezo JENA (9222) versus applied force at RT.	68
Figure 5.19	Capacitance of PICMA piezoelectric actuator versus preloading force at $T=4.4$ K, vacuum pressure 10^{-5} mBar. Test performed at IPN-Orsay in July 2005.[Fouaidy 2005]	68
Figure 5.20	Sensitivity of piezoelectric actuator to preload force versus temperature	69
Figure 6.1	Overview of control system	71
Figure 6.2	Photograph of CTS tuning system attached to the cavity.	72
Figure 6.3	The idea of fast tuner based on piezoelectric stack	72
Figure 6.4	Panel for piezoelectric devices control	75
Figure 6.5	Shape of the pulse with variable parameters.	76
Figure 6.6	Coefficients of detuning linearization and standard deviation from measurement in function of delay time between beginnings of RF pulse and piezostack signal.	77
Figure 6.7	Coefficients of detuning linearization and standard deviation from measurement in function of width of the piezostack signal.	78
Figure 6.8	Coefficients of detuning linearization and standard deviation from measurement in function of rise time of the piezostack signal.	79
Figure 6.9	Coefficients of detuning linearization and standard deviation from measurement in function of amplitude $A1$ (a) and $A2$ (b) of the piezostack signal, when changed independently.	80
Figure 6.10	Coefficients of detuning linearization and standard deviation from measurement in function of amplitude $A1$ and $A2$ increased simultaneously.	81
Figure 6.11	Shape of the pulse with variable parameters	82
Figure 6.12	Coefficients of detuning linearization and standard deviation from measurement in function of delay time.	82
Figure 6.13	Coefficients of detuning linearization and standard deviation from measurement in function of amplitude of multi-pulse signal.	83
Figure 6.14	Coefficients of detuning linearization and standard deviation from measurement in function of frequency of multi-pulse signal. The end of the 4 pulses is fixed.	84

Figure 6.15	<i>Illustration of difference in fixing point. Left figure present situation when end of the pulse is fixed in respect to RF pulse (not shown). Right figure present situation when signal applied to piezostack is fixed in respect to RF pulse after 3.5 periods.</i>	84
Figure 6.16	<i>Coefficients of detuning linearization and standard deviation from measurement in function of frequency of multi-pulse signal. The point after 3.5 pulses is fixed. Bottom plots are the zoom of the top figure around 285 and 435 Hz respectively.</i>	85
Figure 6.17	<i>Measured amplitude of signal applied to piezostack needed for optimal compensation of Lorentz force in function of accelerating field gradient.</i>	86
Figure 6.18	<i>Prediction of amplitude of signal applied to piezostack needed for optimal compensation of Lorentz force in function of accelerating field gradient.</i>	87
Figure 6.19	<i>Cavity detuning with and without piezostack-based system measured in cav5, ACC1, FLASH accelerator. The accelerating field gradient is 20MV/m.</i>	89
Figure 6.20	<i>Beam energy deviation from mean value in function of time measured after the ACC1 module. The fast piezostack-based tuner was switched on after 160 s and switched off after 350 s.</i>	90
Figure 6.21	<i>Amplitude and phase of accelerating field gradient. CHECHIA horizontal cryostat, 35MV/m.</i>	91
Figure 7.1	<i>Piezo Control Panel – division into four section</i>	106
Figure 7.2	<i>Description of first section of PCP</i>	107
Figure 7.3	<i>Description of second section of PCP.</i>	107
Figure 7.4	<i>Description of third section of PCP.</i>	108
Figure 7.5	<i>Amplitude of signal applied to piezostack to obtain a flat detuning during the RF pulse and its approximation for different accelerating field gradients.</i>	115
Figure 7.6	<i>Residuals and theirs norm for different approximations in function of accelerating field gradients.</i>	115

Index of tables

<i>Table 2.1</i>	<i>Dimension in mm of single cell used in TESLA technology</i>	<i>12</i>
<i>Table 2.2</i>	<i>Parameters of VUV-FEL</i>	<i>13</i>
<i>Table 2.3</i>	<i>Different tuners for TESLA type cavities [Liepe 2005]</i>	<i>16</i>
<i>Table 4.1</i>	<i>Parameters of tested piezoelements</i>	<i>43</i>

Appendix A Piezo Control Panel PCP description

The Piezo Control Panel is a MATLAB based GUI application. It was designed using the embedded tool called GUIDE. The main aim of the software is to control the piezoelement using the system described in Chapter 6 in a way to minimize the detuning caused by the Lorentz force. Nevertheless, the PCP was also used for characterization of the system, especially for measurements presented in subchapters 6.4.1 and 6.4.2 as well as in the Appendix B

The overview of the PCP is presented in Figure 6.4. The panel might be divide into four section, as it is presented in Figure 7.1. The detailed description of each section is presented below.

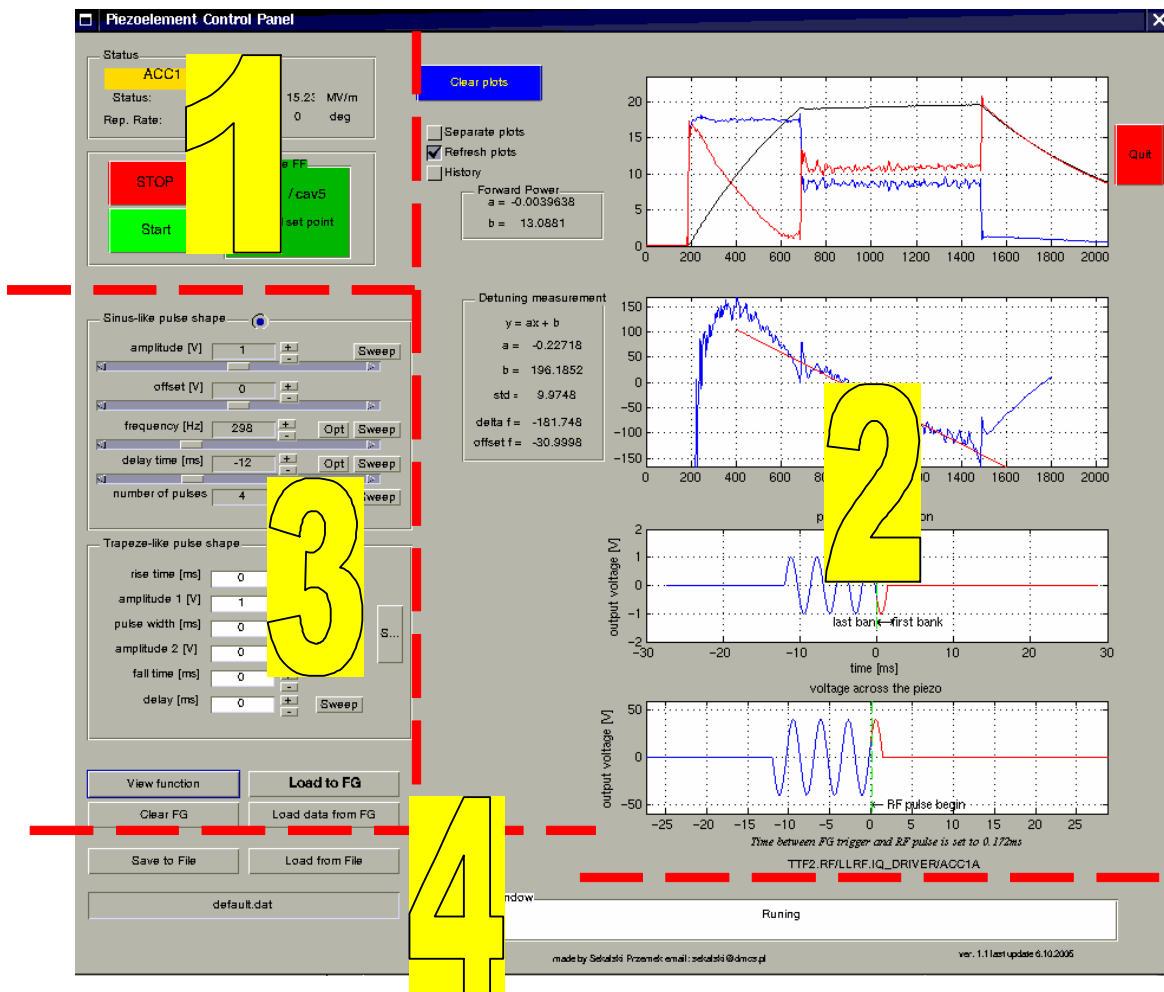


Figure 7.1 Piezo Control Panel – division into four section

The first section presents the main information about the system as the data about the module and the cavity which is currently used, the accelerating field gradient and phase, which is set for particular cavity, repetition rate of RF high power pulses and at least the status of Piezo Control System (see Figure 7.2). Below there are four buttons. Two of them ‘start’ and ‘stop’ initiates and finishes the functioning of PCP. The third of them initiates the adaptive feed-forward based

algorithm used for automatic control of piezoelements. At least, there is possibility to recall the initial settings, which was measured by the author and which are presented in Appendix B

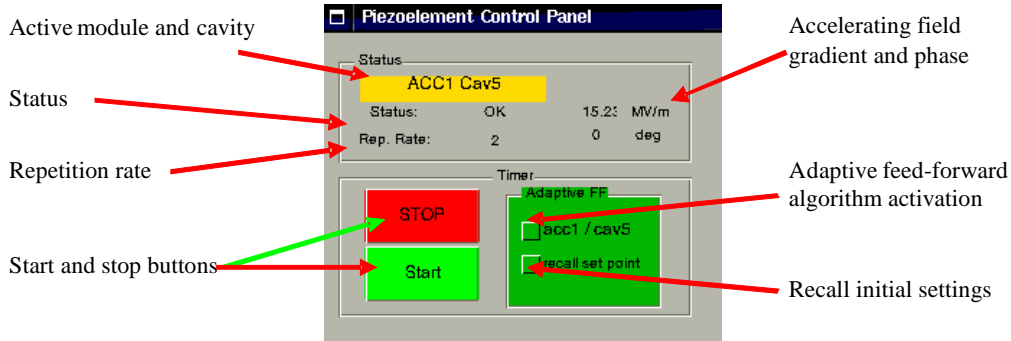


Figure 7.2 Description of first section of PCP

The second section of PCP is dedicated to representation of the results (refer to Figure 7.2). The top plot illustrates the reflected power (red), forward power (blue) and probe signal (black). Below the detuning and its linearization is presented. The value of the coefficients and the value of detuning are showed left to the figures. Two bottom plots illustrates the values saved in the function generator with respect to the last and the first bank, and the signal which is applied to piezoelement with respect to beginning of the RF field.

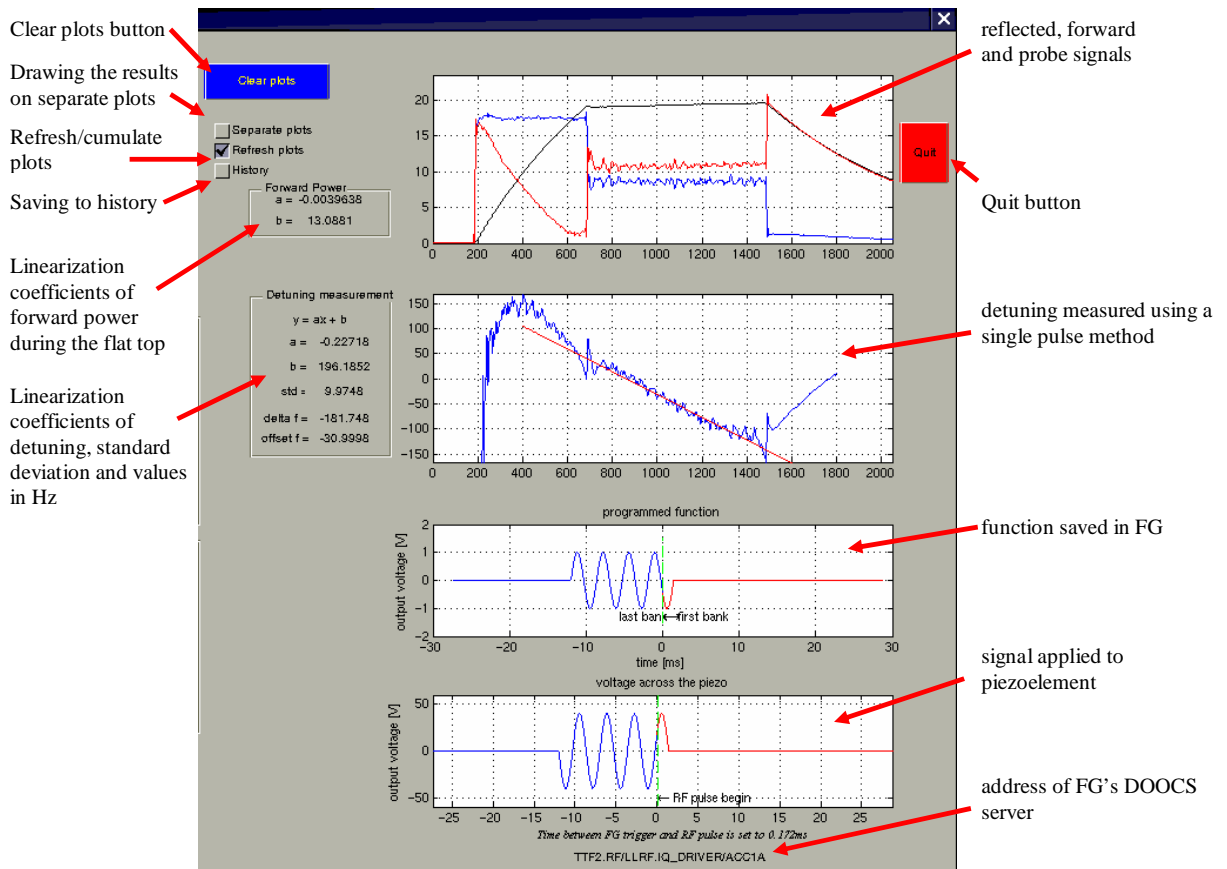


Figure 7.3 Description of second section of PCP.

Additionally, there is possibility to cumulate the figures or shows only the recent one. Moreover, the all above described plots might be saved in separate windows and at least the value of the linearization coefficient with settings of the pulse applied to piezoelement might be saved in separate file ('history').

The third section of PCP is used to manually generate the pulse. If the adaptive feed-forward algorithm is switched off, the settings from this panel is used to set the signal applied to piezoelement. Two types of pulse are allowed – sine-wave like and the trapezoid like one. For sine wave pulse there are five different values which might be used – amplitude, offset, frequency, delay time and number of pulses (refer to Figure 6.11). For the trapezoid like signal there are six parameters – rise, fall, width and delay times, and amplitude A1 and A2 (refer to Figure 6.5).

There are also several buttons called 'sweep'. They were used to change the given value in range indicated in the script. These buttons were used for measurement presented in subchapters 6.4.1 and 6.4.2 as well as in the Appendix B

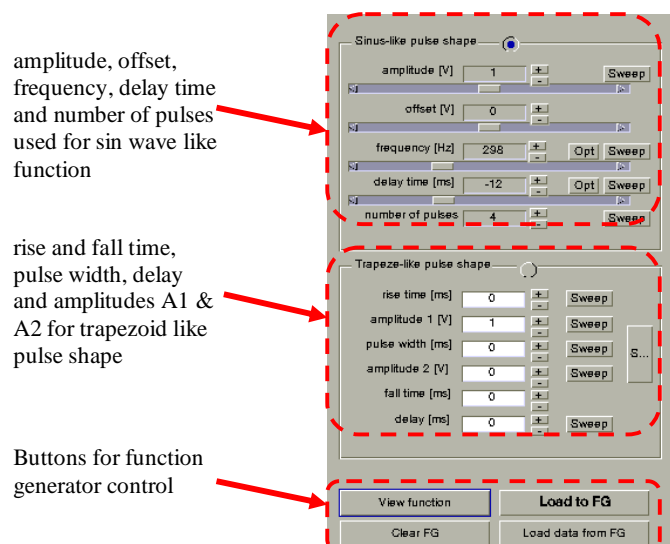


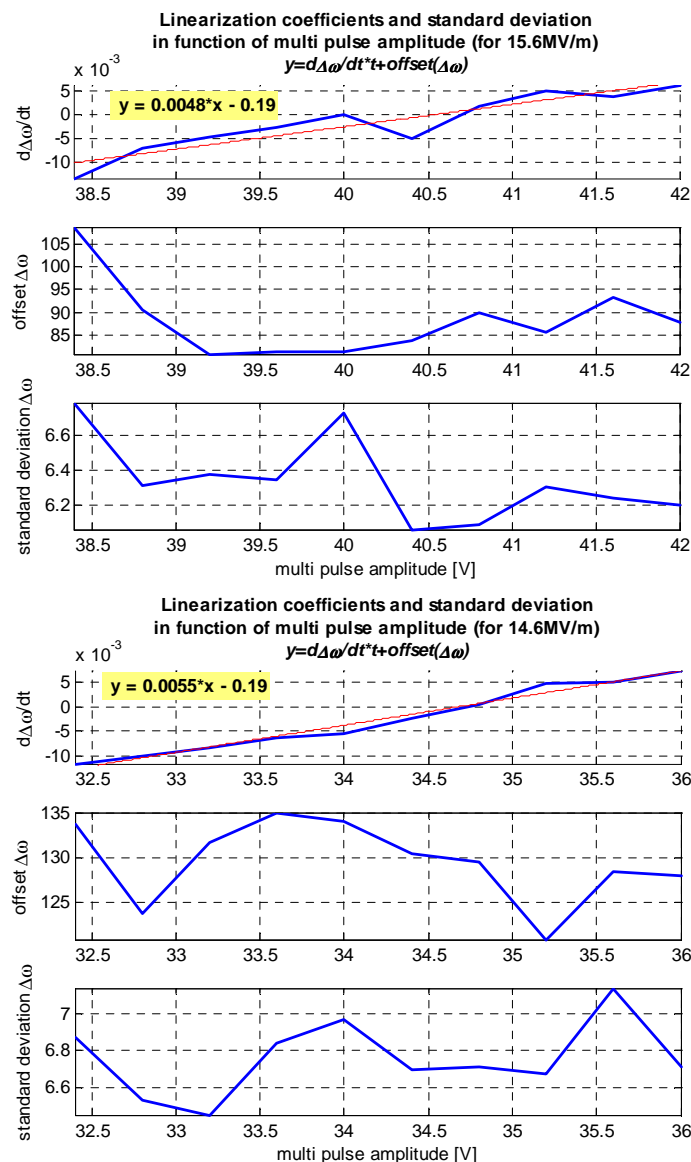
Figure 7.4 Description of third section of PCP.

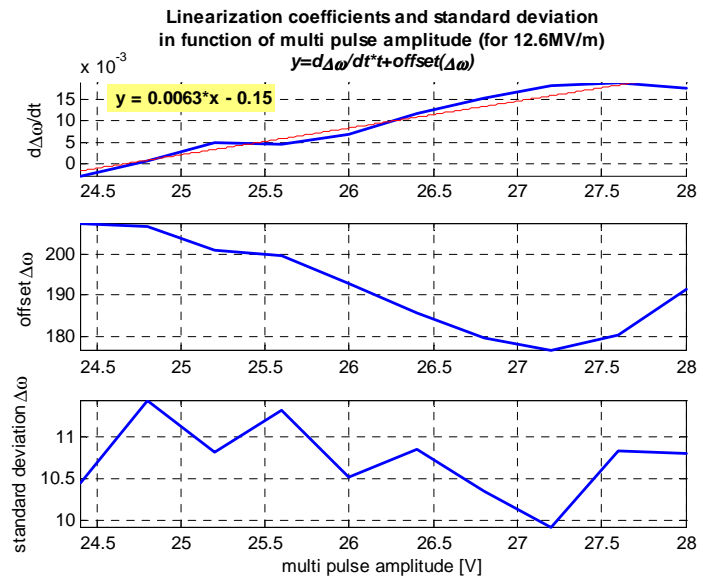
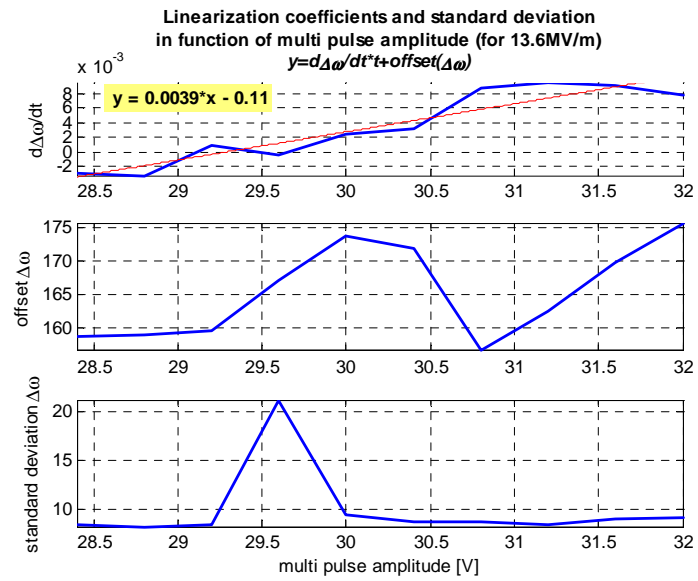
Bellow the settings there are set of four buttons named 'view function', 'load to FG', 'clear FG' and 'load from FG'. The names of these buttons indicates the function which are performed after its activation. To set new value in the FG there is need to set desired settings, then click on the 'view function' button, ant then click on 'load to FG' button. These combination protects the system from the incidentally change of settings. Nevertheless, to protect the piezoelements there are several restriction which are applied to the settings (i.e. the maximal signal must be below 160 V).

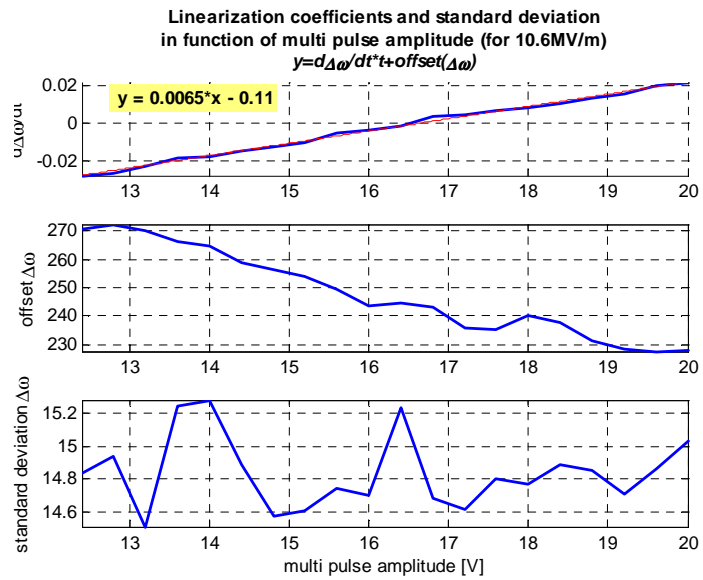
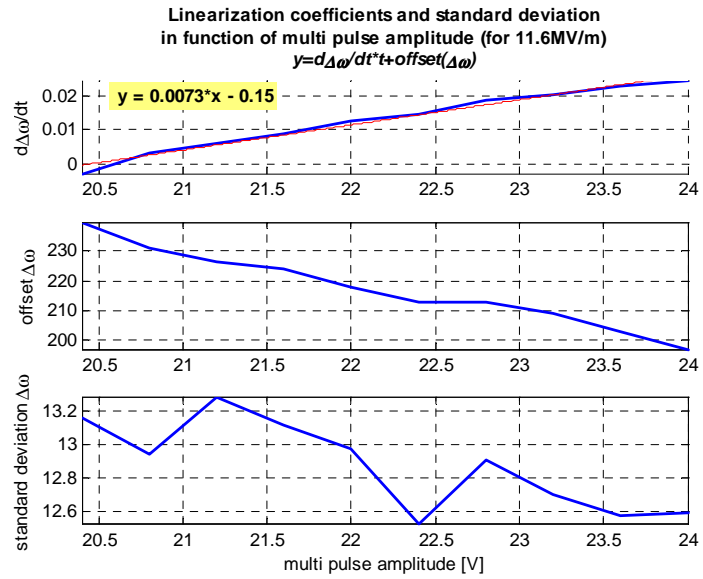
At the end, the fourth section of PCP is used to save and restore previously saved data. There is also a window, in which a results of performed command are shown.

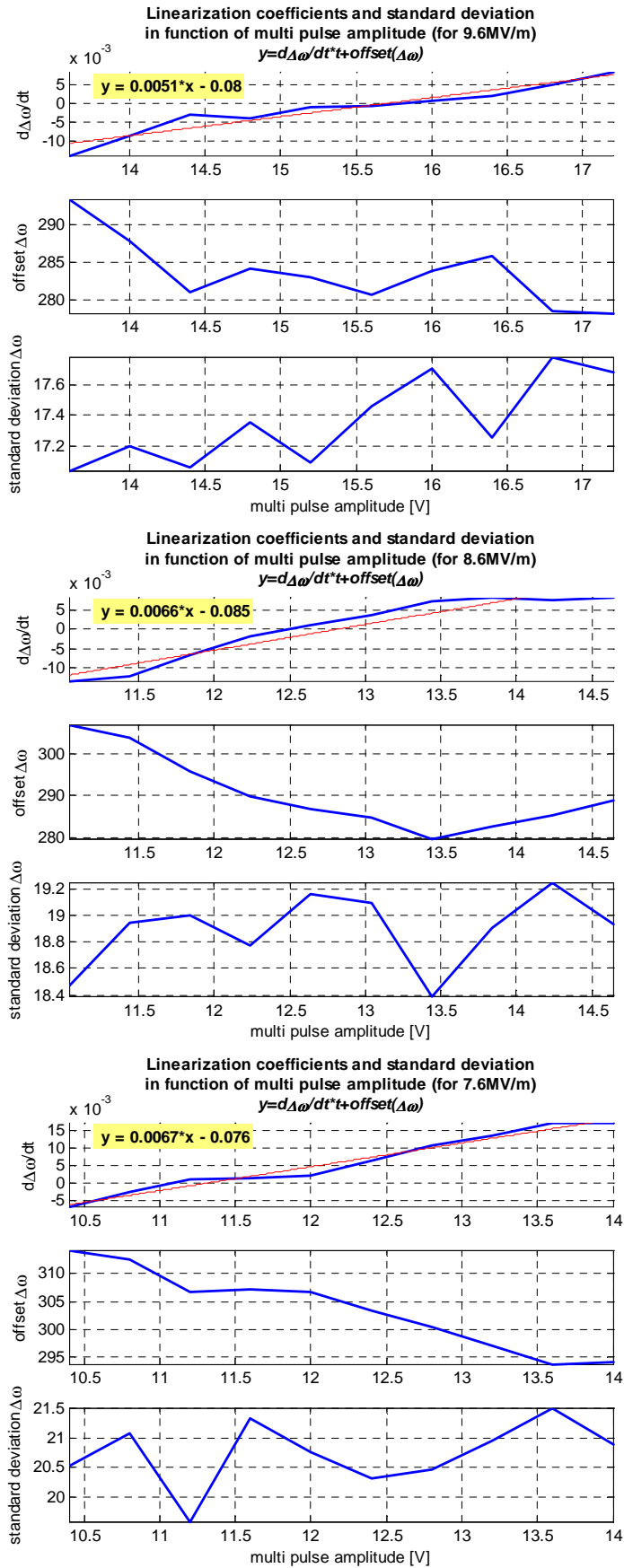
Appendix B Measurements of coefficients of linearized detuning for different accelerating field gradient.

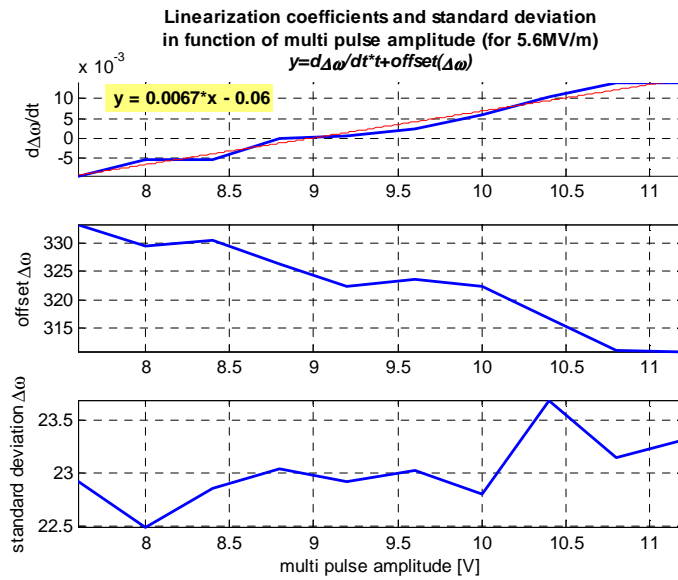
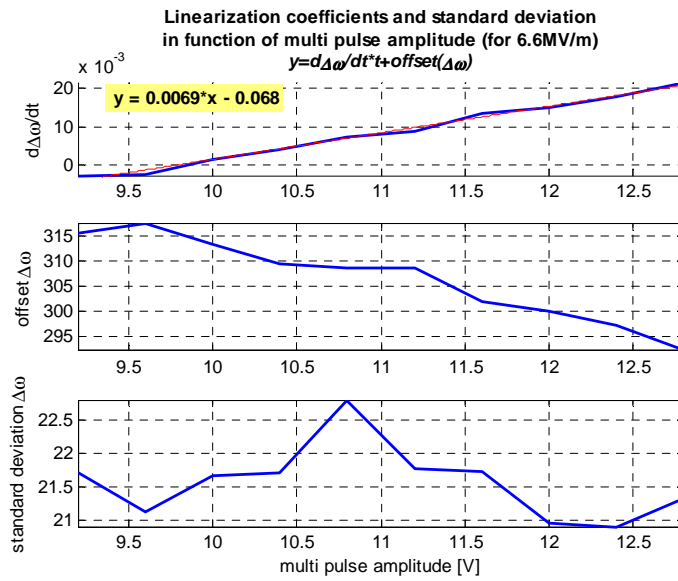
The following pictures illustrate the coefficients of linearization of detuning measured for different field gradients from 3.6 MV/m to 15.6 MV/m (this value corresponds to the settings in DSP, the measured value of probe signal was higher). The top subplot of each single figure presents a slope of Lorentz Force detuning during the RF pulse flat-top (which last 0.8ms). The middle subplot shows an offset of this detuning measured in the middle of flat-top (after 0.4ms from beginning of flat-top). The bottom subfigures illustrate a standard deviation of measurement from the linear approximation.

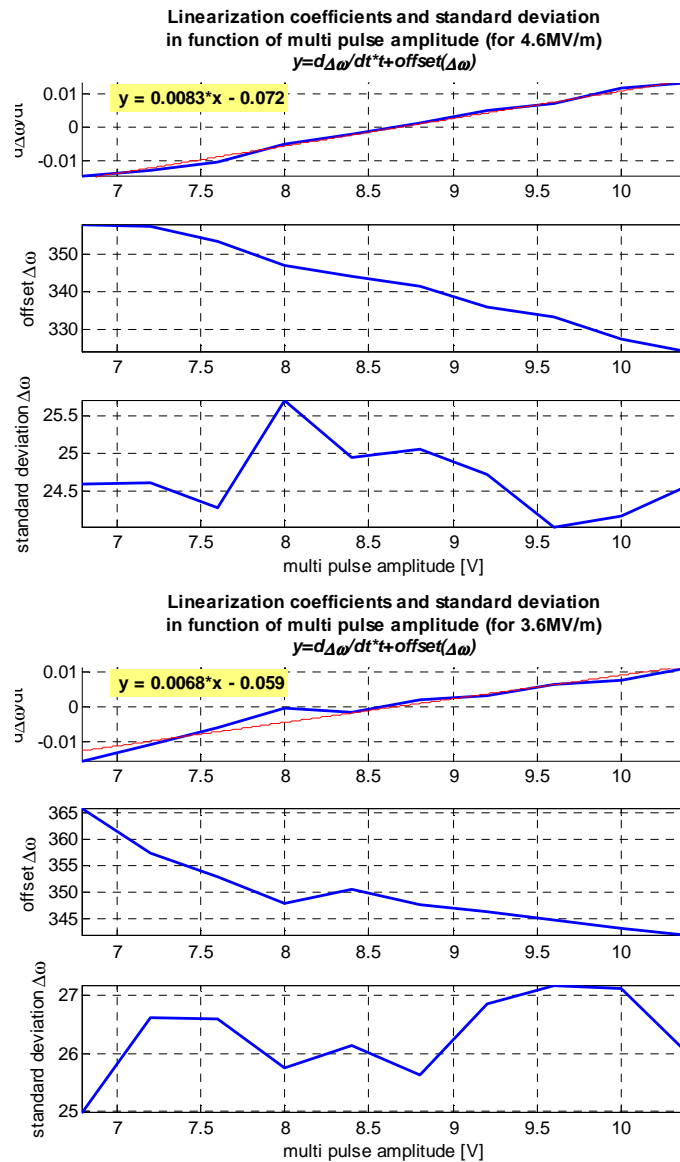












It is possible to find a dependency between the voltages applied to piezostack, when the slope of detuning is equal to zero, and the accelerating field gradient. The measurement and different approximation are shown in Figure B.1. Next figure presents the errors of each approximation for given value. Moreover, norms of residuals are presented. The quadratic estimate is sufficient, however the cubic one gives better correlation. Higher degrees of approximation curves do not give a significant improvement of norm of residuals.

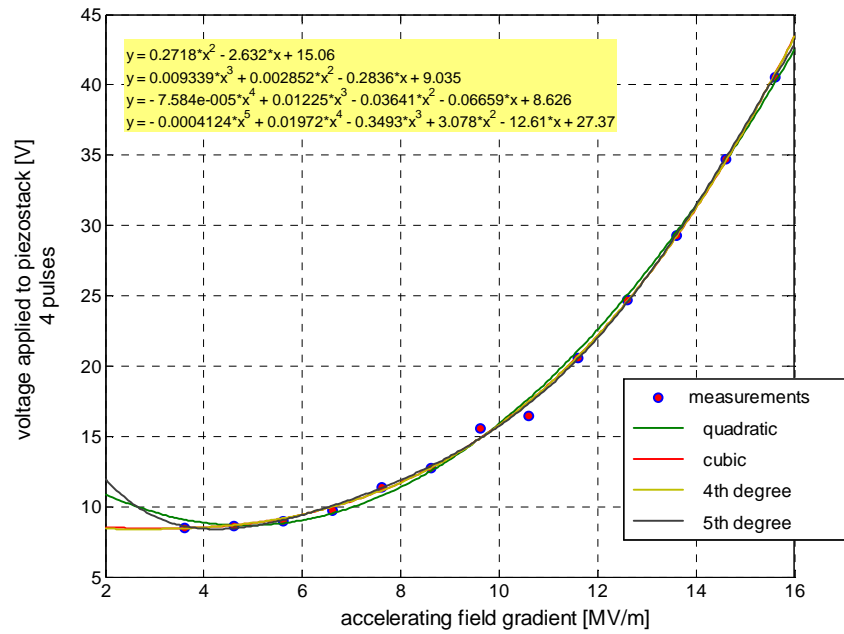


Figure 7.5 Amplitude of signal applied to piezostack to obtain a flat detuning during the RF pulse and its approximation for different accelerating field gradients.

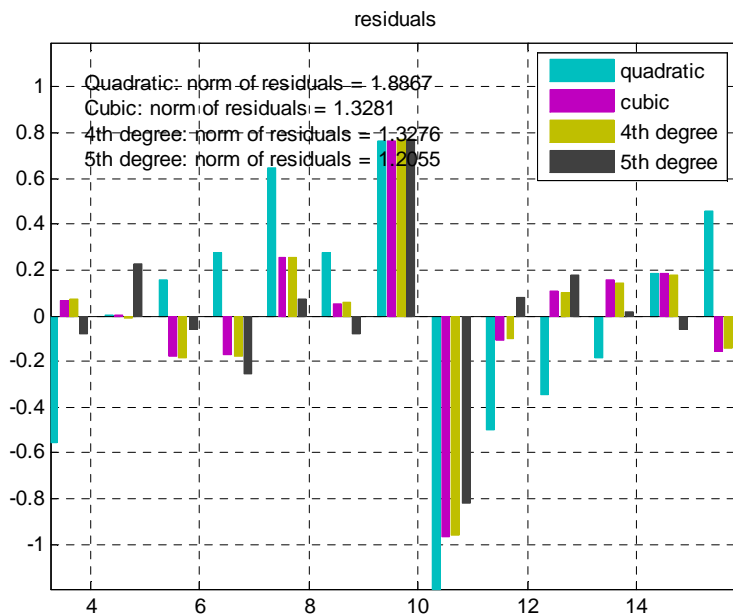


Figure 7.6 Residuals and their norm for different approximations in function of accelerating field gradients.

For higher gradients there is no important difference between cubic and quadratic approximation. However, for low gradients it is more convenient to use a cubic one.

Another conclusion, which might be found from the presented experiment, is the fact that close to the zero value of detuning slope one can find that the first derivative is almost stable for different gradient. It varies from 0.0048 for the highest gradient to 0.0083 for lower ones. This phenomenon is used for fine-tuning implemented in feed forward algorithm.